Tesis doctoral

Programa de Doctorado: Computación avanzada, energía y plasmas

Universidad de Córdoba

Aplicación de Fractales y Redes Complejas de variables meteorológicas en la descripción del cambio climático

Application of Fractals and Complex Networks of meteorological variables in the description of climate change

Autor:

Javier Gómez Gómez

Directores:

Prof. Dr. Francisco José Jiménez Hornero

Prof. Dr. Eduardo Gutiérrez de Ravé Agüera

Córdoba, mayo de 2022

TITULO: *Aplicación de Fractales y Redes Complejas de variables meteorológicas en la descripción del cambio climático*

AUTOR: *Javier Gómez Gómez*

TÍTULO DE LA TESIS:
Aplicación de Fractales y Redes Complejas de variables meteorológicas en la descripción del cambio climático

Application of Fractals and Complex Networks of meteorological variables in the description of climate change

DOCTORANDO:
Javier Gómez Gómez

INFORME RAZONADO DE LOS DIRECTORES DE LA TESIS
(se hará mención a la evolución y desarrollo de la tesis, así como a trabajos y publicaciones derivados de la misma).

El desarrollo de la tesis doctoral ha permitido alcanzar los objetivos inicialmente planteados en el plan de investigación en los plazos previstos.

Respecto a las tres publicaciones que constituyen el compendio presentado en esta tesis doctoral, hay que destacar que una de ellas está indexada en el primer cuartil de su categoría de JCR y el resto en el segundo. Como consecuencia, la difusión internacional de los resultados presentados en esas publicaciones y, por tanto, en esta tesis está asegurada. Estas publicaciones recogen los estudios de series temporales de temperatura y precipitación en España en el periodo (1969-2019) aplicando el análisis multifractal y las redes complejas.

El análisis multifractal se usó para evitar el tener que asumir una función subyacente ajustada y derivable que represente de forma aproximada los datos de las series temporales. El análisis multifractal trabaja directamente con los datos, en concreto, con sus singularidades. Esto impide la inclusión de información errónea obteniendo una descripción más precisa de los procesos estudiados.

En el caso de la temperatura, la observación del espectro multifractal reveló una relación entre el cambio climático y las propiedades fractales de las series de datos, pudiendo discriminar entre localidades costeras y de interior. Se detectaron comportamientos diferentes para los valores máximos y mínimos de la temperatura, siendo esta circunstancia una consecuencia del cambio climático. Los resultados descritos sugieren la inclusión de alguno de los parámetros estudiados en las bases de datos usadas por los modelos predictivos de los diferentes escenarios de evolución de la temperatura.

Respecto a la precipitación, al analizar los parámetros multifractales (no lineales) de las series de datos diarios registrados, se observó que en el cinturón mediterráneo de la Península Ibérica se están produciendo modificaciones en el comportamiento de las tormentas relacionadas con el cambio climático. Por otro lado, para las fluctuaciones de la precipitación, se demostró la existencia de una fuerte persistencia a largo plazo para las escalas temporales de estudio pequeñas, mientras que para las más grandes existía una correlación débil. Los patrones detectados por el análisis multifractal muestran una complejidad notable en la distribución espacial de la precipitación. De

hecho, la complejidad de las fluctuaciones pequeñas es muy relevante en la costa Atlántica y en la zona norte del interior. Por el contrario, en la zona este de España, las precipitaciones exhiben menor número de singularidades. Los resultados encontrados reflejan la irregularidad temporal y espacial de la distribución de la precipitación en España comparando con los proporcionados por el análisis lineal.

Por último, se investigaron las propiedades topológicas derivadas de transformar las series temporales de temperatura en redes complejas. Para esta finalidad se aplicó el enfoque del gráfico de visibilidad horizontal. Los resultados muestran la falta de tendencias significativas, a diferencia de los valores medios anuales de anomalías, que presentan una tendencia ascendente característica. Las principales conclusiones obtenidas son que las estructuras de redes complejas y las características no lineales, como las correlaciones débiles, parecen no verse afectadas por el aumento de las temperaturas derivado de las condiciones climáticas globales. Además, diferentes ubicaciones presentan un comportamiento similar y la naturaleza intrínseca de estas señales parece estar bien descrita por los parámetros de la red.

Los resultados descritos han sido vinculados con la ocurrencia del cambio climático, de tal forma que pueden ser considerados como evidencias del mismo. Este es el aspecto más innovador de esta tesis doctoral.

Por todo ello, se autoriza la presentación de la tesis doctoral.

Córdoba, 31 de mayo de 2022

Firma de los directores

Fdo.: Francisco José Jiménez Hornero Fdo.: Eduardo Gutiérrez de Ravé Agüera

A la memoria de mi abuelo Pedro,

de quien echaré de menos sus historias,

su humilde talento musical y su habilidad

y paciencia para trabajar la madera,

que siempre han sido una gran fuente

de inspiración para mi

AGRADECIMIENTOS

Agradecimientos

No puedo dar por finalizada esta tesis sin haber agradecido a todas las personas que me han acompañado en este viaje y que me han ayudado directa o indirectamente en la realización de este trabajo, a pesar de las dificultades y también una pandemia que aún no sabemos si hemos superado totalmente.

En primer lugar, agradecer a mis directores de tesis, Prof. Dr. Francisco José Jiménez Hornero y Prof. Dr. Eduardo Gutiérrez de Ravé Agüera, por su confianza en mí, su cercanía, paciencia, dedicación y estímulo que en todo momento han mostrado, ayudándome a avanzar en mis investigaciones y en el desarrollo de mi etapa doctoral.

A mis compañeros del departamento, Rafa, Ana Belén A., Elena, Alberto, Fernando, Valle y Ana Belén C. Os agradezco esas charlas distendidas más allá de los temas típicos del trabajo y esos desayunos que tanto han ayudado a desconectar y renovar fuerzas.

A mis padres, Pedro y Rosario, quiero darles las gracias por apoyarme, y por el cariño y paciencia que siempre han tenido tanto en los buenos momentos como en los malos.

A mi hermana Patricia y mi cuñado Carlos, por su respaldo y por esos buenos ratos que echamos juntos.

Finalmente, quiero dar las gracias al resto de mi familia, mis tíos/as, primos/as, abuelos/as. Porque siempre han confiado en mis capacidades, más incluso que yo mismo, aun cuando apenas sabían qué era exactamente lo que estaba haciendo o a qué dedicaba mis investigaciones.

RESUMEN

Resumen

El cambio climático está provocando distintos efectos según la región del planeta que se trate. Para estudiar estos cambios, se analizan largas series de registros de variables meteorológicas, como la temperatura o la precipitación, a través de modelos y técnicas predictivas. Estos están basados principalmente en bases de datos que se apoyan en análisis estadísticos e ignoran ciertas propiedades no lineales y multifractales de las series temporales implicadas.

Esta tesis se presenta como compendio de tres trabajos publicados en revistas indexadas en Journal Citation Reports. En ella se busca encontrar posibles patrones espaciales y temporales en las propiedades de las series y mejorar la descripción de la temperatura del aire en superficie y la precipitación. Para este propósito, se utilizan los análisis multifractal y de redes complejas. Para el primer análisis, se aplica el método de Análisis Multifractal de Fluctuación sin Tendencia (MF-DFA, por sus siglas en inglés), mientras que para el segundo se usa la técnica del Grafo de Visibilidad Horizontal (HVG). Este permite transformar las series temporales en redes complejas que heredan las propiedades de las series originales. Las estaciones meteorológicas analizadas se distribuyen a lo largo del territorio peninsular español y abarcan un mismo periodo de 60 años: 1960-2019.

En el primer trabajo, se lleva a cabo el análisis multifractal de las series de temperatura máxima, mínima, media y rango térmico diario (DTR, por sus siglas en inglés) en los subperiodos 1960-1989 y 1990-2019. Tras aplicar el método MF-DFA, se observa que las series son multifractales. Las temperaturas mínima y media experimentan una reducción del grado de multifractalidad en el último periodo en la mayoría de las estaciones. Además, muestran un mayor grado de multifractalidad en las estaciones costeras.

En el segundo trabajo, se usa el método HVG para analizar las series anuales de temperatura media diaria que se estudiaron en el primero. Los resultados indican que las estructuras de las redes complejas y sus propiedades no parecen estar afectadas por

el ascenso de las temperaturas derivado de las condiciones climáticas globales y son similares para las diferentes localizaciones consideradas.

Finalmente, en el tercer trabajo, se usa de nuevo el método MF-DFA en series de precipitación. Como resultado, se observa que la precipitación presenta un carácter multifractal más complejo que el de la temperatura, con al menos tres regímenes de escala distintos para las pequeñas fluctuaciones de estas señales. A escalas pequeñas, la precipitación diaria tiene una gran persistencia y la magnitud de las correlaciones sigue el gradiente espacial de la precipitación anual característico de la Península Ibérica. Estas correlaciones se reducen de manera uniforme en el segundo periodo. Los principales cambios observados a grandes escalas comprenden un aumento en la complejidad de las pequeñas fluctuaciones y una disminución de las singularidades de las series en la zona oriental de la Península.

ABSTRACT

Abstract

Climate change is causing different effects depending on the region of the planet concerned. To study these changes, long record series of meteorological variables, such as temperature or precipitation, are analyzed by means of models and predictive techniques. These are mainly based in data bases which are supported by statistical analysis and ignore some nonlinear and multifractal properties of the time series involved.

This thesis is presented as a compendium of three works published in journals indexed in Journal Citation Reports. It aims to find possible spatial and temporal patterns in the properties of series and to improve the description of the air surface temperature and the precipitation. For that purpose, multifractal and complex networks analysis are used. For the first analysis, the Multifractal Detrended Fluctuation Analysis (MF-DFA) is applied, while for the second one the Horizontal Visibility Graph (HVG) technique is employed. This allows to transform time series into complex networks which inherit the features of the original series. The analyzed meteorological stations are distributed over the Spanish peninsular territory and span the same 60-year period: 1960-2019.

In the first work, the multifractal analysis of the series of maximum, minimum, mean temperature, and diurnal temperature range (DTR) is carried out in the subperiods 1960-1989 and 1990-2019. After the MF-DFA method is applied, it is observed that the time series are multifractal. Minimum and mean temperatures experience a reduction of the degree of multifractality in the last period in most stations. Furthermore, they show a higher degree of multifractality in the coastal stations.

In the second work, the HVG method is used on the annual series of daily mean temperature which were studied in the first one. Outcomes denote that the complex network structures and their properties seem not to be affected by the rise of temperatures derived from the global climatic conditions and they are similar for the different locations considered.

Finally, in the third work, the MF-DFA method is used again on precipitation series. As a result, it is observed that the precipitation exhibits a more complex multifractal character than the temperature, with at least three different scaling regions for the small fluctuations of these signals. At small scales, daily precipitation has a high persistence, and the magnitude of correlations follows the characteristic spatial gradient of annual precipitation in the Iberian Peninsula. These correlations are reduced uniformly in the second period. The main changes observed at large scales include a rise in the complexity of small fluctuations and a decrease of singularities of series in the eastern part of the Peninsula.

Índice

1. INTRODUCCIÓN

1. Introducción

En las últimas décadas, el calentamiento de la atmósfera, los océanos y la superficie del planeta está provocando un cambio global en el sistema climático. Este cambio climático, así como el impacto y los riesgos derivados del mismo, están siendo el foco de estudio de distintas investigaciones en las que se fundamentan los informes del Grupo Intergubernamental de Expertos sobre el Cambio Climático (IPCC, por sus siglas en inglés). El último informe, publicado en el año 2021, habla de un aumento observado en la temperatura media global de la superficie de casi un grado en las primeras dos décadas del siglo XXI respecto al periodo 1850-1900 (IPCC, 2021). De hecho, en el periodo transcurrido entre la publicación de este informe y el anterior, se constata que continúa este ascenso (IPCC, 2013). Además, también hay claras evidencias de un aumento en la frecuencia de ciertos eventos extremos, como olas de calor, precipitaciones intensas o sequías, entre otros (Coumou y Rahmstorf, 2012). Estos fenómenos tienen un impacto severo en los sistemas naturales y antrópicos. Algunos problemas observados abarcan: un cambio en las precipitaciones, el deshielo y el derretimiento de la nieve, que alteran considerablemente los diversos sistemas hidrológicos del planeta; la alteración en la actividad y las migraciones de muchas especies marinas y terrestres; y un impacto negativo en el rendimiento de las cosechas (IPCC, 2014). Como puede apreciarse, dos de las magnitudes más importantes que influyen en la variabilidad climática, son la temperatura y la precipitación. Estas son las magnitudes en las que se centra esta tesis.

Una de las magnitudes frecuentemente analizadas para el estudio del clima es la temperatura del aire en superficie (Brunet et al., 2007; Eensaar, 2021; Jones et al., 1999; Jones y Moberg, 2003; Perevedentsev et al., 2017). Esta se obtiene fundamentalmente a partir de observaciones de estaciones meteorológicas en superficie, que se agrupan en distintas bases de datos (Brunet et al., 2007; IPCC, 2021, 2013; Jones y Moberg, 2003). En numerosas ocasiones, esta magnitud física se estudia a través de las variables siguientes: las temperaturas máxima y mínima diarias (Abaurrea et al., 2001; Brunet et al., 2007; Horton, 1995), la temperatura media diaria (Fuwape et al., 2017; Javanshiri et al., 2021; Millán et al., 2010) y el rango térmico diario (El Kenawy et al., 2012; Ongoma

et al., 2020; Zhuang y Zhang, 2020). Esta última variable (en adelante, DTR, por sus siglas en inglés) es una magnitud derivada de la diferencia entre las temperaturas máxima y mínima diarias.

En diversos estudios realizados en las dos últimas décadas, se han observado evidencias coherentes de calentamiento sobre el territorio peninsular español (Brunet et al., 2007, y sus referencias). A pesar de las diferencias en la metodología empleada, todos coinciden en el aumento de las temperaturas que ha sido destacado fundamentalmente en la segunda mitad del pasado siglo. Sin embargo, este incremento de las temperaturas no ha sido uniforme temporalmente, detectándose un mayor ritmo en las temperaturas de los meses invernales. También se han observado diferentes ritmos en el incremento de las temperaturas máximas y mínimas. No obstante, se pueden encontrar resultados contradictorios en este aspecto en la literatura científica (Brunet et al., 2007, y sus referencias).

En el estudio de la variabilidad climática de las precipitaciones también es bastante común el análisis de las series temporales obtenidas a partir de estaciones de medida en superficie (Brunetti et al., 2001; López-Moreno et al., 2010; Rodrigo, 2010). Se ha observado un aumento de las sequías y de la frecuencia e intensidad de las fuertes precipitaciones en la mayor parte de la superficie terrestre, aunque hay poca consistencia en los cambios de las precipitaciones intensas sobre algunas áreas del planeta, en particular, en la región del Mediterráneo (IPCC, 2021). Sin embargo, sí se tienen evidencias de un aumento de la frecuencia de las borrascas en verano y otoño y un descenso en invierno y primavera en la región Mediterránea occidental (Bartholy et al., 2009). Estos cambios dan lugar en verano a un aumento de las borrascas de corta duración frente a las de larga duración, que derivan en un descenso significativo de las precipitaciones en esta época del año. En el caso de la Península Ibérica, contrariamente a lo observado en general en la precipitación global, se tienen evidencias de que la probabilidad de los periodos de precipitaciones intensas no ha aumentado, pero sí la de los periodos de sequía (López-Moreno et al., 2010; Rodrigo, 2010; Rodrigo y Trigo, 2007). Además, se han encontrado evidencias de un descenso general en la precipitación anual y en la intensidad de la precipitación diaria.

Tradicionalmente, el estudio de estas series temporales se ha realizado mediante el uso de análisis de tendencias u otros métodos estadísticos que dan una descripción limitada de su compleja dinámica e ignoran sus características no lineales (de Lima et al., 2013; El Kenawy et al., 2012; Horton, 1995; Jones y Hulme, 1996; Katsoulis y Kambetzidis, 1989). Sin embargo, en las últimas décadas ha habido un interés creciente en el estudio de estas propiedades en el análisis de series meteorológicas, en particular, con los llamados métodos multifractales (Baranowski et al., 2015; Burgueño et al., 2014; da Silva et al., 2020; García-Marín et al., 2015; Sarker y Mali, 2021).

La autosimilitud es una característica no lineal que tienen algunos sistemas que consiste en la repetición de sus propiedades a distintas escalas. Si esta autosimilitud ocurre para las infinitas escalas posibles, es decir, si existe invariancia de escala, este sistema se denomina fractal (Mandelbrot, 1982). Un ejemplo de curva fractal es la curva de Koch, representada en la Figura 1. Esta curva se construye repitiendo sucesivamente el siguiente procedimiento: se divide un segmento en tres partes iguales y se sustituye la parte central por dos segmentos de igual longitud que forman un ángulo de 60 grados. El resultado de este proceso puede apreciarse en las diferencias que existen entre la primera y segunda iteración mostradas en la figura mencionada. Como se puede apreciar, esta curva mantiene la misma forma cuando ampliamos un fragmento de ella. Esto significa que es invariante ante traslaciones y cambios de escala, es decir, es autosimilar. Por tanto, se trata de un sistema fractal (Feder, 1988).
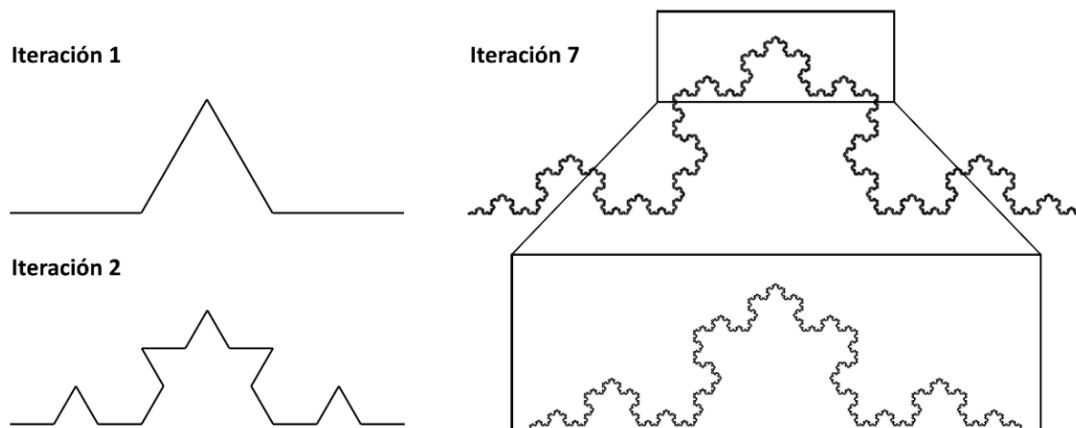
Figura 1: (Izquierda) Primera y segunda iteraciones de la curva de Koch. (Derecha) Séptima iteración y su parte superior ampliada. Fuente: Elaboración propia basada en el código de Durrani (2022)

Un sistema fractal como el de la figura quedaría completamente descrito por la llamada dimensión fractal, que para estos sistemas no es entera y es mayor que su dimensión topológica, D_T. Hay diferentes formas de definir la dimensión fractal de un sistema. Algunas de ellas son la dimensión de información; la dimensión de box-counting (conteo de cajas) o de Minkowski-Bouligand; y la de Hausdorff-Besicovitch (Feder, 1988; Mandelbrot, 1982). Por ejemplo, para la curva de Koch, la dimensión de Hausdorff-Besicovitch es $D_{HB} \approx 1.26 > D_T = 1$.

Muchos objetos de la naturaleza en realidad son estadísticamente autosimilares. Esto significa que en estos objetos son las propiedades estadísticas las que se repiten a diferentes escalas, como ocurre, por ejemplo, con las líneas de costa (Mandelbrot, 1967).

En el contexto de las series temporales, $x(t)$, se observa que la dinámica de estas es más compleja y, en lugar de ser autosimilares, son autoafines. Esto significa que las variables x y t se modifican a razones distintas cuando se cambia la escala de análisis (Feder, 1988). Además, gracias al llamado exponente de Hurst, H, se ha demostrado que muchas series temporales de variables presentes en la naturaleza, como la lluvia, el caudal de los ríos o la temperatura, poseen una relación de escala empírica entre el rango ajustado de la serie y un periodo de tiempo suficientemente amplio, τ,

normalmente de años. Dicha relación está dada por $R/S = (\tau/2)^H$, donde S es la desviación estándar. Bajo ciertas condiciones, este exponente de escala se relaciona con la dimensión fractal de la curva mediante la expresión $D = 2 - H$, válida para series que cumplen la propiedad que se ha mencionado antes, es decir, para series autoafines (Feder, 1988, y sus referencias).

Frecuentemente, se requiere de distintos exponentes de escala (temporal) para describir satisfactoriamente las series temporales encontradas en la naturaleza. La diversidad de exponentes que las describen puede deberse a diferentes factores, como los que se expondrán a continuación. Algunas variables presentan escalas temporales de transición que separan regímenes con distintos exponentes de escala (Hu et al., 2001; Pavón-Domínguez et al., 2013; Tadić et al., 2019). En otros casos, se observa que se necesitan distintos exponentes para describir diferentes segmentos de la serie, indicando una evolución temporal de los mismos (Drożdż et al., 2018; Telesca et al., 2001; Telesca y Lapenna, 2006). Otras magnitudes muestran series con una jerarquía de subconjuntos fractales mezclados, cada uno con un exponente de escala distinto. En este caso, se dice que el proceso es multifractal, mientras que un proceso con una única dimensión fractal se denomina comúnmente como monofractal (Kantelhardt et al., 2002; Telesca y Lapenna, 2006).

Debido a estos factores, el uso del análisis multifractal de las series temporales para tratar de describir sus propiedades no lineales, sus singularidades y sus propiedades de escala ha suscitado un gran interés en las últimas décadas. Algunos de estos estudios abarcan campos tan diversos como la contaminación atmosférica (Carmona-Cabezas et al., 2019), la astronomía (Movahed et al., 2006) o la música (Telesca y Lovallo, 2011a). En particular, varios trabajos han demostrado el éxito de estas técnicas cuando se han aplicado a variables meteorológicas como la evapotranspiración (Ariza-Villaverde et al., 2019), la temperatura del aire en superficie (da Silva et al., 2020), la precipitación (Rodríguez-Solà et al., 2017), la humedad relativa, la radiación global o la velocidad del viento (Baranowski et al., 2015).

Una técnica ampliamente usada en el análisis de series fractales es el método de Análisis de Fluctuación sin Tendencia (o DFA, por sus siglas en inglés). Este método permite la determinación de las propiedades de escala monofractales y de la persistencia o correlaciones de largo alcance en series temporales con ruido y no estacionarias. Sin embargo, para aquellas series que presentan distintos subconjuntos fractales entremezclados, un análisis multifractal es más adecuado. Por ello, Kantelhardt et al. (2002) propusieron el método denominado Análisis Multifractal de Fluctuación sin Tendencia (MF-DFA) para extender su uso a series multifractales no estacionarias. Su utilidad radica en que permite determinar el exponente de Hurst generalizado para distintos momentos estadísticos. Además, estos autores establecieron una relación con el formalismo multifractal estándar. Esto posibilita relacionar dicho exponente con el llamado espectro multifractal o de singularidad, $f(\alpha)$, donde α es el exponente de singularidad (o de Lipschitz-Hölder). Este espectro caracteriza las singularidades de cada subconjunto fractal de la serie analizada (Feder, 1988), donde f puede interpretarse como la probabilidad de ocurrencia de un evento que pertenece a un subconjunto con singularidad α (Nilsson, 2007).

Otra perspectiva del análisis de las características no lineales de las series temporales fue la propuesta de Lacasa et al. (2008), que desarrollaron un método conocido como Grafo de Visibilidad (VG) que trazaba un puente entre el análisis de series temporales y la teoría de grafos. Aunque los grafos ya han sido usado con anterioridad en varios estudios climáticos (Gozolchiani et al., 2011; Paluš et al., 2011; Tsonis y Roebber, 2004), estos se centran en construir las llamadas redes climáticas representando en cada nodo las estaciones o puntos geográficos analizados. El método VG, en cambio, permite transformar series temporales en grafos que heredan las propiedades de las series originales. Para ello, hace uso de un criterio de visibilidad que establece si dos puntos de la serie (nodos) cualesquiera están conectados en la red. Con este método, las series aleatorias se transforman en grafos aleatorios, las series periódicas en grafos regulares y las series fractales en redes libres de escala. Además, la distribución de probabilidad del grado, una medida de centralidad ampliamente utilizada en redes complejas, permite distinguir entre los distintos tipos de redes y, por tanto, entre distintos tipos de series temporales (Lacasa et al., 2008).

Una versión del Grafo de Visibilidad más simple, es el llamado Grafo de Visibilidad Horizontal (HVG), usado por primera vez en un estudio realizado por Luque et al. (2009). En este trabajo, los autores hallaron resultados obtenidos de forma analítica para varias propiedades topológicas de estas redes cuando provenían de series aleatorias no correlacionadas. Otro trabajo (Lacasa y Toral, 2010) demostró que, gracias a una propiedad de estas redes, era posible distinguir entre procesos estocásticos correlacionados, no correlacionados y caóticos. Un ejemplo de aplicación a series reales de esta técnica puede verse en el trabajo de Braga et al. (2016), donde se describe la evolución anual de las fluctuaciones en el caudal de distintos ríos en Brasil a través de las propiedades de las redes.
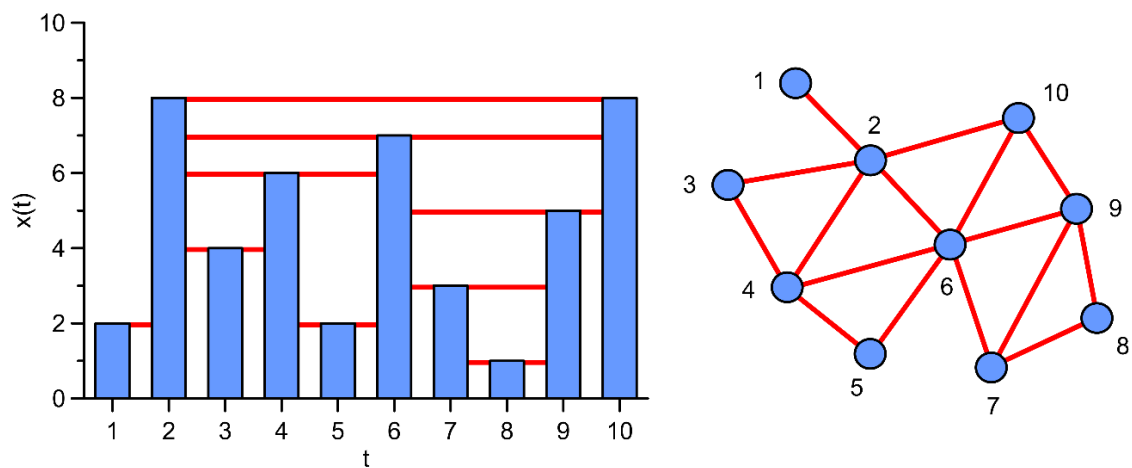

Figura 2: (Izquierda) Ejemplo de una serie temporal representada en diagrama de barras donde se establecen enlaces entre los distintos puntos según el método HVG (Luque et al., 2009). (Derecha) Grafo de Visibilidad obtenido tras aplicar el método, donde cada nodo representa un punto de la serie y cada arista un enlace. Fuente: Elaboración propia.

La hipótesis de partida de esta tesis doctoral es que la descripción de la evolución de la temperatura y la precipitación en un contexto de cambio climático está incompleta al no considerar la información derivada del análisis multifractal y de redes complejas. Actualmente, lo más frecuente es tener en cuenta la información estadística y el análisis de tendencias, entre otros. Sin embargo, estos resultados dan lugar a una descripción parcial y poco precisa, en muchos casos basados en modelos lineales que no reflejan la verdadera dinámica de estas series. El análisis multifractal y de redes complejas supera esta limitación al analizar sus propiedades no lineales. Estos resultados no son

habitualmente contemplados en las bases de datos usadas para la aplicación de modelos predictivos y podrían mejorar su precisión. Este trabajo se centra en la Península Ibérica, presentando el análisis multifractal de la temperatura y la precipitación y la aplicación del Grafo de Visibilidad Horizontal en la temperatura para un periodo de 60 años (1960-2019). Los resultados obtenidos de esta investigación se han descrito en las tres publicaciones que forman el cuerpo de esta tesis. A continuación, para aclarar el contenido de estas, en la Figura 3 se muestra el contenido de cada una de ellas.
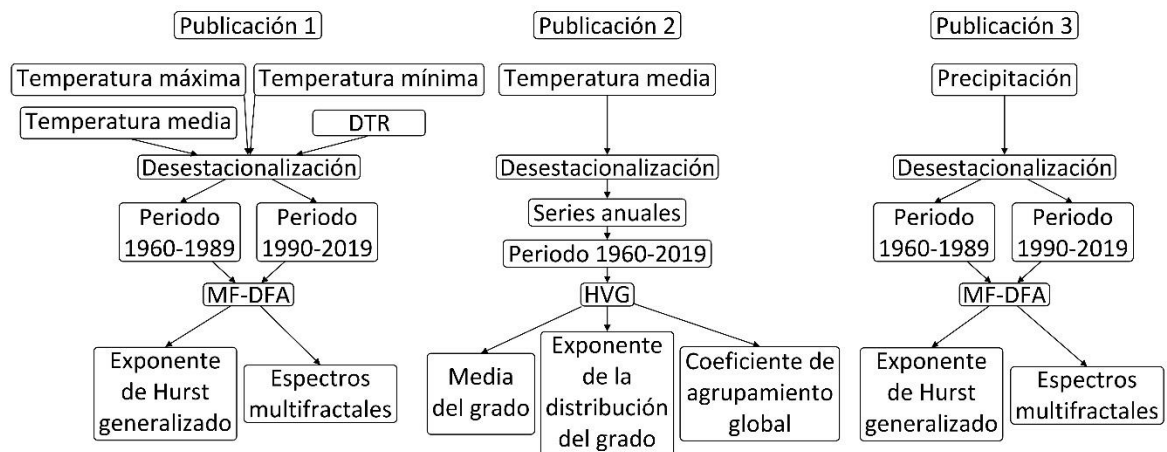

Figura 3: Esquema simplificado del contenido de cada publicación. Fuente: Elaboración propia.

En el primer estudio (Gómez-Gómez et al., 2021a), el método MF-DFA se aplica a cuatro variables de temperatura (máxima, mínima, media diarias y DTR) en diez estaciones distintas distribuidas por la Península Ibérica y en dos periodos: 1960-1989 y 1990-2019. En este trabajo se analizan el exponente de Hurst generalizado y los espectros multifractales de estas series de temperatura con el objetivo de buscar evidencias de una posible influencia del cambio climático en estas propiedades y obtener una mejor descripción de la dinámica de estas series.

En el segundo estudio (Gómez-Gómez et al., 2021b), se exploró la aplicación del método HVG a diez series de temperatura media diaria. Se analizó la relación de las propiedades de las series originales con las características topológicas de los grafos, estudiando si estas últimas cambian en un contexto de ascenso generalizado de las temperaturas. Para ello, se estudiaron tres de estas características (la media del grado, el exponente de la distribución del grado y el coeficiente de agrupamiento global) y sus

tendencias. Las estaciones en las que se analiza esta variable y el periodo abarcado (1960-2019) coinciden con aquellos considerados en el primer estudio.

Finalmente, en el tercer trabajo (Gómez-Gómez et al., 2022), se analizó la complejidad de las series de precipitación, usando de nuevo el MF-DFA, para los mismos periodos de 30 años considerados en el primer estudio. En este caso, se abordó el análisis sobre un total de 29 estaciones. Para esta variable, también se estudiaron tanto el exponente de Hurst generalizado como distintas características de los espectros multifractales, atendiendo especialmente a la posible variación de estas propiedades entre ambos periodos.

2. HIPÓTESIS Y OBJETIVOS

2. Hipótesis y objetivos

La descripción de la evolución de la temperatura y la precipitación ha sido tradicionalmente llevada a cabo a través de diversos métodos estadísticos, con la frecuente inclusión de distintos análisis de tendencias (de Lima et al., 2013; El Kenawy et al., 2012; Horton, 1995; Jones y Hulme, 1996; Katsoulis y Kambetzidis, 1989). La principal hipótesis que aborda esta tesis es que los resultados derivados del análisis multifractal y de redes complejas pueden mejorar la descripción de estas variables meteorológicas en el contexto actual de cambio climático, dando una información complementaria acerca de las propiedades de escala y no lineales de las series implicadas.

El uso de la técnica de MF-DFA para estudiar series meteorológicas se ha extendido mucho en la literatura científica (Baranowski et al., 2015; Burgueño et al., 2014; da Silva et al., 2020; Krzyszczak et al., 2019; Mali, 2015; Sarker y Mali, 2021; Telesca y Lovallo, 2011b). La metodología seguida en la gran mayoría de las publicaciones se fundamenta en analizar las fluctuaciones de las series completas con los datos disponibles. Por tanto, ignoran el posible cambio en las fluctuaciones que puede transcurrir entre distintos periodos, a semejanza de lo encontrado por algunos autores en el marco de las series sísmicas (Telesca et al., 2001; Telesca y Lapenna, 2006). Respecto a las series de precipitación y temperatura en la Península Ibérica, hay pocos estudios y están fundamentalmente centrados en algunas de sus subregiones (Burgueño et al., 2014).

Por otra parte, la aplicación del método de HVG permite trabajar en el marco de las redes complejas con grafos que contienen las propiedades de las series originales (Lacasa y Toral, 2010; Luque et al., 2009). Este método también permite distinguir la naturaleza caótica o estocástica de estas series y describir sus correlaciones, como se expone en las conclusiones de un trabajo publicado en la pasada década (Lacasa y Toral, 2010). Braga et al. (2016) observaron una evolución en las propiedades topológicas en un estudio que aplicaba HVG al caudal anual de los ríos. Por tanto, siguiendo a estos autores, es conveniente explorar los posibles cambios en las propiedades de estas redes

complejas derivadas de series de variables meteorológicas y observar si pueden estar relacionados con el cambio climático.

El objetivo principal de la tesis es, por tanto, completar la descripción de las series temporales de temperatura y precipitación en la Península Ibérica aplicando el análisis multifractales y de redes complejas. Este objetivo se desglosa por publicación en los siguientes objetivos específicos:

1. Publicación 1 (Gómez-Gómez et al., 2021a). El objetivo general de este trabajo es buscar evidencias de cambios en las propiedades multifractales de las series de temperatura del aire en superficie. Para alcanzarlo, se llevaron a cabo las siguientes tareas:

    1.1. Obtención de las anomalías o series temporales desestacionalizadas de cuatro variables de temperatura (máxima, mínima, media y DTR), procedentes de diferentes localizaciones geográficas.

    1.2. Implementación del algoritmo con el método MF-DFA aplicados a estas series en dos periodos consecutivos de 30 años: 1960-1989 y 1990-2019.

    1.3. Obtención de los exponentes de Hurst generalizados de cada variable y localización, y evaluación de sus cambios entre los periodos mencionados.

    1.4. Cálculo de los espectros de singularidad y análisis de las propiedades más importantes que los caracterizan (el máximo, la anchura y la asimetría) y sus cambios entre ambos periodos.

2. Publicación 2 (Gómez-Gómez et al., 2021b). El objetivo de este estudio es explorar si el marco teórico de los Grafos de Visibilidad puede aplicarse a series de temperatura media diaria y verificar si las propiedades topológicas de las redes obtenidas cambian en un contexto de cambio climático. A continuación, se exponen los aspectos tratados para llegar a este objetivo:

2.1. Realización de un análisis preliminar para identificar la evolución anual de los valores promedios de las anomalías de temperatura media diaria en el periodo 1960-2019.

2.2. División de las series de las anomalías en periodos anuales y transformación de cada segmento en sus respectivos HVGs.

2.3. Cálculo del grado y el coeficiente de agrupamiento global de cada red compleja.

2.4. Obtención de la media y el exponente de la distribución del grado para evaluar, junto al coeficiente de agrupamiento, la evolución de estos parámetros en el periodo de 60 años, considerando sus posibles tendencias.

3. Publicación 3 (Gómez-Gómez et al., 2022). El objetivo general de este estudio es investigar si las propiedades multifractales de la precipitación cambian entre dos periodos consecutivos de 30 años, similares a los del primer estudio, y verificar si estos cambios siguen patrones geográficos o temporales. Para desarrollar este objetivo se acometieron las siguientes tareas:

3.1. Realización de un análisis preliminar de la tendencia de la precipitación anual acumulada en distintas localizaciones en el periodo completo de 60 años, 1960-2019. Comparación de sus resultados con los de la estadística descriptiva en cada subperiodo de 30 años (1960-1989 y 1990-2019).

3.2. Desestacionalización de las series de precipitación diaria.

3.3. Cálculo de los exponentes de Hurst generalizados en cada localización y análisis de sus cambios entre los dos subperiodos.

3.4. Determinación de los espectros de singularidad en las distintas localizaciones y estudio de sus propiedades más relevantes (el máximo, la anchura y la asimetría) y los cambios entre ambos subperiodos.

3. PUBLICACIONES

Publicación 1

Multifractal detrended fluctuation analysis of temperature in Spain (1960–2019)

Journal Citation Reports (Clarivate™)

Revista

Physica A: Statistical Mechanics and its Applications

Editorial

Elsevier

Factor de impacto (2020)

3.263

Categoría

Physics, multidisciplinary

Posición y cuartil (2020)

28/86, Q2

Multifractal detrended fluctuation analysis of temperature in Spain (1960–2019)

Javier Gómez-Gómez [*], Rafael Carmona-Cabezas, Ana B. Ariza-Villaverde,
Eduardo Gutiérrez de Ravé, Francisco José Jiménez-Hornero

GEPENA Research Group, University of Cordoba, Gregor Mendel Building (3rd floor), Campus Rabanales, 14071 Cordoba, Spain

ARTICLE INFO

ABSTRACT

In the last decades, an ever-growing number of studies are focusing on the extreme weather conditions related to the climate change. Some of them are based on multifractal approaches, such as the Multifractal Detrended Fluctuation Analysis (MF-DFA), which has been used in this work. Daily diurnal temperature range (DTR), maximum, minimum and mean temperature from five coastal and five mainland stations in Spain have been analyzed. For comparison, two periods of 30 years have been considered: 1960–1989 and 1990–2019. By using the MF-DFA method, generalized Hurst exponents and multifractal spectra have been obtained. Outcomes corroborate that all these temperature variables have multifractal nature and show changes in multifractal properties between both periods. Also, Hurst exponents values indicate that all time series exhibit long-range correlations and a stationary behavior. Coastal locations exhibit in general wider spectra for minimum and mean temperature than for maximum and DTR, in both periods. On the contrary, the mainland ones do not show this pattern. Also, width from multifractal spectra of these two variables (minimum and mean temperature) is shortened in the last period in almost every case. To authors' mind, changes in multifractal features might be related to the climate change experienced in the studied region. Furthermore, reduction of spectra width for minimum and mean temperature implies a decrease of the complexity of these temperature variables between both studied periods. Finally, the wider spectra found in coastal stations might be useful as a discriminator element to improve climate models.

© 2021 Published by Elsevier B.V.

1. Introduction

For decades, it has been widely known the fact that air temperatures are increasing (on different spatial and time scales), as it has been proven by a number of different studies [1–3]. All of the last three decades have been characterized by being consecutively the warmest since 1850 [4], in terms of Earth's surface temperature. It is obvious that this temperature rise has a negative impact on life on Earth: changes in migration and number of many species; increase of the susceptibility of numerous ecosystems and human environments; great impacts to crops (wheat or maize among others), etc. All these complications have an added negative influence on global politics, society and demographics [5].

Due to all this, there is an increasing interest in the scientific community regarding climate variability. The main approaches consist in climate models and statistical analyses that investigate extreme episodes which are supposed to be

---

* Corresponding author.
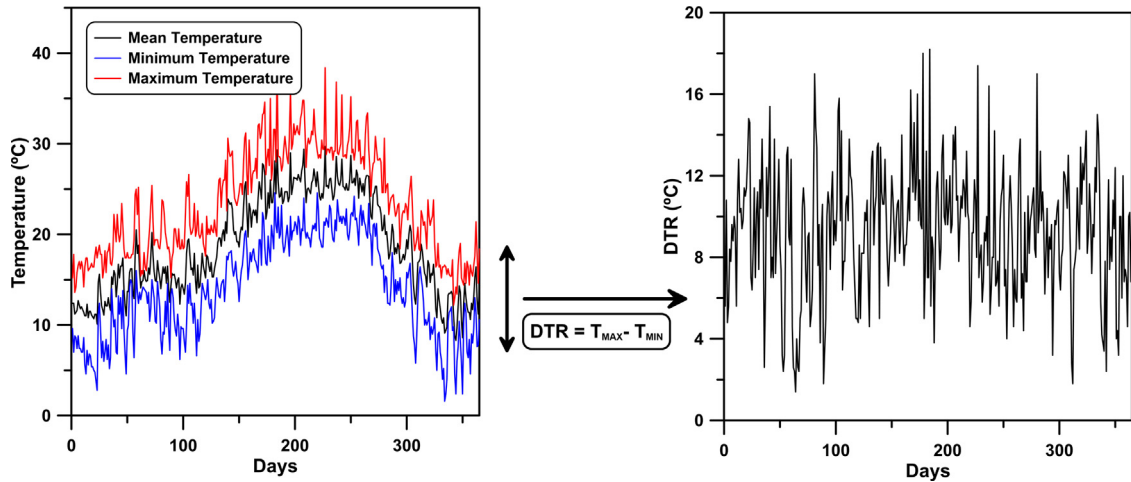 *E-mail address:* f12gogoj@uco.es (J. Gómez-Gómez).

Fig. 1. Example of temperature variables records for 1990 in Málaga station. Daily mean, minimum and maximum temperature are shown on the left part, while diurnal temperature range (*DTR*) is depicted on the right. This last variable was directly computed by subtracting minimum temperature values to the maximum temperature.

related to global warming. In these cases, the highest confidence levels are usually associated to unusually extreme cold and heat events [6]. Thus, the study of temperature variables time series is a widespread approach in the field [7–11].

In the case of Spain (which is where this work is focused), all findings seem to point to the fact that the main change in temperature during the twentieth century was recorded from the 1970s onward. This change was characterized by an abrupt and remarkable increase in temperatures. Nonetheless, this warming does not have a marked continuity nor regularity throughout the century. Neither it has been along the year, being winters typically when the strongest changes were identified. Also, several studies have shown that this change has been more pronounced for the maximum than for the minimum temperature in the Iberian Peninsula and in some subregions [12–15]. However, the opposite was found in other researches [16,17].

Classical statistical methods have been widely used traditionally in order to gain information from time series and to confirm climate models [18,19]. Furthermore, in the last decade, several advanced techniques have gain importance in the context of analysis of complexity and non-linearity of signal. Some of them are the so-called fractal and multifractal analysis [20–22]. Among these last ones, Multifractal Detrended Fluctuation Analysis (MF-DFA) [23] has become an extensively used technique for analyzing climatic time series [7,24–27]. This technique combines the Detrended Fluctuation Analysis (DFA) with the fractal theory, providing a reliable tool that yields information about complex and non-linear time series. DFA is used to determine fractal properties of non-stationary time series. However, it fails when it comes to characterizing series with more than one scaling exponent (multifractal), which is why MF-DFA has advantages over the first one.

The objective pursued in the presented work is to seek evidence of the influence of climate change in the multifractal properties of temperature time series in Spain. Furthermore, these multifractal properties will be analyzed to gain information on the nature and dynamics of the temperature time series. For such purpose, authors have selected four variables related to temperature (daily maximum, minimum and average temperature and the diurnal temperature range) at ten different locations across Spain and for two different time periods: 1960–1989 and 1990–2019. The employed technique for this analysis is the MF-DFA.

2. Materials and methods

2.1. Data

The studied data in this document correspond to four temperature time series of two periods of 30 years: 1960–1989 and 1990–2019. The data that support the findings of this study are openly available. They are provided by the Spanish Meteorological Agency ("Agencia Estatal de Meteorología") from the AEMET OpenData website at http://www.aemet.es/es/datos_abiertos/AEMET_OpenData. The four temperature variables are daily maximum (T_{max}), minimum (T_{min}) and mean temperature (T_{max}), and the diurnal temperature range (*DTR*), which is computed from the maximum and minimum temperatures (see Fig. 1). Raw data are recorded at 10 different meteorological stations located over the Iberian Peninsula, in Spain (Fig. 2). Half of stations belongs to coastal regions and the rest are mainland. Furthermore, they cover the Atlantic and the Mediterranean semiarid climates. Descriptive statistic shows a global increase of temperature variables, especially for mean temperature.

J. Gómez-Gómez, R. Carmona-Cabezas, A.B. Ariza-Villaverde et al.

Physica A 578 (2021) 126118

Fig. 2. Map of the studied meteorological stations localized in the Iberian Peninsula, Spain.

Before applying the MF-DFA, data must be preprocessed in order to remove the seasonality from time series. To this aim, average month values of temperature time series over all 30 years for each period have been computed. Next, these mean values are subtracted from the original signals to obtain the deseasonalized ones. To check that correlations due to seasonal effects are eliminated, authors have computed the autocorrelation functions of the original and the deseasonalized time series. In Fig. 3, an example of these functions is depicted. As it can be observed, the autocorrelation functions before this procedure is applied, give an almost sinusoidal behavior in the interval $[-1, +1]$ which soften when increasing scale. After month values are subtracted, these functions decay rapidly to zero.

2.2. Multifractal detrended fluctuation analysis

MF-DFA was a method proposed by Kantelhardt et al. [28] for multifractal analysis of nonstationary time series and it is based on detrended fluctuation analysis (DFA). The main advantage of these both approaches is that they can obtain the scaling behavior of the fluctuations in time series. Although the studied system is affected by artificial correlations derived from unknown underlining trends, these techniques allow to retrieve the intrinsic fluctuations of the system [29]. DFA was invented in order to deal with monofractal time series and the main concepts were extended by Kantelhardt et al. to multifractal signals. The five steps to implement the MF-DFA algorithm are the following [28]:

(1) Firstly, compute the integrated time series, also known as the "profile". Let x_k be a time series of length N and $\langle x \rangle$ the mean value. Then, the profile is defined as:

$$Y(i) \equiv \sum_{k=1}^{i} [x_k - \langle x \rangle], i = 1, \ldots, N \tag{1}$$

(2) Next, divide the profile $Y(i)$ into $N_s \equiv \text{int}(N/s)$ nonoverlapping segments of equal length s. The length N of the series is often not a multiple of the time scale s, thus, a short part at the end of the profile may remain. To hold this part, the same procedure is repeated from the end of the series to the beginning. Thereby, $2N_s$ segments are obtained for each time scale s.

(3) Compute the local trend for each segment ν by means of the least-squares fit of the series. The fitting polynomial $y_\nu(i)$ can be linear, quadratic, cubic, or higher order polynomial. Different order of the polynomial fit differs in the capability to eliminate trends in the series [30]. In mth order of MF-DFA, trends of order m in the profile (or, equivalently, of order $m - 1$ in the original series) are eliminated. Therefore, by subtracting $y_\nu(i)$ for each segment, one can compute the variance for each s value:

$$F^2(\nu, s) \equiv \frac{1}{s} \sum_{i=1}^{s} \{Y[(\nu - 1)s + i] - y_\nu(i)\}^2 \tag{2}$$
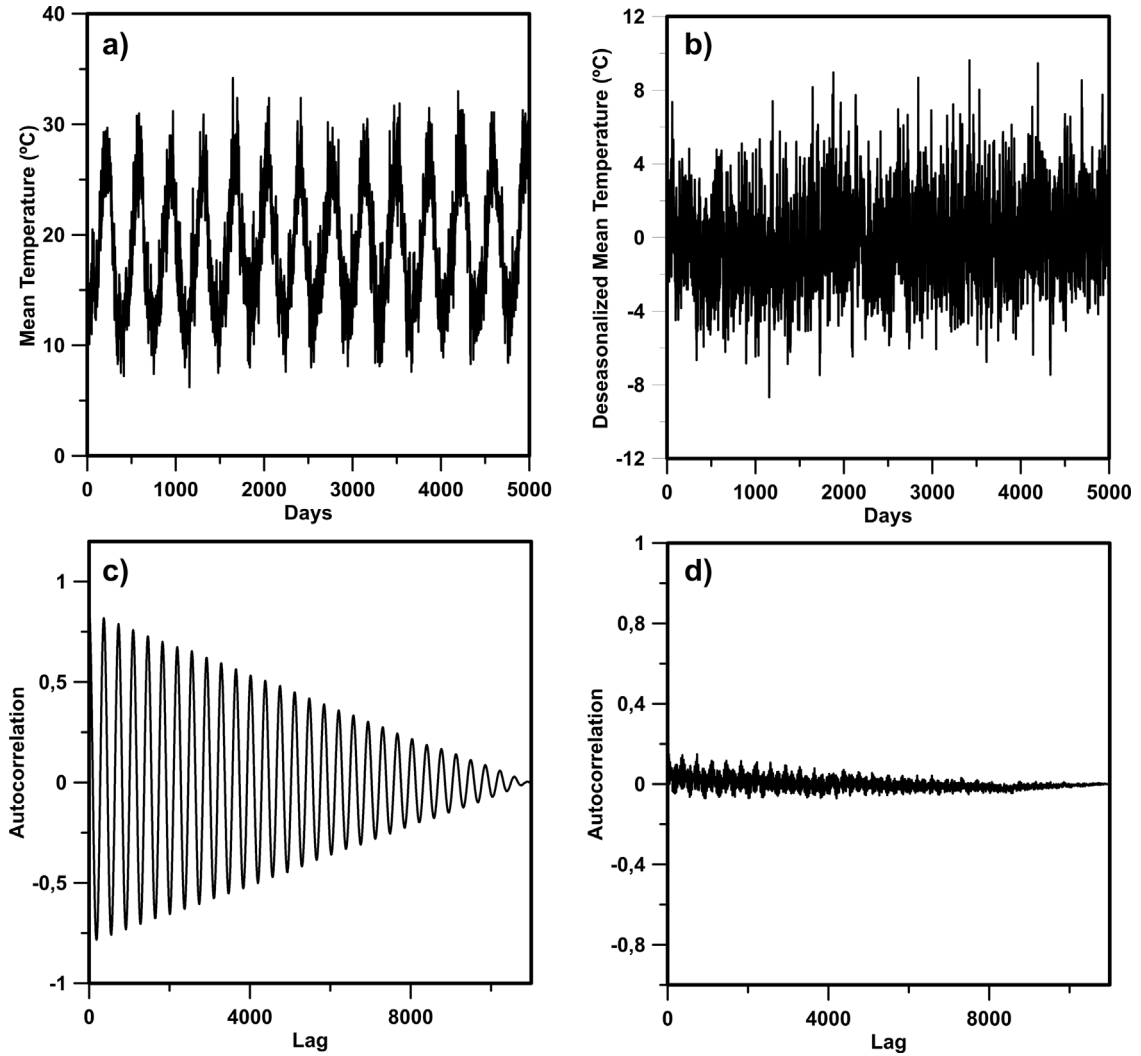
Fig. 3. Example of original (a) and deseasonalized (b) mean temperature time series for Málaga station in the period 1990–2019 and their corresponding autocorrelations functions (c and d, respectively). For clarity reasons, time series are plotted only for the first 5000 data (or days)

for each segment v, $v = 1, \ldots, N_s$ and

$$F^2 (v, s) \equiv \frac{1}{s} \sum_{i=1}^{s} \{Y [N - (v - N_s) s + i] - y_v (i)\}^2 \tag{3}$$

for each segment v, $v = N_s + 1, \ldots, 2N_s$.

(4) Average over all segments to obtain the qth order fluctuation function:

$$F_q (s) \equiv \left\{ \frac{1}{2N_s} \sum_{v=1}^{2N_s} \left[F^2 (v, s) \right]^{q/2} \right\}^{1/q} \tag{4}$$

where the index q can take any real value except zero, because of the diverging exponent. For $q = 0$, a logarithmic averaging procedure must be performed and the fluctuation function is computed as follows:

$$F_{q=0} (s) \equiv \exp \left\{ \frac{1}{4N_s} \sum_{v=1}^{2N_s} \ln \left[F^2 (v, s) \right] \right\} \tag{5}$$

For $q = 2$, the standard DFA method is obtained. To retrieve the scaling behavior of the generalized q dependent fluctuation functions, steps 2 to 4 must be repeated for different time scales s. $F_q (s)$ will increase with increasing s.

Besides, this fluctuation function depends on the m order of the polynomial fit and, by construction, is only defined for $s \geq m + 2$ [30].

(5) To determine the scaling behavior of the fluctuation functions, it is necessary to analyze the log–log plots of $F_q(s)$ vs s for each value of q. If the series x_k is long-range power-law correlated, then $F_q(s)$ increases for large values of s as a power law:

$$F_q(s) \sim s^{h(q)} \tag{6}$$

Hence, the scaling exponent $h(q)$ can be computed by obtaining the slopes of the log–log plots of $F_q(s)$ vs s for each q. For very large scales, $F_q(s)$ becomes statistically inaccurate for the averaging procedure, since the number of segments $2N_s$ becomes very small. Also, systematic deviations from the scaling behavior occur for very small scales ($s \approx 10$). Thus, a thorough analysis is needed in order to determine the best range for the least-squares fits.

In general, $h(q)$ can depend on q. For stationary time series, $h(2)$ is the well-known Hurst exponent H whereas, for non-stationary signals, the Hurst exponent is $H = h(2) - 1$ [31]. For this reason, $h(q)$ is called as generalized Hurst exponent. On the other hand, the Hurst exponent value (H) gives information about the correlation properties of the signals. For a white noise process (uncorrelated time series), $H = 0.5$. When $0 < H < 0.5$, the signal is long-range anti-correlated, meaning that a large value is more likely to be followed by a small value and vice versa. Finally, when $H > 0.5$, time series is long-range correlated and large values are more likely to be followed by other large values and vice versa [29].

For monofractal time series, $h(q)$ is independent of q and Eq. (4) gives an identical scaling behavior for all values of q. Only if small and large fluctuations scales differently, $h(q)$ will depend significantly on q. Segments with large variance $F^2(v, s)$ or large deviations from the fit will dominate the average value $F_q(s)$ for $q > 0$. On the contrary, segments with small variance $F^2(v, s)$ will dominate $F_q(s)$ for $q < 0$. Therefore, $h(q)$ describes the scaling behavior of the segments with large fluctuations (when $q > 0$) and the scaling behavior of the segments with small fluctuations (when $q < 0$).

2.3. Relation to standard multifractal analysis

In order to relate MF-DFA method to the standard multifractal analysis based on the box counting formalism, Kantelhardt et al. also demonstrated that the scaling exponent $h(q)$ is related to the scaling exponent $\tau(q)$, which is defined by the partition function of the multifractal formalism [28]. This relationship is established by the expression:

$$\tau(q) = qh(q) - 1 \tag{7}$$

Another way to characterize a multifractal series in the standard formalism is by means of the so-called multifractal spectrum or singularity spectrum $f(\alpha)$, which can be computed from $\tau(q)$ via the Legendre transform:

$$\alpha = \frac{d\tau(q)}{dq} \text{ and } f(\alpha) = q\alpha - \tau(q) \tag{8}$$

where α is the singularity strength or Hölder exponent and the shape of $f(\alpha)$ is usually a concave-down parabola with a maximum value which correspond to the most dominant scaling behavior [25]. The corresponding value of the singularity strength at this maximum is often denoted by α_0 and the width of the multifractal spectrum (i.e., $W = \alpha_{max} - \alpha_{min}$) gives information about the degree of the multifractality of the signal [32]. When the time series is monofractal, the width of the spectrum will be close to zero.

If the curve is fitted by a second order polynomial, it can be obtained an asymmetry parameter B to discern between right-skewed or left-skewed distributions. Hence, the multifractal spectrum can be parametrized by:

$$f(\alpha) = A(\alpha - \alpha_0)^2 + B(\alpha - \alpha_0) + C \tag{9}$$

When $B = 0$, the spectrum is symmetrical, whereas for $B > 0$ is left-skewed and for negative values is right-skewed [33,34]. A right-skewed spectrum is related to relatively strongly weighted high fractal exponents. Its broadness is mainly due to small fluctuations ($q < 0$) and the time series is more regular (with "fine-structure") [35,36]. On the contrary, a left-skewed spectrum indicates a relatively strongly weighted low fractal exponents associated to large fluctuations ($q > 0$) and a more singular signal. Thus, it shows a richer multifractal structure in the arrangement of the large fluctuations.

3. Results and discussion

3.1. Generalized Hurst exponents

To calculate the generalized Hurst exponent $h(q)$ of temperature variables, fluctuation functions $F_q(s)$ with a range of q values from -5 to 5 with step 0.5 has been chosen. The interval selected for the scale values s is from 5 to 2000 days with step of 5 days. In Fig. 4, values of $\log[F_q(s)]$ vs $\log(s)$ is shown for Málaga in the period 1990–2019 as an example. It is observed that fluctuation functions increase with scale. As it can also be appreciated, curves can be fitted
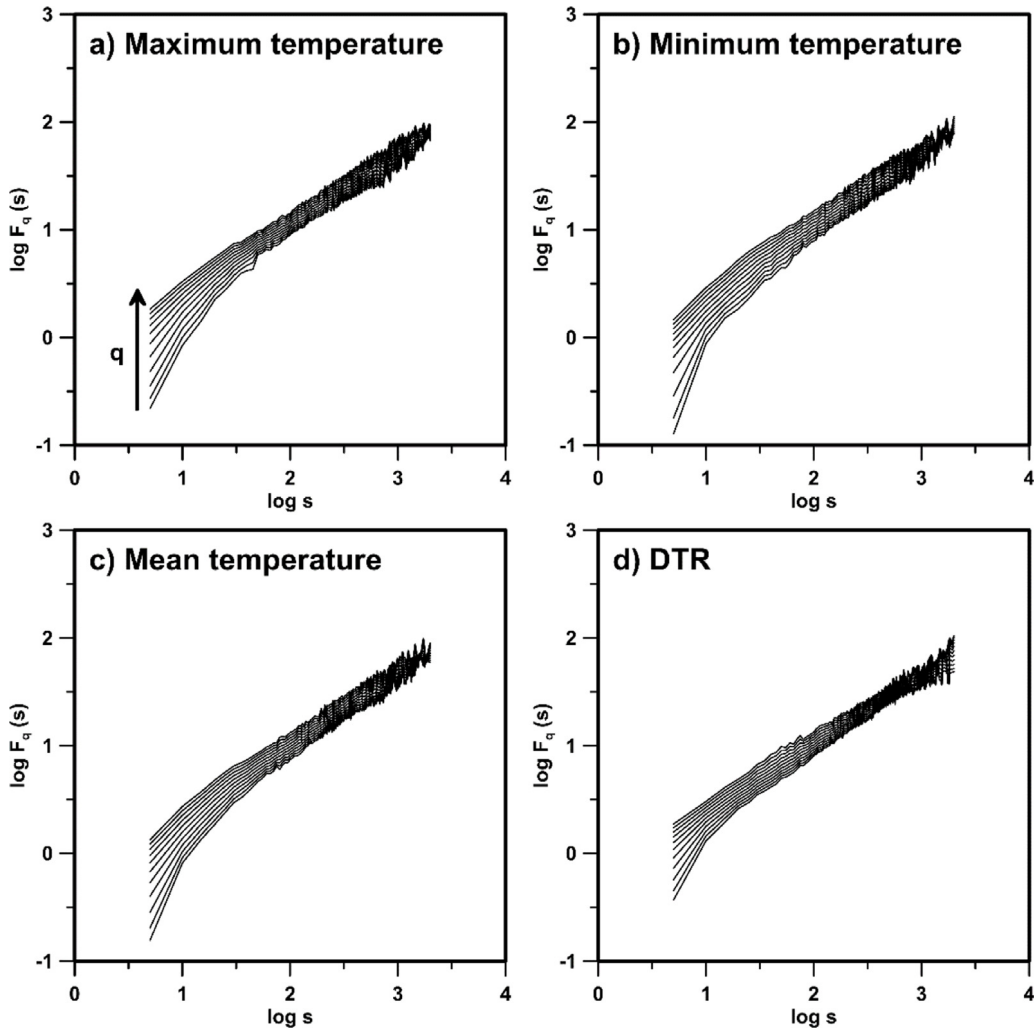
Fig. 4. Fluctuation functions vs scale values of segments for Málaga station in the period 1990–2019. Each curve corresponds to one *q* value. To make clearer charts, only half of the analyzed curves are depicted.

by a linear regression to obtain the sought generalized Hurst exponent $h(q)$. The optimal range to compute the linear fit is approximately between 18 and 355 days (almost one year). Nonetheless, in some cases it is necessary to shorten this range (down to 126 days) to avoid artifacts that worsen the analysis.

The generalized Hurst exponent for every location and period of time has been retrieved from their respective least squares regressions and results are plotted in Fig. 5 for the five coastal locations and in Fig. 6 for the mainland ones.

On the one hand, looking at the five coastal stations, it can be observed that, in general, the scaling exponent is a decreasing function of q. One can define a quantity $\Delta h(q) = h_{max} - h_{min}$, being h_{max} the maximum value of the generalized Hurst exponent in the interval and h_{min} the minimum. The value of $\Delta h(q)$ gives information about the multifractality degree of the signal. Meaning that a greater multifractality degree is related to more violent temperature fluctuations [37]. $\Delta h(q)$ is higher for mean and minimum temperature variables. This fact indicates a more multifractal behavior from these signals which derives from more complex systems [23].

Furthermore, the only case where $\Delta h(q)$ is almost zero occurs for *DTR* in Málaga station in the years 1960–1989 (Fig. 5g). This is a characteristic behavior of monofractal time series. Apparently, for the next 30 years, the *DTR* evolves slightly to a more multifractal signal in this case, as shown in Fig. 5h. However, this will be clearer when multifractal spectra are discussed further in the text.

On the other hand, the mainland stations in Fig. 6 present a similar behavior such as the decreasing trend. Here, negligible differences in $\Delta h(q)$ are shown, contrary to the coastal locations where minimum and mean temperature had a more pronounced value of $\Delta h(q)$. Physically speaking, the major degree of multifractality for mean and minimum temperature in the coastal stations might be related to the oceanic influence. Looking at Zaragoza, a monofractal nature
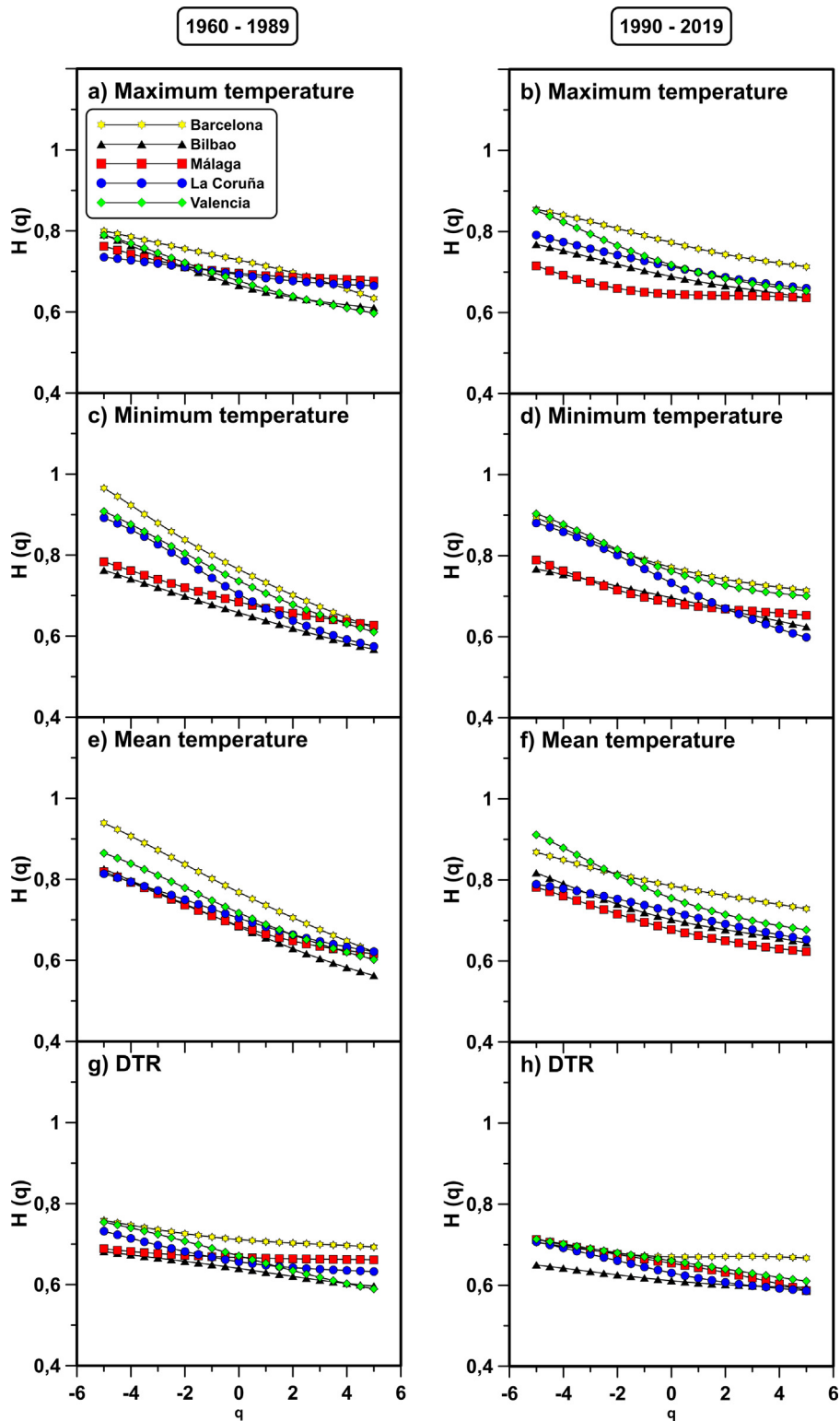
J. Gómez-Gómez, R. Carmona-Cabezas, A.B. Ariza-Villaverde et al.

Physica A 578 (2021) 126118

Fig. 5. Generalized Hurst exponents for T_{max} (a and b), T_{min} (c and d), T_{mean} (e and f) and *DTR* (g and h) in the five coastal stations (Barcelona, Bilbao, Málaga, La Coruña and Valencia). Charts on the left side are from the years 1960–1989 (a, c, e and g), while the ones on the right side correspond to the years 1990–2019.

Fig. 6. Generalized Hurst exponents for T_{max} (a and b), T_{min} (c and d), T_{mean} (e and f) and DTR (g and h) in the five mainland stations (Burgos, Sevilla, Zaragoza, Badajoz and Albacete). Charts on the left side are from the years 1960–1989 (a, c, e and g), while the ones on the right side correspond to the years 1990–2019.
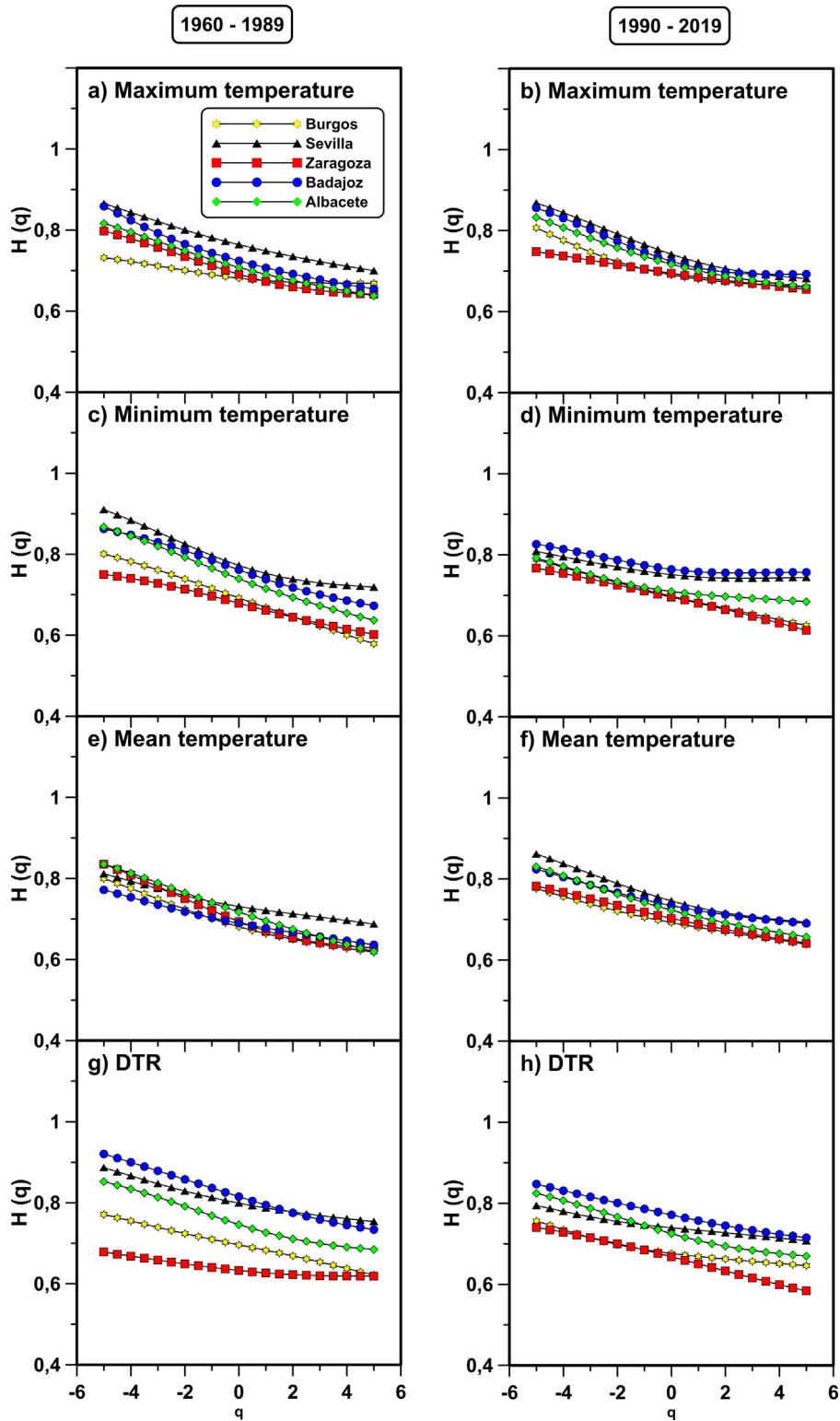
is identified as well in this case for DTR in the 1960–1989 period. This tendency changes for the next period, exhibiting a higher multifractal degree (same phenomenon happened with Málaga, as discussed before).

Overall, the Hurst exponent H value can be calculated from these curves for $q = 2$. Because all these times series have a value of $h(2) < 1$, they are demonstrated to be stationary signals and the Hurst exponent is exactly this value [38]. All values of this parameter are in the range $[0.601, 0.777]$. As $H > 0.5$ for all the cases, time series are long-range correlated, meaning that a relative high value of signals are likely to be followed by other high value and vice versa [25]. Regarding the $\Delta h(q)$, it must be point out the fact that for the studied series, their values belong to the interval $[0.027, 0.187]$. This shows that there is a high variability of the multifractal degree among the different series: from almost monofractal (as seen with Málaga and Zaragoza) to clearly multifractal ones.

3.2. Multifractal spectra

Multifractal spectra are obtained by means of the computed scaling exponent $\tau(q)$, which is yielded from the relation between this quantity and the generalized Hurst exponent (see Eq. (7)). Hölder exponents α and $f(\alpha)$ are finally retrieved from the Legendre transform of this scaling exponent. In Figs. 7 and 8, it can be seen the multifractal spectra for every city, period and temperature variable used in this analysis in the same order as Figs. 5 and 6. Next, the coastal stations will be discussed.

Looking at the maximum temperature variable in Fig. 7a and b, it can be observed that some differences are present between both periods. For all stations except for Málaga, the position of the maxima α_0, which denotes the dominant singularity strength, is slightly shifted to the right from years 1960–1989 to 1990–2019. On the contrary, Málaga spectrum is shifted to the left, meaning that Málaga changes to more correlated signal and more regular structure in the last 30 years. Meanwhile, the other four do the opposite, becoming more complex signals [24]. When it comes to the width ($W = \alpha_{max} - \alpha_{min}$), La Coruña is the coastal station that changes the most between both periods, increasing the degree of multifractality (see Table 1). Barcelona and Valencia spectra have a rather shorter left tail for the last period in contrast to the first one, denoting that, in the last 30 years, there is more homogeneity in the large fluctuations for this series.

Minimum temperature signals (Fig. 7c and d) show that in this case the peaks of the spectra (α_0) experience a shift to the right in the second time period (the series become less correlated, as explained before). The width of the spectra is in this case reduced for every case, pointing to a reduction of the multifractality of the minimum temperature time series over the years. Again, it is possible to see that the left tail corresponding to Barcelona and Valencia is shorter for 1990–2019, as happened with the maximum temperature.

For mean temperature (Fig. 7e and f), again α_0 slightly moves to the right and the widths of the spectra are shortened for every location from years 1960–1989 to 1990–2019. Furthermore, the most highlighted stations that present a reduced left tail between both periods are Barcelona and Valencia again, being coherent with the previous results.

DTR results (Fig. 7g and h) also depict slight shifts in the value of α_0. The difference in this case is that these changes are now towards the left direction of the x-axis. Now the changes in the value of W are not as consistent as in the previous variables. Multifractal degree of La Coruña and Málaga are increased, while the others decrease. The last mentioned station (Málaga) stands out by having a much larger left tail for the last years.

In general, multifractal spectra for minimum and mean temperature are wider than in the other variables, meaning that the degree of multifractality of these variables is larger and that these time series have more complex behavior. This fact is coherent with the outcomes obtained from the generalized Hurst exponent. On the other hand, the asymmetry parameter B, which is shown in Table 2, indicates change in the sign of symmetry for several stations and variables. La Coruña and Valencia do not change the sign of B. Barcelona alters its symmetry for T_{max} from negative to positive, which denotes that spectrum changes from right to left-skewed and becomes more singular in the last period, as discussed in Section 2.2. Bilbao modify its symmetry from positive to negative in T_{min}, i.e., it becomes smoother or less singular for the last years. On the contrary, it is altered from negative to positive in spectra for DTR (see Table 2). Lastly, Málaga changes from positive to negative in T_{max} and DTR.

Once the discussion of the results for the coastal stations has been done, the equivalent for the mainland ones is described, which can be seen in Fig. 8. Focusing on the maximum temperature (Fig. 8a and b), it seems that there is no common behavior when it comes to the shift of α_0 for the five stations. Regarding the shape and the width of the spectra, it must be pointed out that most of them are very similar, especially for the second period, except for Zaragoza.

Moving to the minimum temperature spectra (Fig. 8c and d), the α_0 positions shifts vary from one city to another. While for Sevilla and Albacete they become more correlated (move to the left), the rest do the opposite. The width of the spectra decreases this time for all of them, except for Zaragoza, that remains almost the same. It can be clearly seen in the corresponding figure.

For mean temperature, in every mainland station it can be observed how spectra are shifted to the right (see Fig. 8e and f), meaning that signals become more complex. By looking at the width, it decreases in all locations except for Sevilla. Again, the shape of spectra is very alike, more notably for the last 30 years.

Lastly, DTR charts (Fig. 8g and h) depict shifted spectra to the left in every case except for Zaragoza. For the width, almost all the locations show a decrease of the degree of multifractality. Again, Zaragoza has a different behavior, increasing the width instead of decreasing. Indeed, the spectrum changes from almost monofractal in the years 1960–1989 to multifractal in the last period. This agrees with the results of the generalized Hurst exponent.

Table 1
Multifractal spectra width W of daily maximum (T_{max}), minimum (T_{min}), mean temperature (T_{mean}) and diurnal temperature range (DTR) for the periods 1960–1989 and 1990–2019 in every station.

Station	T_{max}		T_{min}		T_{mean}		DTR	
	1960–1989	1990–2019	1960–1989	1990–2019	1960–1989	1990–2019	1960–1989	1990–2019
Barcelona	0,336	0,243	0,638	0,336	0,577	0,273	0,137	0,099
Bilbao	0,332	0,247	0,362	0,266	0,475	0,348	0,147	0,098
Málaga	0,188	0,198	0,296	0,283	0,355	0,283	0,063	0,261
La Coruña	0,116	0,239	0,514	0,466	0,330	0,235	0,192	0,215
Valencia	0,340	0,351	0,524	0,340	0,454	0,419	0,286	0,197
Burgos	0,110	0,295	0,401	0,313	0,331	0,271	0,294	0,229
Sevilla	0,311	0,318	0,323	0,130	0,244	0,299	0,254	0,184
Zaragoza	0,255	0,172	0,248	0,291	0,343	0,253	0,109	0,277
Badajoz	0,405	0,282	0,308	0,126	0,260	0,249	0,325	0,241
Albacete	0,324	0,318	0,403	0,221	0,393	0,321	0,271	0,259

Table 2
Asymmetry parameter B of multifractal spectra of daily maximum (T_{max}), minimum (T_{min}), mean temperature (T_{mean}) and diurnal temperature range (DTR) for the periods 1960–1989 and 1990–2019 in every station.

Station	T_{max}		T_{min}		T_{mean}		DTR	
	1960–1989	1990–2019	1960–1989	1990–2019	1960–1989	1990–2019	1960–1989	1990–2019
Barcelona	−0,408	0,457	0,447	0,487	0,367	0,480	0,561	0,520
Bilbao	0,495	0,560	0,345	−0,264	0,354	0,627	−0,364	0,407
Málaga	0,294	−0,218	0,516	0,425	0,472	0,493	0,004	−0,336
La Coruña	0,432	0,413	0,487	0,361	0,418	0,284	0,345	0,498
Valencia	0,489	0,486	0,451	0,440	0,425	0,492	−0,269	−0,211
Burgos	0,221	0,085	0,248	0,411	0,541	0,519	0,233	0,421
Sevilla	0,508	0,455	0,377	−0,147	0,620	0,452	0,516	0,518
Zaragoza	0,399	0,488	0,269	−0,329	0,385	0,448	0,232	−0,355
Badajoz	0,452	0,554	0,382	0,055	0,516	0,525	0,381	0,412
Albacete	0,519	0,488	0,432	0,414	0,399	0,521	0,447	0,492

Overall, it cannot be said that the minimum and mean temperature spectra are wider, as happened to the coastal stations. Hence, the multifractal degree in this case is relatively similar for all the variables. In this case, the asymmetry parameter B (see Table 2) maintains its sign for every city and variables, except for Sevilla (T_{max}) and Zaragoza (T_{min} and DTR). In these cases, the sign always changes from positive to negative, which means, as explained before, that the spectra change from left to right-skewed. Therefore, the signals become more regular in the last period.

4. Conclusions

The analyzed air surface temperature variables show all distinct scaling exponents when looking at the fluctuation functions ($F_q(s)$) versus scales (s) at different q moments. This fact demonstrates the intrinsic multifractal nature of signals. It can be concluded that all the series are stationary and long-range correlated. A way to understand the long-range correlation is that an increase in temperature would be more likely followed by another increase and vice versa.

The main multifractal features of the four temperature signals vary between years 1960–1989 and 1990–2019, to a greater or lesser extent. This result might be interpreted as a possible relation between the climatic change and the fractal properties. However, in most cases, the symmetry of multifractal spectra remains almost the same between both periods and changes that we found lacked any consistency.

Regarding the coastal locations, a higher degree of multifractality is mostly present in both periods in T_{min} and T_{mean}, since they show wider spectra than T_{max} and DTR. This result is a discriminator element between coastal and mainland stations in both periods because the last ones do not show this pattern. Thus, authors conclude that ocean might have an impact on the higher complexity of minimum and mean temperature time series on these locations.

Nevertheless, a more relevant result obtained from T_{min} and T_{mean} is a spectral narrowing on the vast majority of mainland and coastal stations over time. This means that the complexity of the temperature series decreases. However, authors believe that changes in complexity for the mean might be derived from minimum temperature values. Since this effect is not consistent with the maximum temperature, there is an asymmetry in the temperature behavior. Brunet et al. already found an asymmetric behavior between maxima and minima only in mainland stations over the Iberian Peninsula in their statistical study between 1850 and 2003 [15]. In that study, maximum temperature increased at greater rates than minimum temperature. On the contrary, other investigations made by Esteban-Parra et al. in 2003 [16] or Staudt et al. in 2004 [17] obtained the opposite behavior (higher rates of change for minima than for maxima). According to this, the climatic change experienced in this region might be linked to different behaviors in maxima and minima. A relation between this asymmetry found in the Iberian Peninsula and the different multifractality shown by their singularity spectra could exist.
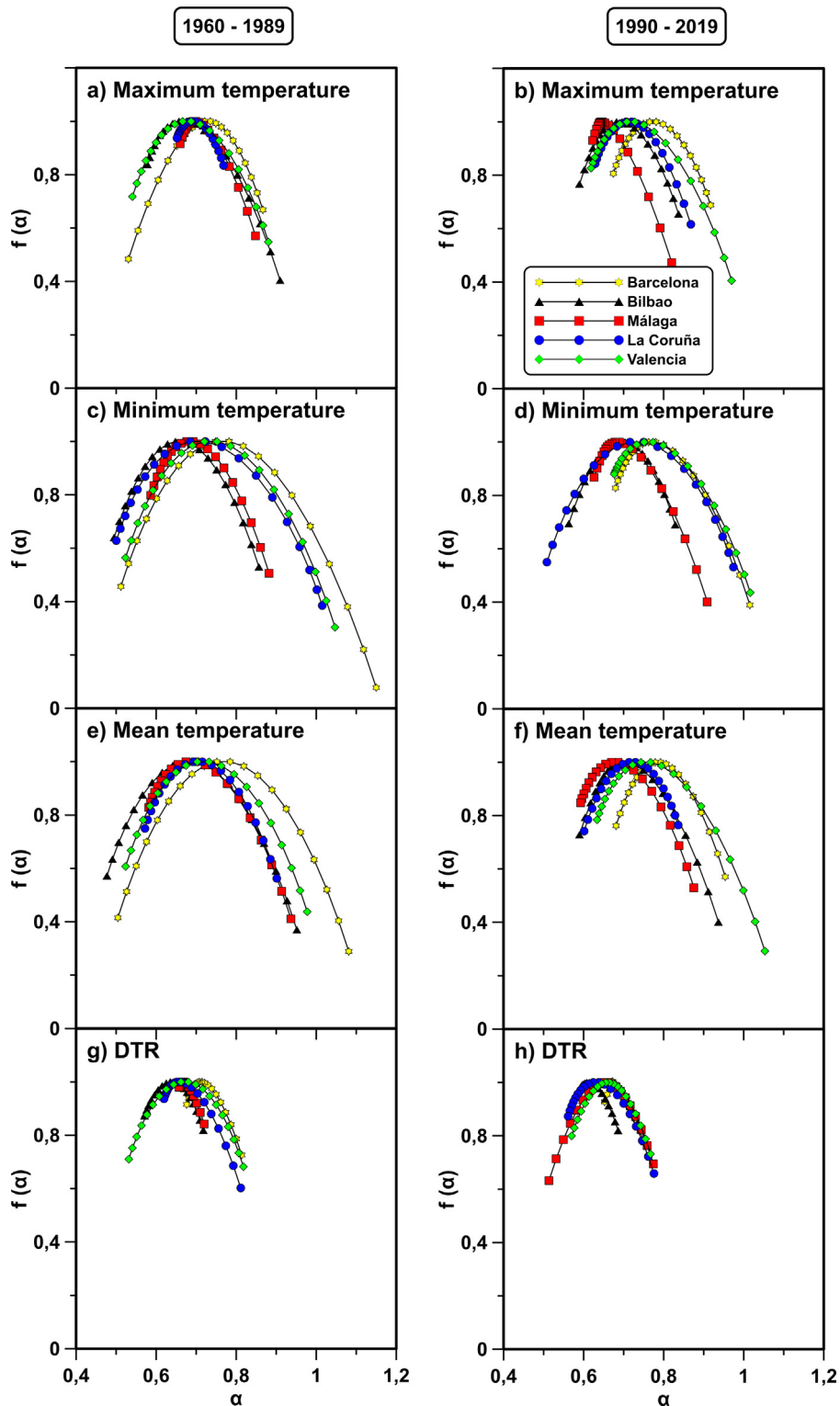
J. Gómez-Gómez, R. Carmona-Cabezas, A.B. Ariza-Villaverde et al.

Physica A 578 (2021) 126118

Fig. 7. Multifractal spectrum of T_{max} (a and b), T_{min} (c and d), T_{mean} (e and f) and *DTR* (g and h) for every coastal station (Barcelona, Bilbao, Málaga, La Coruña and Valencia). Charts on the left side are from the years 1960–1989 (a, c, e and g), while the ones on the right side correspond to the years 1990–2019.
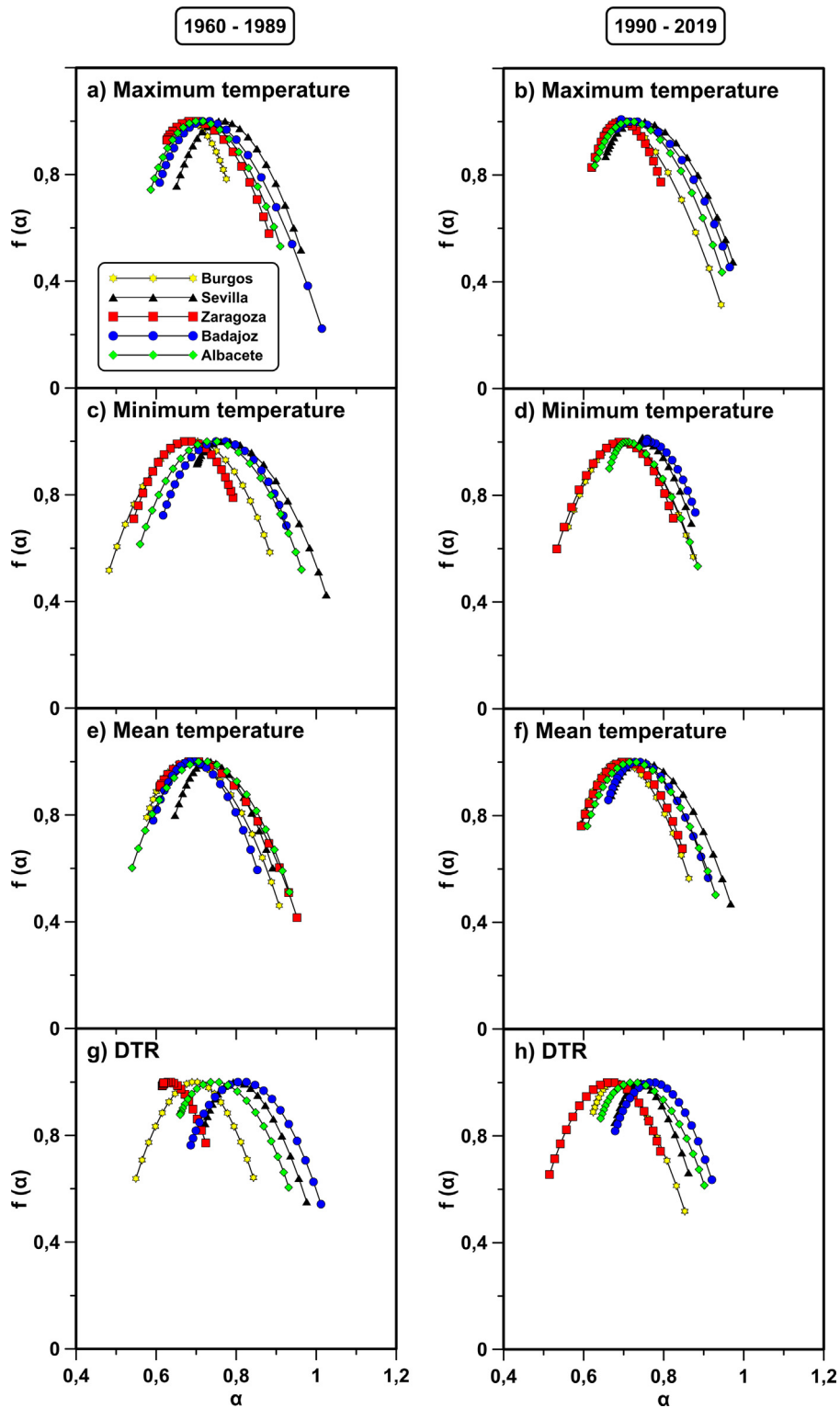
Fig. 8. Multifractal spectrum of T_{max} (a and b), T_{min} (c and d), T_{mean} (e and f) and DTR (g and h) for every mainland station (Burgos, Sevilla, Zaragoza, Badajoz and Albacete). Charts on the left side are from the years 1960–1989 (a, c, e and g), while the ones on the right side correspond to the years 1990–2019.

The conclusions drawn from these results can help testing models related to the climate change. One important point extracted from this analysis is that multifractal properties are not conserved over time for temperature time series. Hence, to improve future simulations, studies involving greater periods of time should be done. By doing so, a better understanding of how these parameters evolve with time could be achieved. Additionally, it must be pointed out the importance of seeking relations among the multifractal features and the atmospheric processes involved. A search of the applicability of these outcomes for assessing different climate models will be the aim of future works.

CRediT authorship contribution statement

Javier Gómez-Gómez: Conceptualization, Methodology, Software, Validation, Formal analysis, Data curation, Investigation, Writing - original draft. **Rafael Carmona-Cabezas:** Conceptualization, Software, Investigation, Resources. **Ana B. Ariza-Villaverde:** Conceptualization, Resources, Supervision. **Eduardo Gutiérrez de Ravé:** Project administration, Funding acquisition, Supervision. **Francisco José Jiménez-Hornero:** Project administration, Funding acquisition, Supervision.

Declaration of competing interest

The authors declare that they have no known competing financial interests or personal relationships that could have appeared to influence the work reported in this paper.

Acknowledgments

References

[1] B. Horton, Geographical distribution of changes in maximum and minimum temperatures, Atmos. Res. 37 (1995) 101–117, http://dx.doi.org/10.1016/0169-8095(94)00083-P.
[2] P.D. Jones, M. New, D.E. Parker, S. Martin, I.G. Rigor, Surface air temperature and its changes over the past 150 years, Rev. Geophys. 37 (1999) 173–199, http://dx.doi.org/10.1029/1999RG900002.
[3] P.D. Jones, A. Moberg, Hemispheric and large-scale surface air temperature variations: An extensive revision and an update to 2001, J. Clim. 16 (2003) 206–223.
[4] T.F. Stocker, D. Qin, G.-K. Plattner, M. Tignor, S.K. Allen, J. Boschung, A. Nauels, Y. Xia, V. Bex, P.M. Midgley, Summary for policymakers WG I, in: Climate Change 2013: The Physical Science Basis. Contribution of Working Group I to the Fifth Assessment Report of the Intergovernmental Panel on Climate Change, Cambridge University Press, Cambridge, United Kingdom and New York, NY, USA, 2013, https://www.ipcc.ch/pdf/assessment-report/ar5/wg1/WG1AR5_SPM_FINAL.pdf.
[5] C.B. Field, V.R. Barros, D.J. Dokken, K.J. Mach, M.D. Mastrandrea, T.E. Bilir, M. Chatterjee, K.L. Ebi, Y.O. Estrada, R.C. Genova, B. Girma, E.S. Kissel, A.N. Levy, S. MacCracken, P.R. Mastrandea, L.L. White, Summary for policymakers WG II, in: Climate Change 2014: Impacts, Adaptation, and Vulnerability. Part A: Global and Sectoral Aspects. Contribution of Working Group II to the Fifth Assessment Report of the Intergovernmental Panel on Climate Change, Cambridge University Press, Cambridge, United Kingdom and New York, NY, USA, 2014, pp. 1–32, https://www.ipcc.ch/pdf/assessment-report/ar5/wg2/ar5_wgII_spm_en.pdf.
[6] D.L. Swain, D. Singh, D. Touma, N.S. Diffenbaugh, Attributing extreme events to climate change: A new frontier in a warming world, One Earth 2 (2020) 522–527, http://dx.doi.org/10.1016/j.oneear.2020.05.011.
[7] A. Burgueño, X. Lana, C. Serra, M.D. Martínez, Daily extreme temperature multifractals in Catalonia (NE Spain), Phys. Lett. A 378 (2014) 874–885, http://dx.doi.org/10.1016/j.physleta.2014.01.033.
[8] J.J. Gómez-Navarro, J.P. Montávez, P. Jimenez-Guerrero, S. Jerez, J.A. García-Valero, J.F. González-Rouco, Warming patterns in regional climate change projections over the Iberian Peninsula, Meteorol. Z. 19 (2010) 275–285, http://dx.doi.org/10.1127/0941-2948/2010/0351.
[9] Y. Latif, M. Yaoming, M. Yaseen, S. Muhammad, M.A. Wazir, Spatial analysis of temperature time series over the Upper Indus Basin (UIB) Pakistan, Theor. Appl. Climatol. 139 (2020) 741–758, http://dx.doi.org/10.1007/s00704-019-02993-8.
[10] V. Ongoma, M.A. Rahman, B. Ayugi, F. Nisha, S. Galvin, Z.W. Shilenje, B.A. Ogwang, Variability of diurnal temperature range over Pacific island countries, a case study of Fiji, Meteorol. Atmos. Phys. (2020) http://dx.doi.org/10.1007/s00703-020-00743-4.
[11] Y. Zhuang, J. Zhang, Diurnal asymmetry in future temperature changes over the main Belt and Road regions, Ecosyst. Health Sustain. 6 (2020) 1749530, http://dx.doi.org/10.1080/20964129.2020.1749530.
[12] M. Brunet, P.D. Jones, J. Sigró, O. Saladié, E. Aguilar, A. Moberg, P.M. Della-Marta, D. Lister, A. Walther, D. López, Temporal and spatial temperature variability and change over Spain during 1850–2005, J. Geophys. Res. 112 (2007) D12117, http://dx.doi.org/10.1029/2006JD008249.
[13] E. Galán, R. Cañada, F. Fernández, B. Cervera, Annual temperature evolution in the southern plateau of Spain from the construction of regional climatic time series, in: M.B. India, D.L. Bonillo (Eds.), Detecting and Modelling Regional Climate Change, Springer Berlin Heidelberg, Berlin, Heidelberg, 2001, pp. 119–131, http://dx.doi.org/10.1007/978-3-662-04313-4_11.
[14] J. Abaurrea, J. Asín, O. Erdozain, E. Fernández, Climate variability analysis of temperature series in the medium Ebro river basin, in: M.B. India, D.L. Bonillo (Eds.), Detecting and Modelling Regional Climate Change, Springer Berlin Heidelberg, Berlin, Heidelberg, 2001, pp. 109–118, http://dx.doi.org/10.1007/978-3-662-04313-4_10.
[15] M. Brunet, O. Saladié, P. Jones, J. Sigró, E. Aguilar, A. Moberg, D. Lister, A. Walther, D. Lopez, C. Almarza, The development of a new dataset of Spanish daily adjusted temperature series (SDATS) (1850–2003), Int. J. Climatol. 26 (2006) 1777–1802, http://dx.doi.org/10.1002/joc.1338.
[16] M.J. Esteban-Parra, D. Pozo-Vázquez, F.S. Rodrigo, Y. Castro-Díez, Temperature and precipitation variability and trends in northern Spain in the context of the Iberian Peninsula climate, in: H.-J. Bolle (Ed.), Mediterranean Climate, Springer Berlin Heidelberg, Berlin, Heidelberg, 2003, pp. 259–276.
[17] M. Staudt, Detección de cambios térmicos en la Península Ibérica con datos homogéneos regionales (Ph.D.), Univ. of Granada, 2004.

[18] M.G. Bosilovich, J. Chen, F.R. Robertson, R.F. Adler, Evaluation of global precipitation in reanalyses, J. Appl. Meteorol. Climatol. 47 (2008) 2279–2299, http://dx.doi.org/10.1175/2008JAMC1921.1.

[19] R.K. Jaiswal, A.K. Lohani, H.L. Tiwari, Statistical analysis for change detection and trend assessment in climatological parameters, Environ. Process. 2 (2015) 729–749, http://dx.doi.org/10.1007/s40710-015-0105-3.

[20] B. Sivakumar, Fractal analysis of rainfall observed in two different climatic regions, Hydrol. Sci. J. 45 (2000) 727–738, http://dx.doi.org/10.1080/02626660009492373.

[21] H. He, Multifractal analysis of interactive patterns between meteorological factors and pollutants in urban and rural areas, Atmos. Environ. 149 (2017) 47–54, http://dx.doi.org/10.1016/j.atmosenv.2016.11.004.

[22] A.B. Ariza-Villaverde, P. Pavón-Domínguez, R. Carmona-Cabezas, E.G. de Ravé, F.J. Jiménez-Hornero, Joint multifractal analysis of air temperature, relative humidity and reference evapotranspiration in the middle zone of the Guadalquivir river valley, Agricult. Forest Meteorol. 278 (2019) 107657, http://dx.doi.org/10.1016/j.agrformet.2019.107657.

[23] J.W. Kantelhardt, Fractal and multifractal time series, in: R.A. Meyers (Ed.), Mathematics of Complexity and Dynamical Systems, Springer New York, New York, NY, 2011, pp. 463–487, http://dx.doi.org/10.1007/978-1-4614-1806-1_30.

[24] J. Krzyszczak, P. Baranowski, M. Zubik, V. Kazandjiev, V. Georgieva, C. Sławiński, K. Siwek, J. Kozyra, A. Nieróbca, Multifractal characterization and comparison of meteorological time series from two climatic zones, Theor. Appl. Climatol. 137 (2019) 1811–1824, http://dx.doi.org/10.1007/s00704-018-2705-0.

[25] N. Kalamaras, C. Tzanis, D. Deligiorgi, K. Philippopoulos, I. Koutsogiannis, Distribution of air temperature multifractal characteristics over Greece, Atmosphere 10 (2019) 45, http://dx.doi.org/10.3390/atmos10020045.

[26] H.S. da Silva, J.R.S. Silva, T. Stosic, Multifractal analysis of air temperature in Brazil, Physica A 549 (2020) 124333, http://dx.doi.org/10.1016/j.physa.2020.124333.

[27] P. Mali, Multifractal characterization of global temperature anomalies, Theor. Appl. Climatol. 121 (2015) 641–648, http://dx.doi.org/10.1007/s00704-014-1268-y.

[28] J.W. Kantelhardt, S.A. Zschiegner, E. Koscielny-Bunde, S. Havlin, A. Bunde, H.E. Stanley, Multifractal detrended fluctuation analysis of nonstationary time series, Physica A (2002) 28.

[29] L. Telesca, G. Colangelo, V. Lapenna, M. Macchiato, Fluctuation dynamics in geoelectrical data: an investigation by using multifractal detrended fluctuation analysis, Phys. Lett. A 332 (2004) 398–404, http://dx.doi.org/10.1016/j.physleta.2004.10.011.

[30] P. Oświęcimka, S. Drozdz, J. Kwapień, A.Z. Górski, Effect of detrending on multifractal characteristics, Acta Phys. Pol. A. 123 (2013) 597–603, http://dx.doi.org/10.12693/APhysPolA.123.597.

[31] Q. Zhang, C.-Y. Xu, Y.D. Chen, Z. Yu, Multifractal detrended fluctuation analysis of streamflow series of the Yangtze River basin, China, Hydrol. Process. 22 (2008) 4997–5003, http://dx.doi.org/10.1002/hyp.7119.

[32] A.B. Ariza-Villaverde, F.J. Jiménez-Hornero, E. Gutiérrez de Ravé, Multifractal analysis applied to the study of the accuracy of DEM-based stream derivation, Geomorphology 197 (2013) 85–95, http://dx.doi.org/10.1016/j.geomorph.2013.04.040.

[33] Y. Shimizu, S. Thurner, K. Ehrenberger, Multifractal spectra as a measure of complexity in human posture, Fractals 10 (2002) 103–116, http://dx.doi.org/10.1142/S0218348X02001130.

[34] L. Telesca, V. Lapenna, Measuring multifractality in seismic sequences, Tectonophysics 423 (2006) 115–123, http://dx.doi.org/10.1016/j.tecto.2006.03.023.

[35] S. Drozdz, R. Kowalski, P. Oświęcimka, R. Rak, R. Gębarowski, Dynamical variety of shapes in financial multifractality, Complexity 2018 (2018) 1–13, http://dx.doi.org/10.1155/2018/7015721.

[36] S. Drozdz, P. Oświęcimka, Detecting and interpreting distortions in hierarchical organization of complex time series, Phys. Rev. E 91 (2015) 030902, http://dx.doi.org/10.1103/PhysRevE.91.030902.

[37] H. Feng, Y. Xu, Multifractal detrended fluctuation analysis of WLAN traffic, Wirel. Pers. Commun. 66 (2012) 385–395, http://dx.doi.org/10.1007/s11277-011-0347-y.

[38] P. Pavón-Domínguez, S. Serrano, F.J. Jiménez-Hornero, J.E. Jiménez-Hornero, E. Gutiérrez de Ravé, A.B. Ariza-Villaverde, Multifractal detrended fluctuation analysis of sheep livestock prices in origin, Physica A 392 (2013) 4466–4476, http://dx.doi.org/10.1016/j.physa.2013.05.042.

Publicación 2

Analysis of Air Mean Temperature Anomalies by Using Horizontal Visibility Graphs

Revista

Entropy

Editorial

MDPI

Factor de impacto (2020)

2.524

Categoría

Physics, multidisciplinary

Posición y cuartil (2020)

38/86, Q2

Analysis of Air Mean Temperature Anomalies by Using Horizontal Visibility Graphs

Javier Gómez-Gómez *[ID], **Rafael Carmona-Cabezas, Elena Sánchez-López** [ID]**, Eduardo Gutiérrez de Ravé** [ID] **and Francisco José Jiménez-Hornero** [ID]

GEPENA Research Group, University of Cordoba, Gregor Mendel Building (3rd Floor), Campus Rabanales, 14071 Cordoba, Spain; f12carcr@uco.es (R.C.-C.); g02saloe@uco.es (E.S.-L.); eduardo@uco.es (E.G.d.R.); fjhornero@uco.es (F.J.J.-H.)
* Correspondence: f12gogoj@uco.es

Abstract: The last decades have been successively warmer at the Earth's surface. An increasing interest in climate variability is appearing, and many research works have investigated the main effects on different climate variables. Some of them apply complex networks approaches to explore the spatial relation between distinct grid points or stations. In this work, the authors investigate whether topological properties change over several years. To this aim, we explore the application of the horizontal visibility graph (HVG) approach which maps a time series into a complex network. Data used in this study include a 60-year period of daily mean temperature anomalies in several stations over the Iberian Peninsula (Spain). Average degree, degree distribution exponent, and global clustering coefficient were analyzed. Interestingly, results show that they agree on a lack of significant trends, unlike annual mean values of anomalies, which present a characteristic upward trend. The main conclusions obtained are that complex networks structures and nonlinear features, such as weak correlations, appear not to be affected by rising temperatures derived from global climate conditions. Furthermore, different locations present a similar behavior and the intrinsic nature of these signals seems to be well described by network parameters.

Keywords: complex networks; horizontal visibility graph; time series analysis; mean temperature; topological properties

1. Introduction

The global increase of surface air temperatures on different time and spatial scales was confirmed in past decades by distinct studies [1–3]. Each of the last three decades has been successively warmer at the Earth's surface than any other preceding decade since 1850 [4]. Some consequences include change in migrations patterns and abundances of many terrestrial, freshwater, and marine species, an increase of vulnerability of some ecosystems and many human systems, shrinking of glaciers, or negative impacts in crops like wheat or maize yield in many regions, influencing current global politics and society [5]. As a result, a major interest in climate variability has appeared among researchers. Most studies have used climate models and statistical approaches to investigate extreme events linked to global warming. The major level of confidence associated with these extreme events are related to extreme heat and cold events [6]. Therefore, the study of temperature variables is a widespread research field [7–11].

In the last decades, a methodology which transforms time series into complex networks was developed [12]. It is called visibility graph (VG) and it has been demonstrated that these graphs inherit the nature of the underlining time series [12–14]. Furthermore, this method has been proven to be robust when applied to different environmental signals [15–19]. A simpler version of this approach, the horizontal visibility graph (HVG), was firstly published by Luque et al. in 2009, who developed a theoretical framework for uncorrelated time series which supported the numerical results [20]. In addition, Lacasa

and Toral found that a characteristic exponent of a network property, the degree distribution, was a limit which allowed us to distinguish between chaotic and correlated stochastic nature of time series [14]. As an example of application, Braga et al. described annual evolution of river flow fluctuations in Brazil for more of 80 years data series with HVG [21]. They found significant trends in networks properties.

Although graph theory and other particular complex networks techniques have been used in several works for climate studies [22–24], they mainly focus on the spatial description by considering stations and/or grid points as nodes in the so-called climate networks. Moreover, some non-trivial assumptions based on different measures of correlation are generally done to determine connections between nodes. On the contrary, VG's aim is to obtain a graph from each time series with its links following the same visibility criterion. To best of our knowledge, no previous study has applied an HVG approach to investigate the annual evolution of temperature by means of the topological properties of their graphs.

In this work, the authors' objective is to explore whether a VG framework can be applied to air mean temperature time series and to verify how some topological properties might change in a warming context. To that end, we used the HVG approach on yearly temperature anomalies of a 60-year period. Three relevant parameters have been analyzed, as in the work of Braga et al. for flow fluctuations of Brazilian rivers, namely: average degree centrality, degree distribution exponent, and global clustering coefficient.

This manuscript is organized as follows: Section 2 presents a detailed explanation of data and methodology used. Data, stations information and the preprocessing technique employed are introduced respectively in Sections 2.1 and 2.2 The HVG algorithm is presented in Section 2.3 and network topological properties can be found on Section 2.3.1 (degree centrality) and Section 2.3.2 (global clustering coefficient). In Section 3, a description and discussion of the main results are shown, organized as degree centrality computation in Section 3.1 and clustering coefficient computation in Section 3.2. Finally, the most important conclusions are stated in Section 4.

2. Materials and Methods

2.1. Data

To undertake this work, daily mean temperature time series from 10 different meteorological stations of Spain located over the Iberian Peninsula were analyzed (see Figure 1). These locations were chosen in order to have the least number of missing data, retaining a representative amount of stations to cover the Atlantic and the Mediterranean semiarid climates, which are the most representative climates in the Iberian Peninsula. In addition, half of them belong to mainland areas and the rest are coastal. In Table 1, we show their names, coordinates, and altitudes. Raw data are publicly available and provided by Agencia Estatal de Meteorología (Spanish Meteorological Agency). The period considered for this study extend to 60 years, from 1960 to 2019.

Figure 1. Meteorological stations located over the Iberian Peninsula (Spain) selected for this study.

Table 1. Meteorological stations name, coordinates and altitude.

Station Name	Short Name	Latitude (°N)	Longitude (°W)	Altitude (m)
Albacete air base	Albacete	38.95	1.86	702
Badajoz airport	Badajoz	38.88	6.81	185
Barcelona airport	Barcelona	41.29	−2.07	4
Bilbao airport	Bilbao	43.30	2.91	42
Burgos airport	Burgos	42.36	3.62	891
La Coruña	La Coruña	43.37	8.42	58
Málaga airport	Málaga	36.67	4.48	5
Sevilla airport	Sevilla	37.42	5.88	34
Valencia	Valencia	39.48	0.37	11
Zaragoza airport	Zaragoza	41.66	1.00	249

2.2. Seasonality Removal

Before employing the HVG algorithm, seasonal behavior of signals has been removed by computing the mean temperature anomalies. These new time series are obtained by subtracting the average value for each calendar day over the whole period from the original time series (μ) and normalizing by their standard error (σ), i.e., $x'_i = (x_i - \mu_i)/\sigma_i$, for $i = 1 \ldots 366$ day [25]. In Figure 2a,b, two examples of time series have been depicted. For illustrative purposes, only one year is shown (2019). Figure 2c,d contain their respective computed anomalies for the same period.
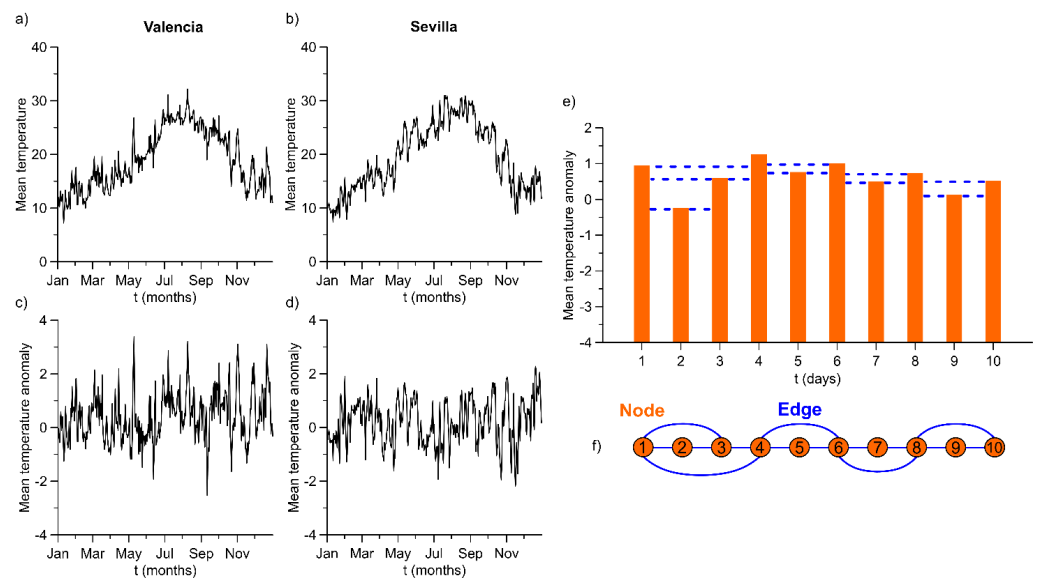

Figure 2. The left margin: (**a**,**b**) Plots that illustrate mean temperature time series of Valencia and Sevilla in the year 2019, respectively. (**c**,**d**) The corresponding anomalies for the same stations and period. The right margin: (**e**) Example of application of the horizontal visibility graph (HVG) algorithm to the first ten values of Sevilla anomalies in 1960. (**f**) Network obtained from the previous plot.

After computing temperature anomalies, one can obtain a better description of annual changes because the seasonal effect has been eliminated. The evolution of annual average values of these anomalies has been explored as a preliminary study. It has been found that all locations show time series with clear upward linear trends (see Figure 3). *t*-tests reject in every case the null hypothesis, which tests whether these slopes are equal to zero; therefore, they are statistically significant. Pearson correlation coefficients are in the range 0.51–0.71 and slopes vary between 0.0098 and 0.0179 °C/year. These trends can be associated to the global climate conditions because they are influenced by the global warming effect.
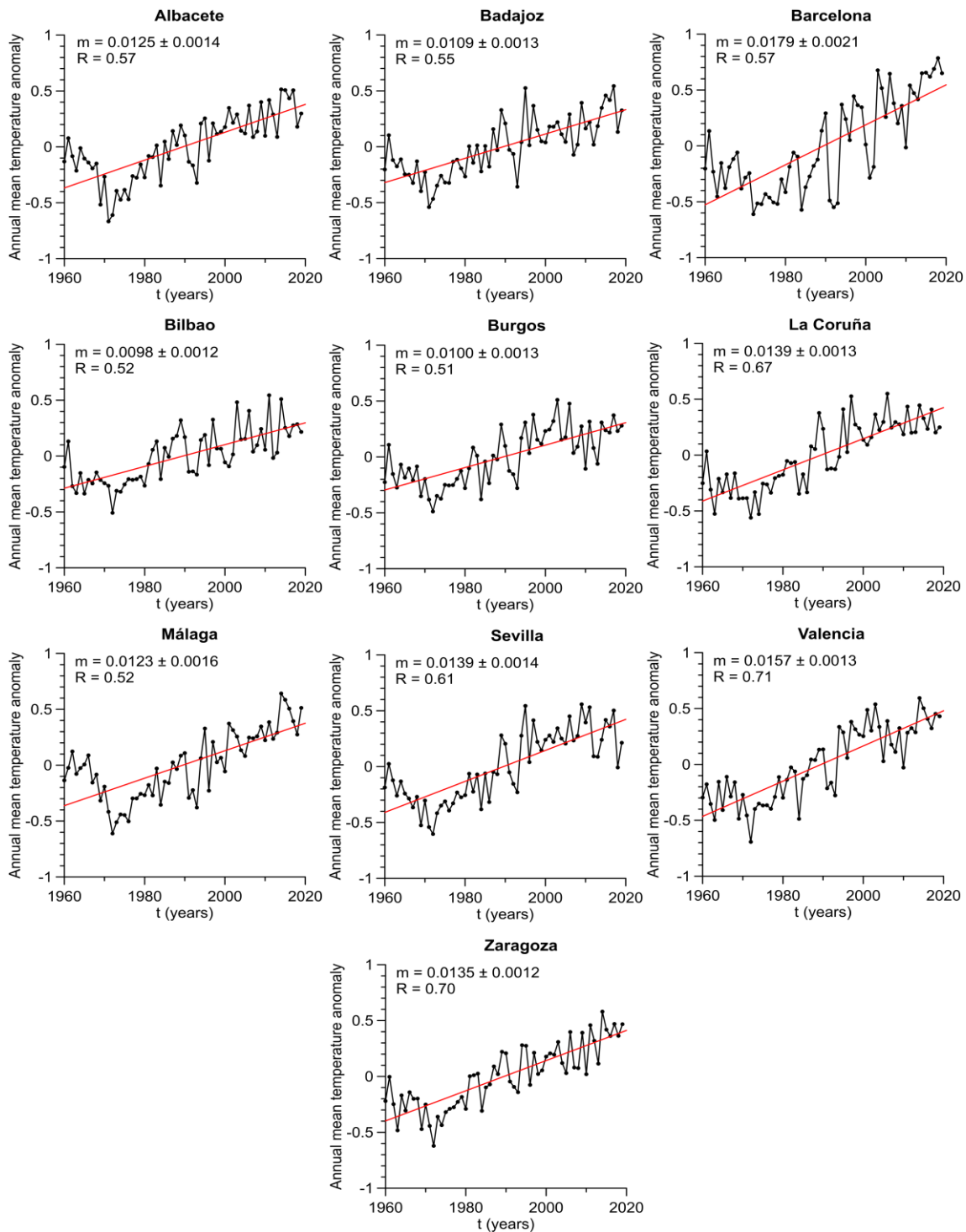
Figure 3. Annual average of daily mean temperature anomalies for every location.

2.3. Horizontal Visibility Graph (HVG)

VGs were conceived by Lacasa et al. in 2008 as an approach that allowed us to transform time series into complex networks [12]. This technique was proven to capture the main nonlinear features of time series such as correlations. One year later, a geometrically simpler procedure of mapping time series was firstly published by Luque et al. with the

advantage of being easier to find a theoretical framework that support the recent findings for uncorrelated time series: the horizontal visibility graph (HVG) [20].

The HVG algorithm states that two nodes (or points in a time series) i and j are connected if every node between them fulfills the following criterion:

$$x_i, x_j > x_p, \ \forall \, p \mid i < p < j \tag{1}$$

An example of the application of this algorithm can be seen in Figure 2e,f. For more details, some properties of HVGs can be found in Ref. [20].

As every node in HVGs is connected and these connections are bidirectional, the resulting network is connected and undirected. Therefore, an HVG can be easily described by their nodes and links, also named edges. By doing so, a natural way of describing this kind of networks is by means of a matrix where each element A_{ij} is one or zero if nodes i and j are connected or not, respectively. The matrix obtained in this way is a $n \times n$ adjacency binary matrix, with n being the size of the time series [16].

Some topological properties from the complex networks have been explored in this work, such as the degree distribution and the global clustering coefficient, which are defined further in the text. The procedure used to obtain the time evolution of these topological properties was: (i) to split each time series into each year; (ii) to transform time series to their respective HVG and (iii) to compute the degree centrality and the global clustering coefficient in each case. After that, we investigated the mean values and trends of both topological properties, as Braga et al. did for river flow fluctuations [21].

2.3.1. Degree Centrality

The first studied topological property is the degree centrality, one of the most widely used in several articles due to the simplicity of its computation and the information which provides about the nonlinear properties of time series [12,18,19,26]. This measure is defined as the number of edges, k_i, that each node i has in the network, i.e., the number of other nodes which node i sees. By using the adjacency matrix, this quantity is formally defined as:

$$k_i = \sum_{j=1}^{n} A_{ij} \ \forall \, j = 1 \dots n \tag{2}$$

After computing the degree of every node, the degree probability distribution, $P(k_i)$, can be obtained. For HVGs, the theoretical degree distribution of a random uncorrelated series was demonstrated in [20] and it fits an exponential function: $P(k) = (1/3)(2/3)^{k-2}$. This expression can be rewritten as $P(k) \sim \exp(-\gamma k)$ with a characteristic exponent value of $\gamma_{un} = \ln(3/2)$.

As commented in Section 1, Lacasa and Toral found that this theoretical result is also a quantitative frontier between chaotic and correlated stochastic processes [14]. They showed that chaotic time series map into HVGs whose degree distribution follow an exponential function with a characteristic exponent $\gamma < \ln(3/2)$ (λ in the original work) whereas correlated stochastic series exhibit exponential degree distributions as well, but with $\gamma > \ln(3/2)$. Moreover, every possible value on the left and the right of γ_{un} slowly tends to this asymptotical value as the correlation dimension increases in chaotic processes or the correlations become weaker in stochastic ones.

2.3.2. Global Clustering Coefficient

Another commonly studied topological property in networks is the global clustering coefficient C, which was introduced by Watts and Strogatz [27]. It gives information about to what extent nodes tend to be clustered together. The coefficient definition is based on triplets of nodes. This term refers to groups of three nodes which are connected by two or three edges. In the last situation, if one of these groups reaches the maximum possible number of edges among the three nodes, then it is called a closed triplet. According to this,

C is defined as the proportion of closed triplets over the total number of triplets (open and closed) and it can be computed through the adjacency matrix of the network [17]:

$$C = \frac{\sum_{i,j,k} A_{ij} A_{jk} A_{ki}}{\sum_i k_i (k_i - 1)} \tag{3}$$

where k_i is the degree of node *i* and if the denominator is null, then *C* is set to zero.

Note that this quantity is a unique value for each network and is in the range [0, 1]. The closer the clustering coefficient is to one, the more clustered the network is.

3. Results

3.1. Degree Centrality Computation

As previously stated, after separating temperature anomalies into annual time series, the HVG algorithm was computed for each case. Next, the degree centrality was obtained from the corresponding networks and the mean values of every network and degree distributions were studied. An example of this can be observed in Figure 4 for Valencia and Sevilla stations.
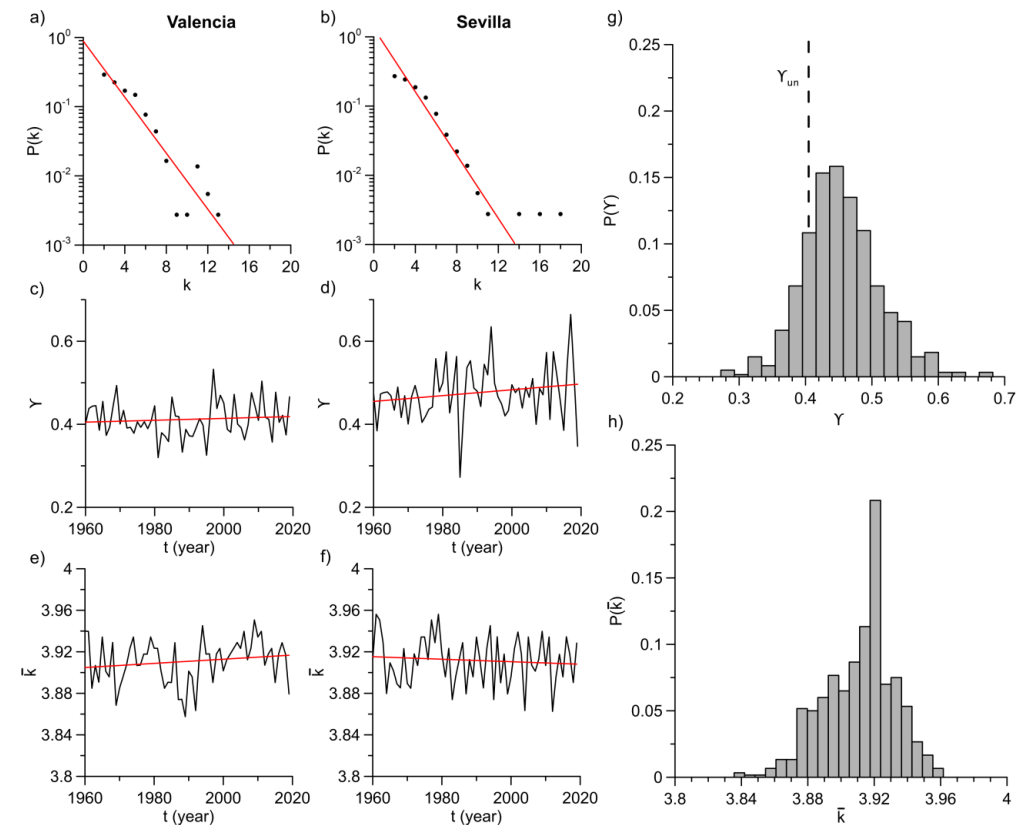

Figure 4. The left margin: (**a**,**b**) Degree distributions of Valencia and Sevilla stations in year 2019, respectively. Red lines are the least-square fits of values. (**c**,**d**) Annual evolution of slopes obtained from the previous linear fits (γ exponent) for Valencia and Sevilla, respectively. (**e**,**f**) Annual evolution of mean values of degree for the same stations. Red lines in every case represent the least-squares fits of curves. The right margin: (**g**) Normalized histogram of γ exponent obtained for all locations and years. Dashed line represents the theoretical value for an uncorrelated random series ($\gamma_{un} = \ln(3/2)$). (**h**) Normalized histogram of mean degree for all locations and years.

Figure 4a,b illustrates the degree distributions of the mentioned stations in year 2019 in log-linear plots. It can be appreciated how these distributions well fit to an exponential function of the form: $P(k) \sim \exp(-\gamma k)$. Slopes obtained from least-square fit are different

values of the characteristic exponent γ. In a similar way, the rest of stations replicate the expected theoretical behavior of these curves.

Figure 4c,d depict the annual evolution of these exponents for the same stations while Figure 4e,f show annual evolution of average degree. Linear fits were computed in every case and outcomes are displayed in Table 2. The authors investigated t-tests of these fits to determine whether these network properties evolve in a similar way to the trends identified in annual means of temperature anomalies (see Figure 3). t-tests verify or reject the null hypothesis of that slope is different from zero. For this reason, if the null hypothesis is rejected, the curve exhibits a statistically significant trend. Interestingly, t-tests approved null hypothesis at a 95% confidence level for annual average degree in every station and for the γ exponent curves in almost every location (see Table 2). This outcome, together with rather low values of Pearson correlation coefficients, suggest that γ and average degree do not show statistically significant trends. As a consequence, they must oscillate around a mean value. These mean values were also computed, and they are discussed next.

Table 2. Slopes with standard errors and Pearson correlation coefficients of linear fits of mean degree (k), characteristic exponent of degree distribution (γ) and global clustering coefficient (C) for each location over time. Values in bold refer to statistically significant trends at a 95% confidence level given by t-tests.

Station	$m_k(\times 10^{-4})$	$\sigma_{m_k}(\times 10^{-4})$	R_k	$m_\gamma(\times 10^{-4})$	$\sigma_{m_\gamma}(\times 10^{-4})$	R_γ	$m_C(\times 10^{-4})$	$\sigma_{m_C}(\times 10^{-4})$	R_C
Albacete	2.2	1.7	0.03	−1.9	4.3	0.00	0.6	0.7	0.01
Badajoz	−0.2	1.7	0.00	7.1	4.2	0.05	1.0	0.7	0.04
Barcelona	−2.4	1.4	0.05	0.7	3.2	0.00	**1.7**	**0.8**	**0.06**
Bilbao	−1.4	1.7	0.01	**7.3**	**3.5**	**0.07**	**1.9**	**0.7**	**0.10**
Burgos	1.7	1.4	0.02	3.6	4.3	0.01	0.8	0.7	0.02
La Coruña	1.7	1.6	0.02	6.4	4.3	0.04	1.1	0.8	0.03
Málaga	0.9	1.4	0.01	−4.7	2.8	0.05	−0.2	0.7	0.00
Sevilla	−1.2	1.7	0.01	7.0	4.8	0.04	1.3	0.7	0.05
Valencia	2.0	1.6	0.03	2.3	3.2	0.01	0.5	0.6	0.01
Zaragoza	−1.8	1.6	0.02	7.4	5.2	0.03	**2.0**	**0.8**	**0.10**

In Table 3, we show the mean values and their corresponding standard errors for γ exponents and average degree in the whole period of 60 years. These values are all quite close to each other despite large distances among stations. In fact, mean degree absolutely coincide in values up to the second decimal with the same error: $\bar{k} = 3.91 \pm 0.02$, while γ is in the range $[0.41, 0.48]$. Mean average degree is associated to the average number of connections that nodes have in networks. This means that a high value of this parameter— and thus, more connected graphs—will be related to irregular time series. In this case, every location time series is smoother, rather than rougher, and this feature remains in time. As $\gamma > \ln(3/2)$, temperature anomalies are situated in the region of correlated stochastic processes. Nonetheless, they are rather close to the limit of an uncorrelated random process, so correlations are very weak [14]. This also contributes to the smoothness of time series, since correlation tends to decrease the number of nodes with high degree.

Table 3. Average values and standard errors of mean degree (k), characteristic exponent of degree distribution (γ) and global clustering coefficient (C) for the 60-year period in each location.

Station	μ_k	σ_k	μ_γ	σ_γ	μ_C	σ_C
Albacete	3.91	0.02	0.46	0.06	0.57	0.01
Badajoz	3.91	0.02	0.47	0.06	0.57	0.01
Barcelona	3.91	0.02	0.43	0.04	0.56	0.01
Bilbao	3.91	0.02	0.46	0.05	0.57	0.01
Burgos	3.91	0.02	0.48	0.06	0.57	0.01
La Coruña	3.91	0.02	0.46	0.06	0.57	0.01
Málaga	3.91	0.02	0.43	0.04	0.56	0.01
Sevilla	3.91	0.02	0.48	0.07	0.57	0.01
Valencia	3.91	0.02	0.41	0.04	0.55	0.01
Zaragoza	3.91	0.02	0.47	0.07	0.57	0.01

When results from each year and station are analyzed together, one can find that their normalized histograms are also centered around one value and take the form of gaussian distributions.

On the one hand, the histogram of γ is depicted on Figure 4g. It is centered around 0.45 with a relatively important amount of values grouped to the right side of the exponent value from a white noise process, γ_{un}. However, it also displays a significant number of them falling on the left side (approximately 19% of all yearly time series analyzed). These last values are all equally distributed along the years and over different stations. This outcome points to the fact that although this parameter suggests a "mean behavior" that has a stochastic character, it also exhibits a chaotic character in a shorter time scale.

On the other hand, we also illustrate the normalized histogram of average degree on Figure 4h. This histogram shows a sharper distribution with the peak being the previously mentioned result from Table 3, what could explain the coincident results for every location.

In summary, degree distributions are quite similar in average independently of locations, although some differences can be observed. Mean degree is the same for all locations and this can indicate that it might not be affected by local conditions, such as coastal proximity or latitude. In contrast, although γ exponents are close to each other, a distinct strength of correlations can be observed among different locations. Contrary to what Braga et al. found for river flow fluctuations [21], we found an absence of trends. This points to the fact that such parameters can be considered as good constant properties for temperature anomalies, without being affected by any kind of trend from climate change.

The study of the character of nonlinearities in temperature anomalies suggests that signals exhibit an overall behavior which can be classified as stochastic, although in shorter time scale some yearly time series can be classified as chaotic. Lacasa and Toral found that although extrinsic noise was well captured by the HVG algorithm, it failed to discern chaotic from stochastic character for intrinsic noise [14]. More sophisticated methods such as the ϵ entropy and the finite size Lyapunov exponent analysis have also shown some difficulties to distinguish nonlinear nature of signals due to the finiteness of the observational data [28]. Nonetheless, climate system has been often defined as a nonlinear system involving both chaotic and stochastic components [29,30]. It is possible that in shorter time scales our results can be strongly affected by mesoscale convective phenomena—such as Atlantic or Mediterranean (cold drop) depressions landfalls in the Iberian Peninsula—that provide a more chaotic nature to signals.

3.2. Clustering Coefficient Computation

The computed global clustering coefficients of HVGs from Valencia and Sevilla stations are depicted vs. time on Figure 5a,b. The rest of locations shows similar behaviors. It can be observed how these plots are analogous to those obtained from the average degree and γ parameters. Again, trends were tested with *t*-tests. It was found that the null hypothesis was accepted in most cases as well as in the degree results leading to no significant trends

for the majority of locations (see Table 2). Only three stations had a significant trend at a 95% confident level. Nonetheless, the orders of magnitude in slopes are too low and their respective Pearson correlation coefficients are no more than 0.10. Therefore, the global clustering coefficient agrees with the previous analyzed topological properties and yearly values can be considered as oscillations around a mean. This result suggests that there is no annual evolution in complexity of time series structure. Moreover, linear trends of anomalies do not affect it.
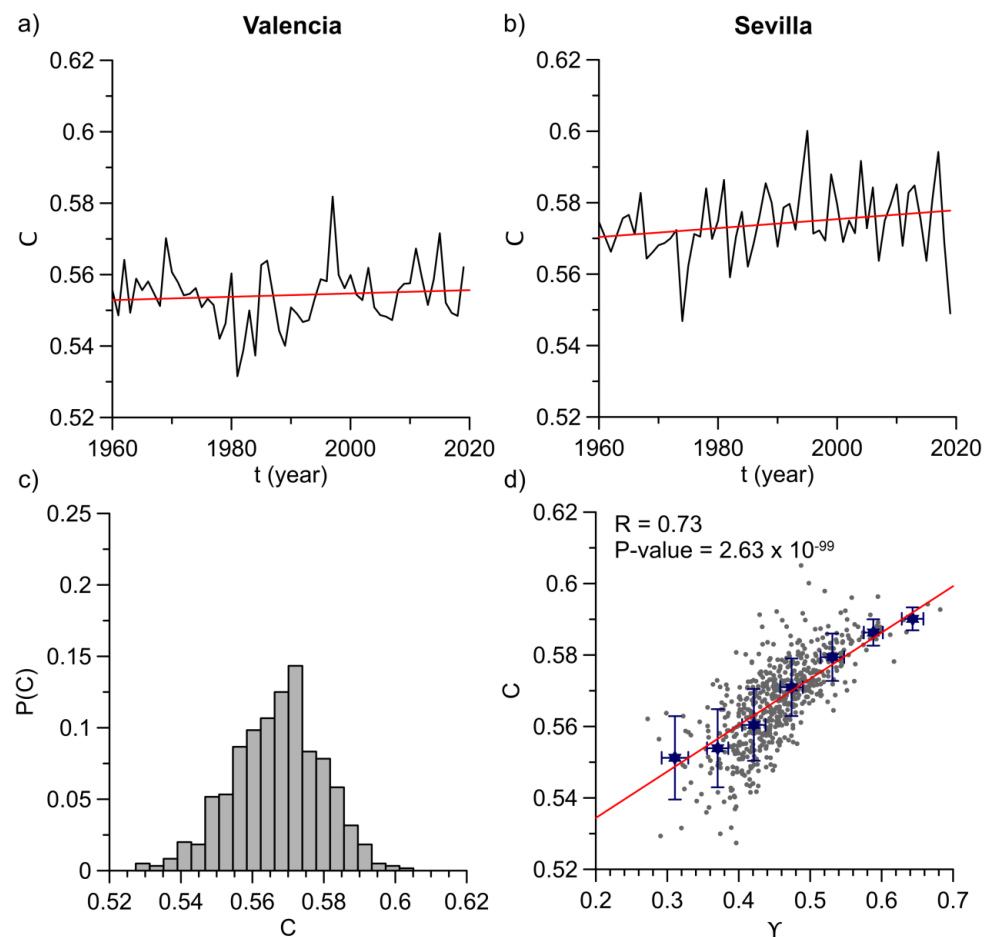

Figure 5. (**a**) Annual evolution of global clustering coefficient (C along the years for Valencia station. Red line represents the least-squares fit of the curve. (**b**) The same plot for Sevilla station. (**c**) Normalized histogram of C for all years and locations. (**d**) Scatter plot (grey dots) of C vs. the characteristic degree exponent (γ). Correlation coefficient and *p*-value for testing the null hypothesis that C and γ are not correlated. This *p*-value is smaller than the 95% significance level (less than 0.05), thus the correlation is statistically significant. Blue stars are window average values obtained from seven bins of equal size in γ axis and error bars are standard deviations. Red line is the least-squares fit of these average values.

Mean values of annual clustering coefficients and their standard errors are displayed on Table 3 for every location. As it can be seen in the table, they are all really close to each other, varying from 0.55 to 0.57, although standard errors are lower than in the case of γ. This shows that the obtained networks exhibit a complex structure where nodes have some tendency to be clustered. It also suggests a quite similar behavior in different stations which, as it was commented before, remain almost constant along the years. For illustrative purposes, Figure 5c shows the normalized histogram obtained from every year and location. This confirms that the complex structure is rather similar in every case with a higher or lower degree of clustering. These results also take the form of a gaussian distribution.

Finally, authors compared all results to check whether some kind of relationship could exist among the three parameters (average degree, degree exponent and clustering coefficient). A statistically significant correlation between clustering coefficient and γ exponent was found. This correlation can be observed on Figure 5d. Grey dots represent the relation between both distributions with a high correlation coefficient of 0.73 and extremely low *p*-value for the correlation test at a 95% confidence level (2.63×10^{-99}). This last outcome is much less than the significance level, which means that we can certainly reject the null hypothesis that C and γ are not correlated. In the same figure, it can also be seen the window average over seven bins of equal size in γ axis. They fit to a straight line with a Pearson coefficient of 0.99 and a slope of 0.13 ± 0.01. Braga et al. also got a coupling on average between these two topological properties when they studied river flow fluctuations in Brazil [21]. In that work, an exponential function was the best fit to the average values. Temperature anomalies, conversely, exhibit a linear coupling of degree exponent and global clustering coefficient. This also corroborates that both properties behave in a similar way.

4. Conclusions

Daily mean temperature anomalies show common HVGs structures over different locations which also remain almost constant in a relative long period of time (up to 60 years). Three studied topological parameters (average degree, degree exponent and global clustering coefficient) do not show statistically significant annually trends in most cases, although annual mean values of anomalies do show them. Indeed, these anomalies are clearly affected by a positive trend which can be related to the global conditions of rising temperatures in the context of climate change, but this fact apparently does not affect the topological properties of networks.

When mean values were analyzed, they showed a coincident mean average degree and similar degree exponents and clustering coefficients in every location. According to this, these properties are more related to the natural process itself than to the local variations in climate or geographical conditions. In fact, one can clearly notice that HVG algorithm characterizes the nature of the time series, as explained below. Firstly, mean degree invariance points to a similar smoothness in every time series, which is characteristic of dissipative processes where the air temperature is involved. Secondly, similar degree exponents are higher than the theoretical value for an uncorrelated process. This fact suggests that the underlining process is mainly stochastic with weak correlations. Lastly, clustering coefficients—which are related to the tendency of nodes to be clustered together—also give some information about these correlations. This last consideration is corroborated since it is found a great correlation between degree exponents and clustering coefficients which can be well fitted to a line.

Finally, the characteristics of these constant properties could be useful to expand databases for climate models validation. However, some problems remain open for future studies, such as the confirmation of these results on more locations governed by other climate conditions, or the appearance of different new outcomes. Other open research fields for future works include the application of other variants from the VG framework or HVGs together with Shannon–Fisher plane method [31]. This last methodology could be studied in future works on real data.

Author Contributions: Conceptualization, J.G.-G. and R.C.-C.; methodology, J.G.-G.; software, J.G.-G. and R.C.-C.; validation, J.G.-G.; formal analysis, J.G.-G.; investigation, J.G.-G. and R.C.-C.; resources, R.C.-C.; data curation, J.G.-G. E.S.-L.; writing—original draft preparation, J.G.-G.; writing—review and editing, J.G.-G.; visualization, J.G.-G., E.S.-L.; supervision, E.G.d.R. and F.J.J.-H.; project administration, E.G.d.R. and F.J.J.-H.; funding acquisition, E.G.d.R. and F.J.J.-H. All authors have read and agreed to the published version of the manuscript. The FLAE approach for the sequence of authors is applied in this work.

Data Availability Statement: Publicly available datasets were analyzed in this study. This data can be found here: http://www.aemet.es/es/datos_abiertos/AEMET_OpenData.

Conflicts of Interest: The authors declare no conflict of interest.

References

1. Horton, B. Geographical distribution of changes in maximum and minimum temperatures. *Atmos. Res.* **1995**, *37*, 101–117. [CrossRef]
2. Jones, P.D.; New, M.; Parker, D.E.; Martin, S.; Rigor, I.G. Surface air temperature and its changes over the past 150 years. *Rev. Geophys.* **1999**, *37*, 173–199. [CrossRef]
3. Jones, P.D.; Moberg, A. Hemispheric and large-scale surface air temperature variations: An extensive revision and an update to 2001. *J. Clim.* **2003**, *16*, 206–223. [CrossRef]
4. Stocker, T.F.; Qin, D.; Plattner, G.-K.; Tignor, M.; Allen, S.K.; Boschung, J.; Nauels, A.; Xia, Y.; Bex, V.; Midgley, P.M. Summary for Policymakers WG I. In *Climate Change 2013: The Physical Science Basis. Contribution of Working Group I to the Fifth Assessment Report of the Intergovernmental Panel on Climate Change*; Cambridge University Press: Cambridge, UK; New York, NY, USA, 2013.
5. Field, C.B.; Barros, V.R.; Dokken, D.J.; Mach, K.J.; Mastrandrea, M.D.; Bilir, T.E.; Chatterjee, M.; Ebi, K.L.; Estrada, Y.O.; Genova, R.C.; et al. Summary for Policymakers WG II. In *Climate Change 2014: Impacts, Adaptation, and Vulnerability. Part A: Global and Sectoral Aspects. Contribution of Working Group II to the Fifth Assessment Report of the Intergovernmental Panel on Climate Change*; Cambridge University Press: Cambridge, UK; New York, NY, USA, 2014; pp. 1–32.
6. Swain, D.L.; Singh, D.; Touma, D.; Diffenbaugh, N.S. Attributing extreme events to climate change: A new frontier in a warming world. *One Earth* **2020**, *2*, 522–527. [CrossRef]
7. Burgueño, A.; Lana, X.; Serra, C.; Martínez, M.D. Daily extreme temperature multifractals in Catalonia (NE Spain). *Phys. Lett. A* **2014**, *378*, 874–885. [CrossRef]
8. Gómez-Navarro, J.J.; Montávez, J.P.; Jimenez-Guerrero, P.; Jerez, S.; García-Valero, J.A.; González-Rouco, J.F. Warming patterns in regional climate change projections over the Iberian Peninsula. *Metz* **2010**, *19*, 275–285. [CrossRef]
9. Latif, Y.; Yaoming, M.; Yaseen, M.; Muhammad, S.; Wazir, M.A. Spatial analysis of temperature time series over the upper Indus Basin (UIB) Pakistan. *Theor. Appl. Climatol.* **2020**, *139*, 741–758. [CrossRef]
10. Ongoma, V.; Rahman, M.A.; Ayugi, B.; Nisha, F.; Galvin, S.; Shilenje, Z.W.; Ogwang, B.A. Variability of diurnal temperature range over Pacific Island countries, a case study of Fiji. *Meteorol. Atmos. Phys.* **2020**. [CrossRef]
11. Zhuang, Y.; Zhang, J. Diurnal asymmetry in future temperature changes over the main belt and road regions. *Ecosyst. Health Sustain.* **2020**, *6*, 1749530. [CrossRef]
12. Lacasa, L.; Luque, B.; Ballesteros, F.; Luque, J.; Nuño, J.C. From time series to complex networks: The visibility graph. *Proc. Natl. Acad. Sci. USA* **2008**, *105*, 4972–4975. [CrossRef]
13. Lacasa, L.; Luque, B.; Luque, J.; Nuño, J.C. The visibility graph: A new method for estimating the hurst exponent of fractional brownian motion. *Europhys. Lett.* **2009**, *86*, 30001. [CrossRef]
14. Lacasa, L.; Toral, R. Description of stochastic and chaotic series using visibility graphs. *Phys. Rev. E* **2010**, *82*, 036120. [CrossRef]
15. Carmona-Cabezas, R.; Ariza-Villaverde, A.B.; Gutiérrez de Ravé, E.; Jiménez-Hornero, F.J. Visibility graphs of ground-level ozone time series: A multifractal analysis. *Sci. Total Environ.* **2019**, *661*, 138–147. [CrossRef]
16. Carmona-Cabezas, R.; Gómez-Gómez, J.; Ariza-Villaverde, A.B.; Gutiérrez de Ravé, E.; Jiménez-Hornero, F.J. Can complex networks describe the urban and rural tropospheric O_3 dynamics? *Chemosphere* **2019**, *230*, 59–66. [CrossRef] [PubMed]
17. Donner, R.V.; Donges, J.F. Visibility graph analysis of geophysical time series: Potentials and possible pitfalls. *Acta Geophys.* **2012**, *60*, 589–623. [CrossRef]
18. Elsner, J.B.; Jagger, T.H.; Fogarty, E.A. Visibility network of United States hurricanes. *Geophys. Res. Lett.* **2009**, *36*, L16702. [CrossRef]
19. Pierini, J.O.; Lovallo, M.; Telesca, L. Visibility graph analysis of wind speed records measured in Central Argentina. *Phys. A Stat. Mech. Appl.* **2012**, *391*, 5041–5048. [CrossRef]
20. Luque, B.; Lacasa, L.; Ballesteros, F.; Luque, J. Horizontal visibility graphs: Exact results for random time series. *Phys. Rev. E* **2009**, *80*, 046103. [CrossRef]
21. Braga, A.C.; Alves, L.G.A.; Costa, L.S.; Ribeiro, A.A.; de Jesus, M.M.A.; Tateishi, A.A.; Ribeiro, H.V. Characterization of river flow fluctuations via horizontal visibility graphs. *Phys. A* **2016**, *444*, 1003–1011. [CrossRef]
22. Tsonis, A.A.; Roebber, P.J. The architecture of the climate network. *Phys. A Stat. Mech. Appl.* **2004**, *333*, 497–504. [CrossRef]
23. Paluš, M.; Hartman, D.; Hlinka, J.; Vejmelka, M. Discerning connectivity from dynamics in climate networks. *Nonlinear Process. Geophys.* **2011**, *18*, 751–763. [CrossRef]
24. Havlin, S.; Kenett, D.Y.; Ben-Jacob, E.; Bunde, A.; Cohen, R.; Hermann, H.; Kantelhardt, J.W.; Kertész, J.; Kirkpatrick, S.; Kurths, J.; et al. Challenges in network science: Applications to infrastructures, climate, social systems and economics. *Eur. Phys. J. Spec. Top.* **2012**, *214*, 273–293. [CrossRef]
25. Lange, H.; Sippel, S.; Rosso, O.A. Nonlinear dynamics of river runoff elucidated by horizontal visibility graphs. *Chaos* **2018**, *28*, 075520. [CrossRef]
26. Mali, P.; Manna, S.K.; Mukhopadhyay, A.; Haldar, P.K.; Singh, G. Multifractal analysis of multiparticle emission data in the framework of visibility graph and sandbox algorithm. *Phys. A Stat. Mech. Appl.* **2018**, *493*, 253–266. [CrossRef]

27. Watts, D.J.; Strogatz, S.H. Collective dynamics of 'Small-World' networks. *Nature* **1998**, *393*, 440–442. [CrossRef]
28. Cencini, M.; Falcioni, M.; Olbrich, E.; Kantz, H.; Vulpiani, A. Chaos or noise: Difficulties of a distinction. *Phys. Rev. E* **2000**, *62*, 427–437. [CrossRef]
29. Millán, H.; Ghanbarian-Alavijeh, B.; García-Fornaris, I. Nonlinear dynamics of mean daily temperature and dewpoint time series at Babolsar, Iran, 1961–2005. *Atmos. Res.* **2010**, *98*, 89–101. [CrossRef]
30. Lorenz, E.N. Deterministic nonperiodic flow. *J. Atmos. Sci.* **1963**, *20*, 130–141. [CrossRef]
31. Ravetti, M.G.; Carpi, L.C.; Gonçalves, B.A.; Frery, A.C.; Rosso, O.A. Distinguishing noise from chaos: Objective versus subjective criteria using horizontal visibility graph. *PLoS ONE* **2014**, *9*, e108004. [CrossRef] [PubMed]

Publicación 3

Multifractal fluctuations of the precipitation in Spain (1960–2019)

Journal Citation Reports (Clarivate™)

Revista

Chaos, Solitons & Fractals

Editorial
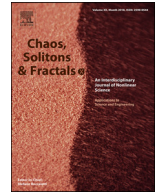
Elsevier

Factor de impacto (2020)

5.944

Categoría

Physics, mathematical

Posición y cuartil (2020)

1/55, Q1

Multifractal fluctuations of the precipitation in Spain (1960–2019)

Javier Gómez-Gómez*, Rafael Carmona-Cabezas, Elena Sánchez-López, Eduardo Gutiérrez de Ravé, Francisco José Jiménez-Hornero

GEPENA Research Group, University of Cordoba, Gregor Mendel Building (3rd floor), Campus Rabanales, Cordoba 14071, Spain

ABSTRACT

In this work, an analysis of multifractal parameters of daily precipitation series over the Iberian Peninsula was performed in two 30-year periods to explore whether these properties follow any pattern. Fluctuations of precipitation series show three different scaling regions. Only two distinct regimes for small and large timescales can be confirmed, while intermediate scales are part of a transition region. It is also observed a certain degree of multifractality, which is higher for small timescales. At these scales, there is a high persistence which follows the spatial gradient of the annual precipitation. Moreover, multifractal parameters of the precipitation are modified according to complex spatial and temporal patterns. Only persistence uniformly decreases in the last period. Other relevant findings are the changes in the asymmetry of multifractal spectra in the eastern belt at larger timescales, which might be related to the change in the behavior of the Mediterranean cyclones.

© 2022 Elsevier Ltd. All rights reserved.

1. Introduction

Climate change might impact natural and human systems in different ways. Some include changes in quantity and quality of water resources, negative impacts on agriculture or an increment in frequency of droughts, floods or wildfires, among others [1,2]. A closely relation between some of these effects and precipitation patterns, makes quite relevant the study of this climatic variable for a better understanding of the hydrological systems [3].

Precipitation is a climatic variable of great relevance for the Iberian Peninsula. This region is located between Africa and Central Europe, more precisely, at the south of Europe and in the western Mediterranean basin. Unlike other Mediterranean regions, this one is characterized by having the Atlantic oceanic influence, what produces a climate with irregularity in water regime [4], which makes this geographic location specially interesting to study rainfall. According to de Luis et al. [5], seasonal precipitation regimes in the Iberian Peninsula can be explained in a simple way, as the sum of three factors that contributes to the high spatial variability: an Iberian inland component, and the Atlantic and Mediterranean oceanic components which becomes more notable at the west and east, respectively. Thus, water resources scarcity is notable in this region, as it is shown by some models that predict a drier precipitation regime, particularly, due to a prolonged dry season [6]. Actually, several authors showed that seasonal precipitation regimes are modifying in this region [5,7–9].

Climate variability studies based on empirical meteorological data are of great importance. Much of them are based on statistical analysis [10–13]. Nevertheless, an growing interest in multifractal analysis is taking place in the last decades [14–16]. Multifractal analysis is useful to study the complexity and non-linearity of time series which cannot be addressed with other linear methods. These techniques are based on the fractal theory [17,18]. A fractal is a geometric object characterized by its self-similarity or scale independency when they are split into smaller parts. Many studies have demonstrated that fluctuations of several environmental variables and, particularly, precipitation, have multifractal nature, and contain a range of scaling exponents which characterize the temporal structure of the time series. Thus, the underlying process can be described by the multifractal parameters. Some of the most important ones studied here are the Hurst exponent, the Hölder exponent with maximum spectrum, the width and the asymmetry of the multifractal spectrum [14,19,20].

In recent years, a technique is being widely used to get information about the multifractal scaling properties of temporal fluctuations in signals. This is the multifractal detrended fluctuation analysis (MF-DFA), which was developed by Kantelhardt et al. [21]. This technique is a useful method to deal with non-stationary time series. Its applications extend to several climatic variables, as exposed in different studies [3,16,20,22].

Due to the high variability in the spatial and temporal distribution of rainfall in the Iberian Peninsula, it is appropriate to analyze the complexity and non-linearity of precipitation series in dif-

ferent time periods. Thus, it will be possible to explore whether these properties follow geographical or temporal patterns. To this purpose, two independent 30-year periods are analyzed with MF-DFA and compared. Because of the data availability and their quality, the two 30-year periods are limited to 1960 - 1989 and 1990 - 2019. Hence, the analysis of the spatial and temporal variability is performed through the study of the changes in multifractal parameters of daily precipitation series between these periods. Furthermore, a preliminary analysis of linear trends of annual precipitation series is carried out to improve the information extracted about the climate variability in this region. This work is structured as follows. Section 2 includes the description of data, gauge stations and methods used; results are collected and discussed in Section 3 and, lastly, Section 4 includes the main conclusions drawn in this study.

2. Materials and methods

2.1. Data

This study is based on daily precipitation data series from 29 meteorological stations distributed over the Spanish region of the Iberian Peninsula during the period 1960 - 2019 (see Fig. 1). This leads to a total amount of 21,915 records, split up into two sub-periods (1960 - 1989 and 1990 - 2019) with $N_1 = 10958$ and $N_2 = 10957$, respectively.

Raw data records were obtained via the Spanish Meteorological Agency ("Agencia Estatal de Meteorología") from the AEMET Open-Data website at http://www.aemet.es/es/datos_abiertos/AEMET_OpenData. This network contains 261 stations across the considered region. To get reliable results, a previous identification of missing data was carried out and we discarded time series which contained more than 0.01% missing values and more than 10 consecutive ones for both periods. After this procedure, the remaining 29 series were collected. Some basic information about these stations can be seen in the Appendix A, in Table A.1. The annual precipitation was also computed from daily rainfall and an analysis of inter-annual trends was performed through simple least-squares fits.

The set of gauge stations covers the main two climate variants of the Iberian Peninsula: the Atlantic climate type and the Mediterranean semiarid subtype [23]. The precipitation climatology in the Spanish region of the Iberian Peninsula is characterized by strong gradients with abundant annual precipitation to the
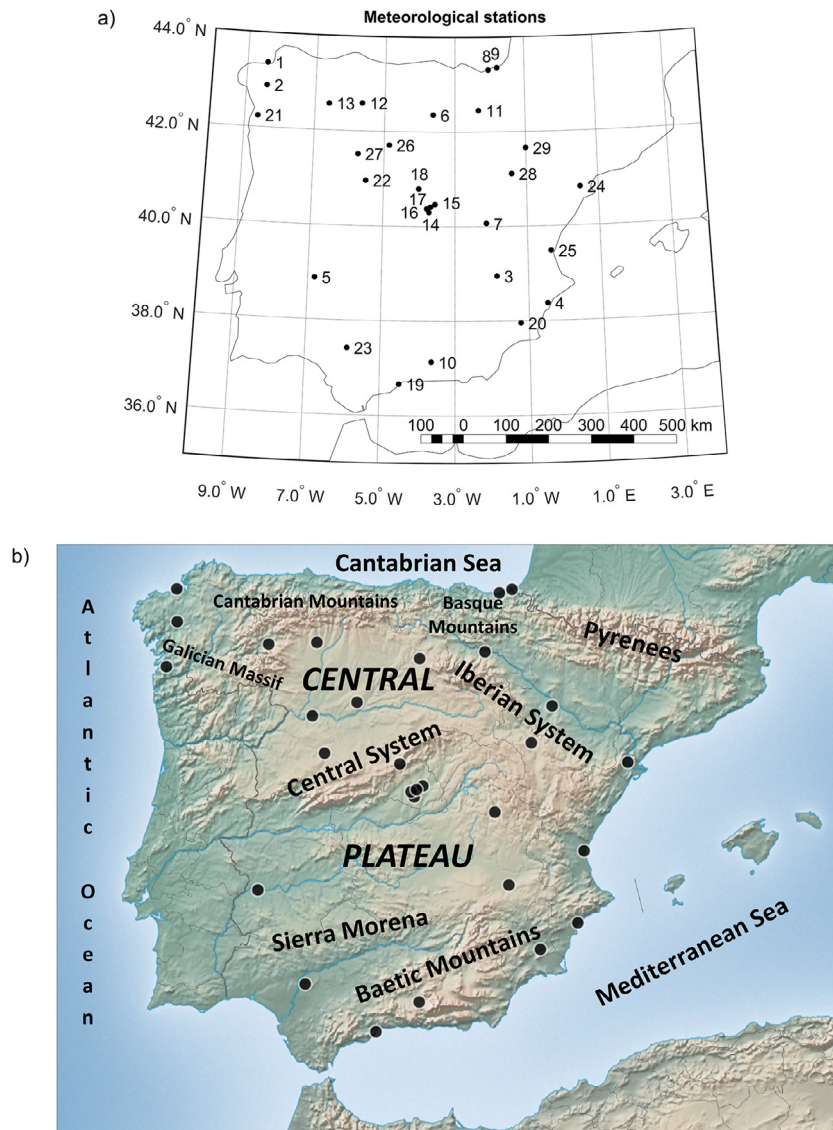

Fig. 1. (a) Meteorological stations. (b) Orographic map of the Iberian Peninsula.

north and northwest ($P > 1000$ mm/year) and lower values towards the southeast ($P < 400$ mm/year) [10]. In this last region, certain areas can even have less than 200 mm/year [24]. However, a higher complexity in the spatial and temporal seasonal variability is present in the study area, because of the two water masses influences and orography [5]. Fig. 1(b) shows the orography of the region.

2.2. Multifractal detrended fluctuation analysis

In order to apply the MF-DFA algorithm, it is common to contemplate the deseasonalized time series when analyzing climatological variables [16,25] and, in particular, hydrological variables [26–28]. In our study, the precipitation (normalized) anomalies were computed similarly to the work of Xavier et al. [29], to avoid that seasonal periodicity affected power law behavior. As an example, the whole time series with daily resolution of station No. 15 and its corresponding deseasonalized version are shown in Fig. 2.

MF-DFA algorithm was developed by Kantelhardt et al. [21]. This method computes the "profile" (the integrated series after subtracting the mean) and obtains its fluctuation function dividing this profile into multiple segments. More precisely, the profile is divided into $N_s \equiv \mathrm{int}(N/s)$ nonoverlapping segments of equal length s and the same procedure is repeated from the end of the series to the beginning. As a result, $2N_s$ segments are obtained altogether for each time scale s (see [21] for more details). Next, the local trend, $y_\nu(i)$, must be determined for each segment ν by the least-squares fit of the values [30,31]. In this document, the simple linear fit has been used. The local trend is subtracted from the

a)

b)

Fig. 2. Complete time series and its corresponding deseasonalized version (precipitation anomalies) of station No. 15.

profile as follows:

$$F^2(\nu, s) \equiv \frac{1}{s} \sum_{i=1}^{s} \{Y[(\nu - 1)s + i] - y_\nu(i)\}^2 \tag{1}$$

for each segment ν, $\nu = 1, \ldots, N_s$ and

$$F^2(\nu, s) \equiv \frac{1}{s} \sum_{i=1}^{s} \{Y[N - (\nu - N_s)s + i] - y_\nu(i)\}^2 \tag{2}$$

for each segment ν, $\nu = N_s + 1, \ldots, 2N_s$.

Finally, to compute the qth order fluctuation function, the average over all segments is computed:

$$F_q(s) \equiv \left\{ \frac{1}{2N_s} \sum_{\nu=1}^{2N_s} \left[F^2(\nu, s) \right]^{q/2} \right\}^{1/q} \tag{3}$$

Since the averaging procedure in Eq. (3) cannot be used for $q = 0$, a logarithmic averaging procedure must be applied instead [21].

If the analyzed series are long-range power law correlated, $F_q(s)$ increases for large s as a power-law:

$$F_q(s) \sim s^{h(q)} \tag{4}$$

Consequently, the scaling exponent $h(q)$ can be obtained by means of the computation of slopes in the log-log plots of $F_q(s)$ vs s for each q.

Negative q values are related to the intervals with small fluctuations whereas positive ones describe the scaling behavior of large fluctuations [32]. In general, $h(q)$ can depend on q, meaning that small and large fluctuations significantly scale in different ways. Only if $h(q)$ is independent of q, the series has monofractal nature.

For stationary signals, $h(2)$ is the Hurst exponent H whereas, for non-stationary signals, it is retrieved from $H = h(2) - 1$ [33]. For this reason, $h(q)$ is called as generalized Hurst exponent [21,26,34]. The standard Hurst exponent, H, provides information about the long-range correlations of the signals [34].

2.3. Relation to standard multifractal analysis

Kantelhardt et al. obtained an analytical expression [21] that connected the MF-DFA to the standard box counting formalism [17,18]. As they demonstrated, the scaling exponent $h(q)$ defined in Eq. (4) is related to the scaling exponent $\tau(q)$, which is determined by the partition function of the multifractal formalism. Therefore, the multifractal spectrum or singularity spectrum, $f(\alpha)$, can be computed via the Legendre transform as [35]:

$$\alpha = \frac{d\tau(q)}{dq} \quad \text{and} \quad f(\alpha) = q\alpha - \tau(q) \tag{5}$$

where α is the singularity strength or Hölder exponent [36].

The shape of $f(\alpha)$ is often a concave-down parabola with a maximum value which is the most dominant scaling behavior [20]. The singularity strength at which $f(\alpha)$ reaches its maximum value is usually denoted by α_0. Large values of this parameter indicates that the underlying process has "fine-structure" and is more complex [15,37]. Another important quantity from this spectrum is its width, w, which provides information about the degree of multifractality of the signal [16]. A monofractal time series will have a spectral width close to zero.

There are different kinds of parameters in literature to measure the asymmetry of multifractal spectra [15,20,37–39]. In this manuscript, it is used one based on the work of Shimizu et al. [37], which takes the multifractal spectrum and compute the second order polynomial fit of the shifted curve:

$$f(\alpha) = A(\alpha - \alpha_0)^2 + B(\alpha - \alpha_0) + C \tag{6}$$

The B coefficient is usually known as the asymmetry parameter. When this parameter is equal to zero, the spectrum itself is
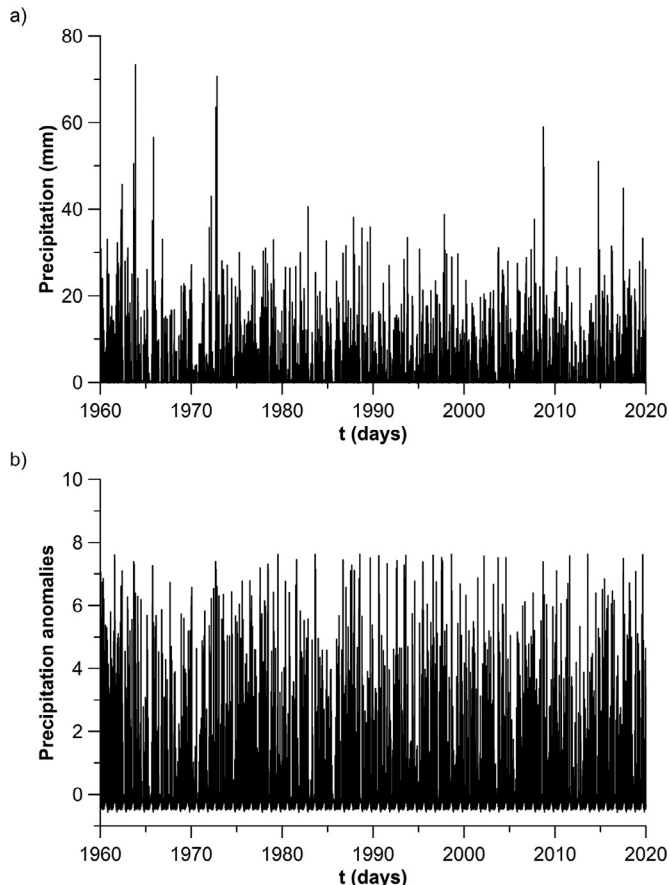
symmetrical. On the other hand, if $B > 0$ the curve is left-skewed and it is right-skewed when $B < 0$ [19,37]. A right-skewed spectrum indicates that small fluctuations ($q < 0$) are favored and the time series is less singular and has "fine-structure" [37,40]. A left-skewed shape is associated to time series which are more singular and are characterized by a "loss of fine-structure".

3. Results and discussion

3.1. Descriptive statistics and trend analysis of annual precipitation

Annual precipitation series were computed from daily records and linear fits, based on least-squares regressions, were applied to these series as a preliminary study of inter-annual variability. The presence of significant linear trends was analyzed for each location. Results are given in Table 1. To this aim, t-tests were performed.

A total amount of 14 stations (48% of sample) shows statistically significant negative trends in the whole period 1960 - 2019. An example of four stations is depicted in Fig. 3, where trends are statistically significant in the considered period. In these stations, trends of -10.90, -1.71, -4.10 and -2.59 mm/year, respectively, were found. The most pronounced decreasing trend corresponds to the station No. 2 (Fig. 3(a)), located at the northwestern coastal subregion of the Iberian Peninsula, which is characterized by abundant precipitation. The second highest decreasing trend belongs to the station No. 21, which is also located at this region. The rest of locations with significant trends belong to the central and southern mainland subregions, except for No. 24 (Fig. 3(d)), which is at the northeastern Mediterranean coastland. Furthermore, all these 14 significant trends are consistent with a decrease in mean and standard deviation of annual precipitation for the same stations between both subperiods 1960 - 1989 and 1990 - 2019 (see Table 1).

3.2. Hurst exponents for different regions and for periods 1960 - 1989 and 1990 - 2019

MF-DFA method was applied to deseasonalized daily precipitation series at 29 locations for each subperiod. The q dependent fluctuation function was obtained from these signals for $q \in [-5, 5]$ with step 0.5 and over a wide range of time scale s, more precisely, from $s = 10$ to 1094 days ($\approx N/10$) and step of 2. Consequently, log-log plots of $F_q(s)$ vs s were obtained for each case. Plots for stations No. 15, 20 and 2 in both subperiods are depicted in Fig. 4. It can be observed that the fluctuation function has three clearly differentiated scaling regions, indicated by (i) - (iii). All stations exhibit these three distinct regimes. However, the amplitudes of these regions vary, and might be shifted depending on the location (see Fig. 4). Moreover, the same location can exhibit different limits for the three regions ((i) – (iii)) in both subperiods of 30 years. Average values of crossovers that separate the three scaling regimes are the following. The average first crossover that separate regions (i) and (ii) is 45 and 41 days for the first and second subperiods, respectively. The second average crossovers are 151 and 134 days.

The power spectra of time series only show two different scaling regions which can be clearly distinguished, as it can be seen for the above-mentioned stations in Fig. 4(g), (h). Most stations display statistically non-significant slopes for low frequencies, while all of them show marked slopes for high frequencies. This means that for a wide range of high frequencies, the precipitation series show a power-law decay of the spectrum, $P(f) \propto f^{-\beta}$, what indicates a strong persistence at small scales [41]. The linear fits in this last interval of frequencies agree the region (i) found for s. As a consequence, both results confirm that fluctuations of precipitation series present mainly two different scaling regimes for large and small timescales, while the region (ii) seems to be a transition region for small fluctuations ($q < 0$).
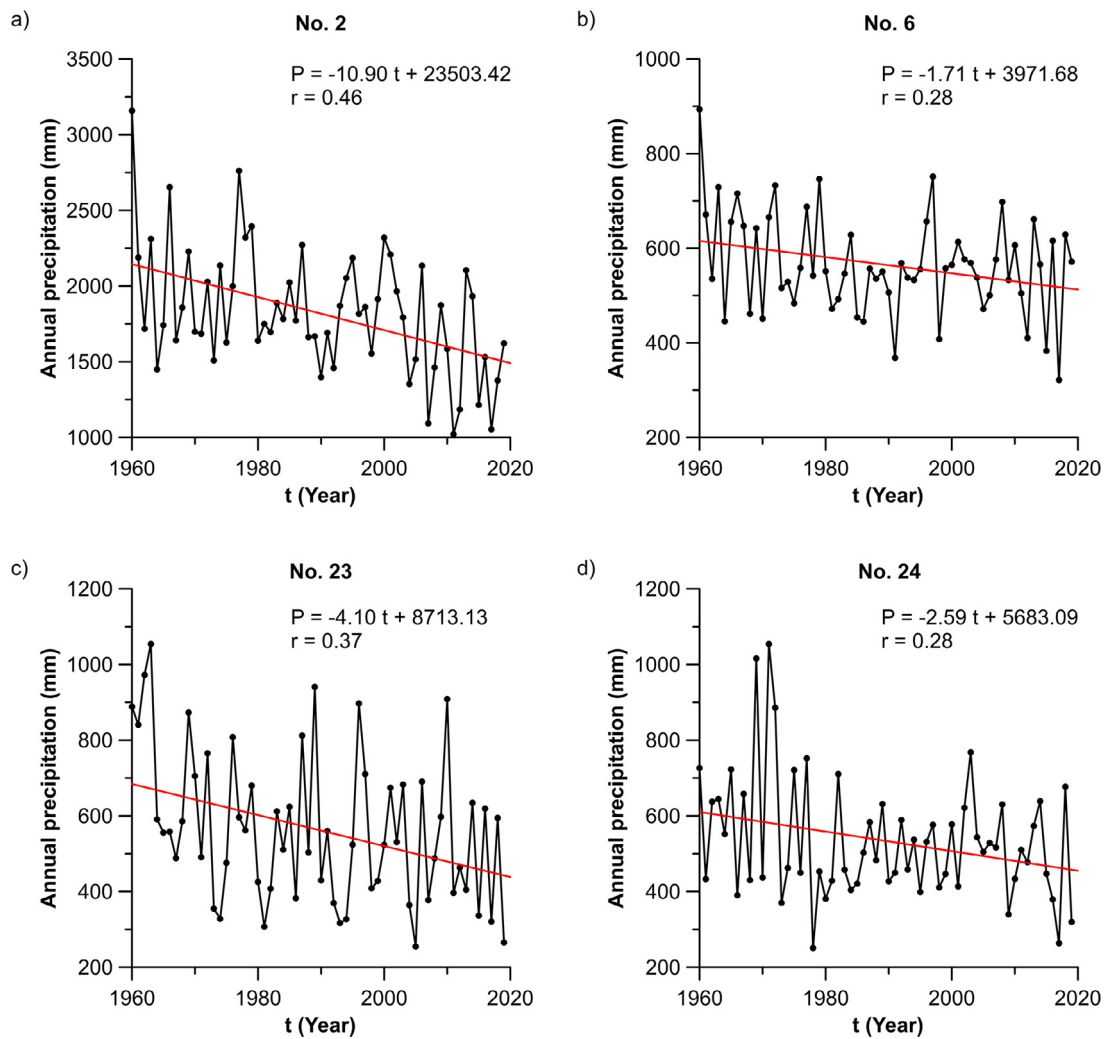
Table 1

Mean, standard deviation (SD) and daily maximum (Max.) of precipitation for each subperiod, together with the slope and Pearson correlation coefficient of linear fits obtained by least-squares regression of annual precipitation series. Slopes highlighted in bold are statistically significant at 95% confidence level.

No.	1960–1989			1990–2019			Annual trends	
	Mean	SD	Max.	Mean	SD	Max.	Slope (mm/year)	R
1	1014.1	169.5	66.6	1017.0	175.7	132.7	−0.06 ± 1.3	0.01
2	1975.4	400.8	218.0	1671.3	366.4	118.6	**−10.90 ± 2.7**	0.46
3	370.2	98.0	78.6	351.5	101.0	146.6	−0.27 ± 0.7	0.05
4	359.6	116.9	220.2	286.3	114.7	270.2	−1.22 ± 0.9	0.18
5	507.8	134.8	70.5	424.8	130.5	119.1	**−2.54 ± 1.0**	0.32
6	584.7	111.4	51.6	545.1	96.9	52.4	**−1.71 ± 0.8**	0.28
7	577.9	151.2	69.6	490.9	115.0	98.2	**−2.84 ± 1.0**	0.35
8	1590.5	242.1	149.8	1560.2	221.1	167.7	−0.20 ± 1.7	0.02
9	1747.0	268.5	130.4	1686.3	257.3	185.2	−2.29 ± 2.0	0.15
10	390.6	89.0	53.6	356.3	117.0	69.3	−0.93 ± 0.8	0.16
11	391.1	78.9	64.6	429.3	87.0	82.6	0.71 ± 0.6	0.15
12	568.5	116.3	98.5	495.5	109.3	56.5	**−1.92 ± 0.8**	0.28
13	668.0	146.6	58.3	638.1	140.9	63.6	−0.50 ± 1.1	0.06
14	429.4	100.7	62.0	352.3	80.5	64.6	**−2.32 ± 0.7**	0.41
15	423.2	133.8	73.4	367.4	95.2	58.9	**−1.89 ± 0.9**	0.28
16	472.4	111.6	66.8	411.7	93.4	79.4	**−2.04 ± 0.8**	0.34
17	464.3	121.3	87.0	411.1	95.8	50.2	**−1.65 ± 0.8**	0.26
18	1438.5	323.0	116.0	1254.6	296.5	150.0	−4.61 ± 2.3	0.25
19	594.2	237.3	151.0	502.2	237.7	132.7	−3.14 ± 1.8	0.23
20	296.5	117.5	99.8	287.4	92.7	179.7	0.34 ± 0.8	0.06
21	2001.6	357.3	175.0	1690.4	347.4	171.9	**−9.89 ± 2.6**	0.45
22	395.8	88.2	48.7	354.6	76.9	50.3	**−1.34 ± 0.6**	0.28
23	623.3	202.7	101.0	503.3	171.5	109.3	**−4.10 ± 1.4**	0.37
24	568.3	192.8	176.5	499.6	111.4	140.8	**−2.59 ± 1.2**	0.28
25	465.1	187.2	148.4	454.4	154.0	178.2	0.22 ± 1.3	0.02
26	486.9	109.6	80.0	422.6	108.8	60.5	**−1.88 ± 0.8**	0.29
27	397.6	121.9	66.1	388.0	89.8	51.4	−0.67 ± 0.8	0.11
28	434.3	97.8	76.6	392.9	95.7	68.8	−0.94 ± 0.7	0.17
29	315.3	77.3	67.3	326.9	88.1	70.8	0.56 ± 0.6	0.12

Fig. 3. Linear fits of annual precipitation in the period 1960–2019 of four meteorological stations.

The best linear fits of $F_q(s)$ in station No. 15 for regions (i) and (iii) are depicted in Fig. 5(a). Generalized Hurst exponents, $h(q)$, obtained from these linear fits are shown against q moments in Fig. 5(b). A non-monotonic function of q can be seen in the region (i) due to the abrupt change of the tendency for negatives q values (see Fig. 5(a), (b)). This phenomenon might be related to the limited resolution of the daily time series which might be causing spurious results when the small fluctuations are magnified by the method in these smaller scales. Similar outcomes have been obtained for the rest of stations.

A clear evidence of multifractality is the q dependence of h. In fact, a measurement of the degree of multifractality is the range of $h(q)$ [32]. There is a wide range of h for small timescales and a small but significant range of values for large timescales, as it is shown in the Fig. 5(b). Therefore, these signals are multifractals and show a greater degree of multifractality at small timescales.

Regarding the well-known Hurst exponent, H, some interesting results have been obtained. All values are lower than 1, what indicates that time series are stationary [33]. The greatest values of H correspond to the smallest timescales (region (i)), as it is also confirmed by the marked slopes found in the power spectra. For this regime, $H_i \in [0.58, 0.79]$, while the region (iii) shows values of $H_{iii} \in [0.38, 0.65]$. These last weak long-term correlations depend on the location and only station No. 16 for the last period has a Hurst exponent similar to a white noise process considering results obtained from MF-DFA. Nevertheless, power spectra at these timescales only exhibit statistically significant slopes for stations No. 3, 8, 13 and 19 for the first period and No. 1, 2, 11, 18 and 21 for the second one. Thus, all precipitation series show a regime with strong long-term persistence for small timescales and other regime where they resemble white noise for large timescales. Due to this discrepancy in the results, the analysis of the possible changes in H has been only performed for the small timescales (region (i)), where the values of H are considerably larger and the persistence is more marked.

The spatial distribution of H in both periods of 30 years have been depicted in Fig. 5(c), (d). Both periods show the highest values ($H \in [0.70, 0.79]$) at the northeastern Atlantic coast, which gradually decrease to the southeast and the east. In this last area, the reduction is even more noticeable. The lowest values in both periods correspond to stations No. 20, 28 and 29. The analysis of changes between periods 1960–1989 and 1990–2019 reveal that there is a little reduction of persistence in most stations of the central and northwestern inland areas and in the southern part. These regions present values of $H \in [0.64, 0.73]$ for the first period and $H \in [0.61, 0.70]$ for the second one.

3.3. Parameters of the singularity spectra for different regions for periods 1960–1989 and 1990–2019

The non-monotonic function of q found for the scaling exponent in the region (i) in most stations leads to unreliable singular-
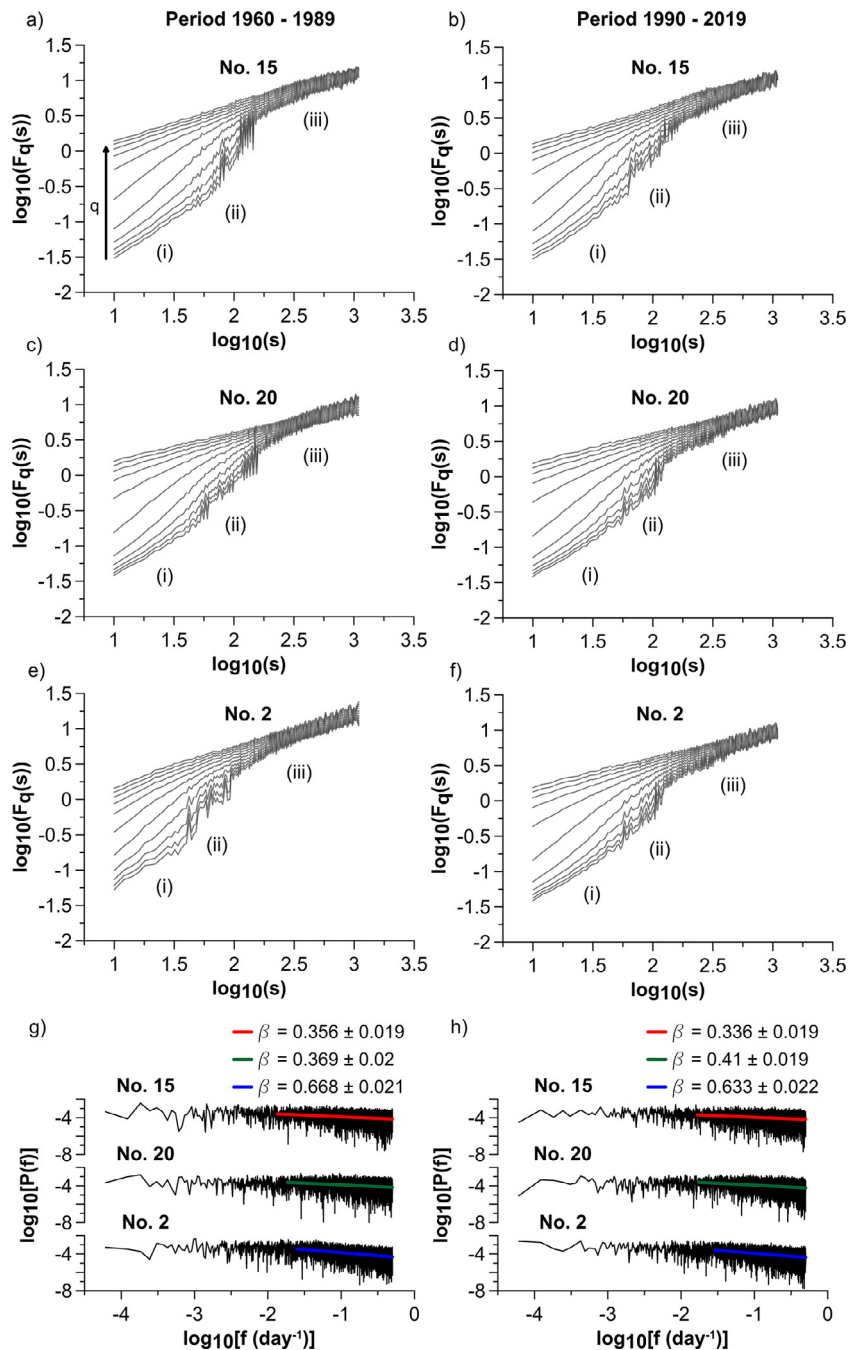
Fig. 4. (a–f) Log-log plots of fluctuations function $F_q(s)$ vs time scale s for different stations and periods. For clarity reasons, only half of the analyzed curves are depicted. (g, h) Power spectrum of the same stations and their corresponding slopes.

ity spectra $f(\alpha)$ when the Eq. (5) is applied. They exhibit a non-parabolic shape with abrupt changes for $q < 0$ and large statistical errors. Therefore, the analysis of changes in parameters that describe the multifractal spectra (α_0, w and B) has been only performed for the region (iii), i.e., for large timescales. An example of these spectra can be found in Fig. 6(a), (b). Similar parabolic shapes have been obtained for every station. In the given example, the multifractal parameters are shown for both subperiods. α_0 increases in the last period and, as a result, the spectrum is shifted to the right. Both curves show widths significantly greater than zero, what proves that signals have a multifractal behavior, although it is more evident for the period 1990 - 2019. Two different behaviors can be found for the asymmetry

parameter B. For the sake of clarity, the shifted curves of spectra with respect to its maximum were depicted together with its respective second order polynomial fit in Fig. 6(c), (d). Additionally, the second order polynomial functions with the same A and C coefficients and null B coefficient are plotted in the same figures. A comparison between both fits is enough to see that this station had approximately symmetric multifractal spectrum (Fig. 6(c)), which changed to a left-skewed spectrum in the last 30 years, with $B = 0.14 \pm 0.04$ (Fig. 6(d)). As explained previously in Section 2.3, this means that this time series becomes more singular, with loss of "fine-structure". The multifractal parameters for all locations are shown with their statistical errors in Table A.2.
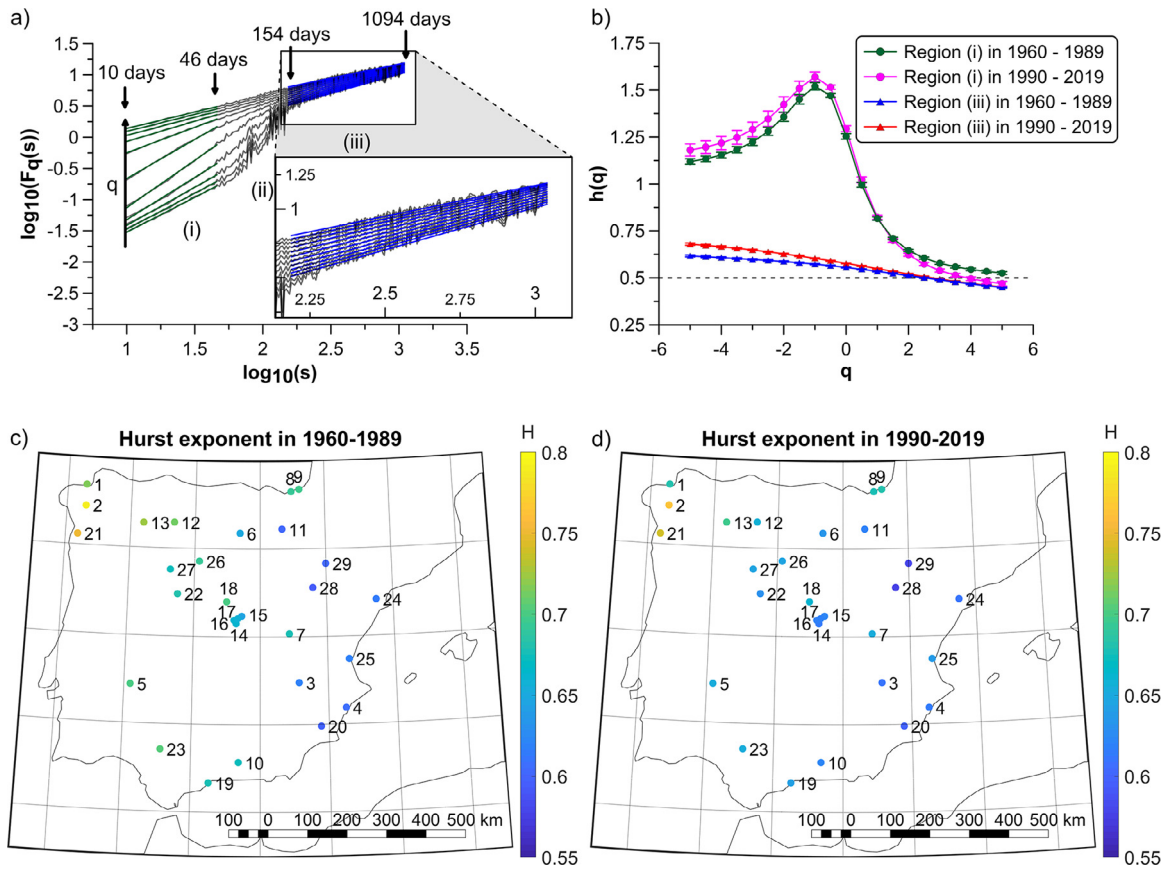
Fig. 5. (a) Log-log plot of fluctuation function $F_q(q)$ vs time scale s for different q values in station No. 15 and subperiod 1960 – 1989. (b) $h(q)$ and their respective statistical errors obtained for regions (i) and (iii) for the same station. (c, d) Spatial distribution of H for the region (i).
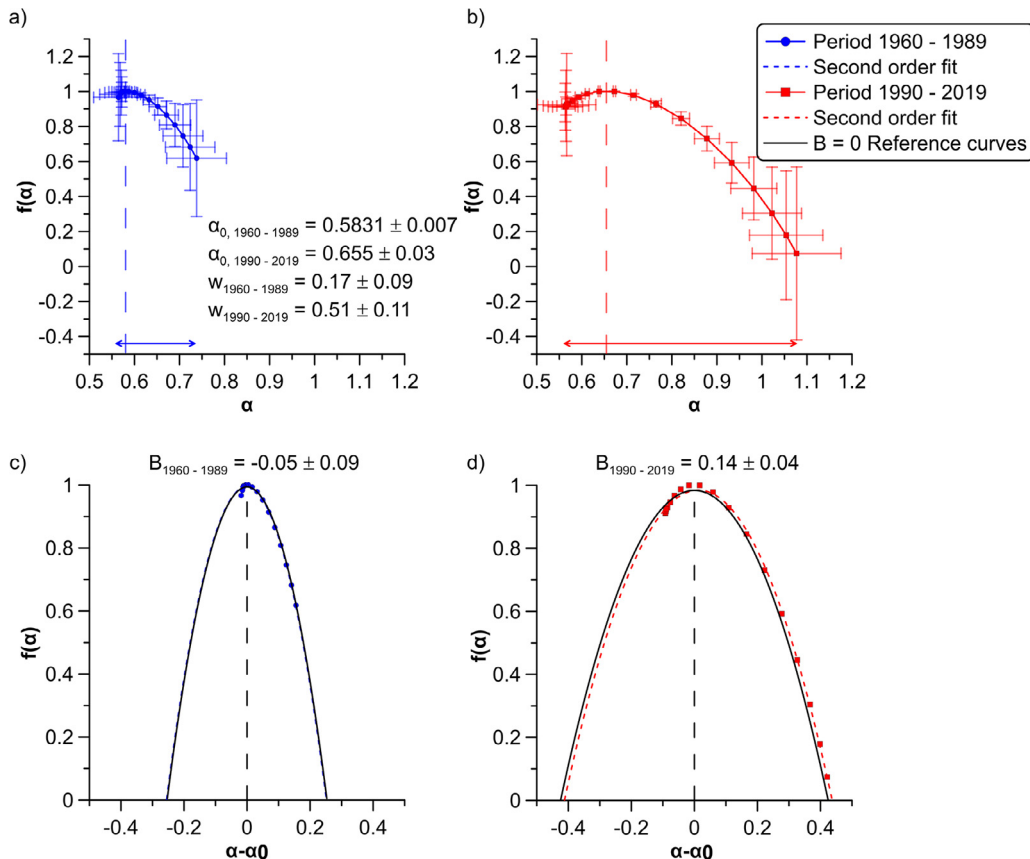

Fig. 6. (a, b) Singularity spectra $f(\alpha)$ in station No. 2 in both subperiods obtained for the scaling region (iii). (c, d) Shifted curves of the spectra shown in panels (a, b). The reference curves with the same A and C coefficients from second order fits and $B = 0$ are depicted as solid black lines. For clarity reasons, error bars have been omitted here.
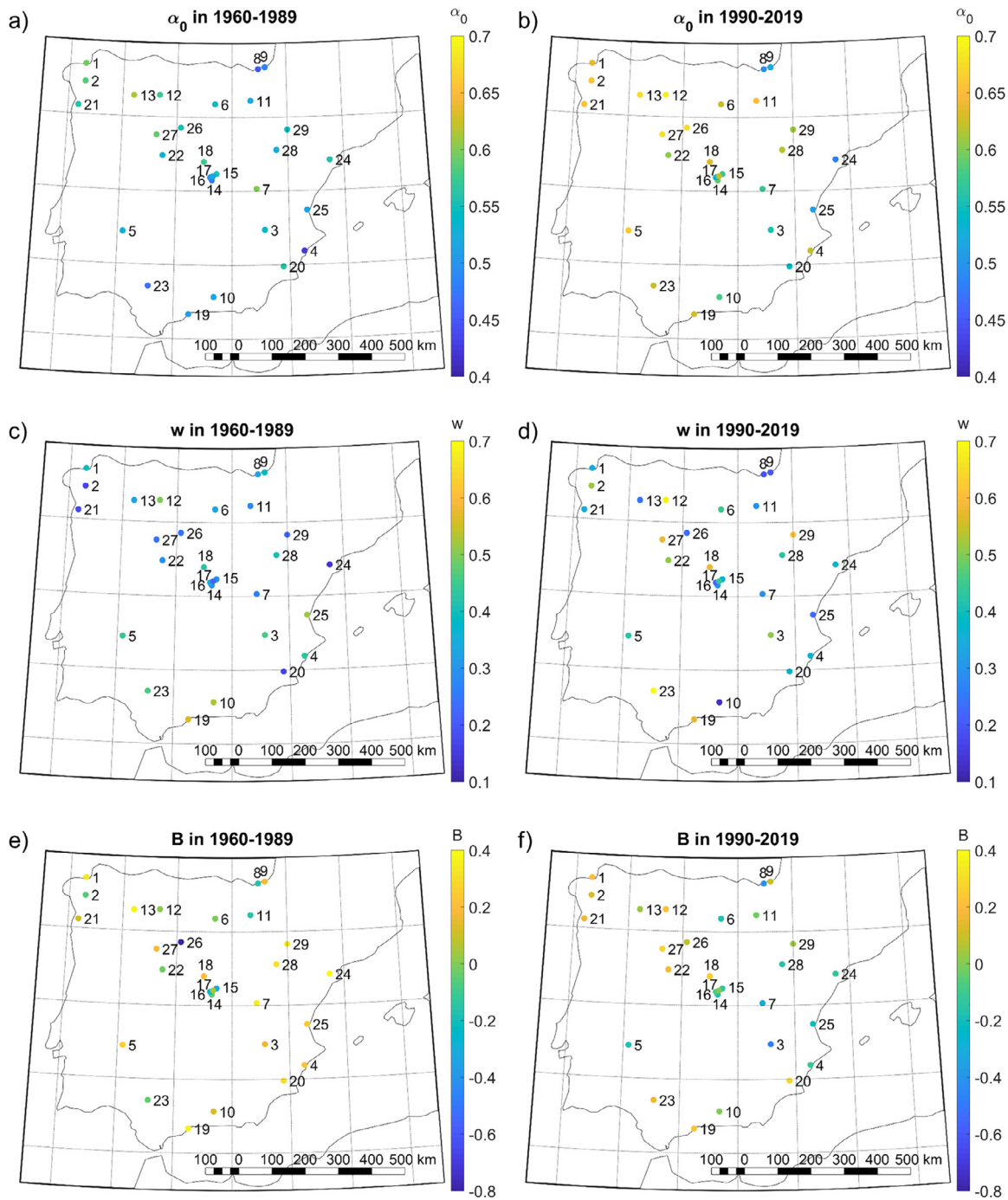
Fig. 7. Spatial distribution of multifractal parameters obtained for the scaling region (iii).

The spatial distribution for the maximum scaling exponent α_0 for period 1960–1989 is depicted in Fig. 7(a). For this period, there is a high variability in α_0. However, some areas which present more homogeneity can be observed. The northwestern coastal part (stations No. 1, 2 and 21), with $\alpha_0 \in [0.56, 0.60]$; the northeastern area of the Iberian Peninsula (stations No. 6, 11, 29 and 28), with $\alpha_0 \in [0.52, 0.55]$; the southern part (No. 19 and 10, $\alpha_0 \sim [0.50, 0.52]$) and the northern Atlantic coast (No. 8 and 9, $\alpha_0 \in [0.45, 0.49]$). This last area shows some of the lowest values of α_0, denoting that these series are more characterized by a "smooth-structure". On the contrary, stations No. 13 and 7 are those with

the highest value (see Table A.2), meaning that these series are more complex (possess "fine-structure").

On the other hand, the plot for the last 30 years is depicted in Fig. 7(b). There is a slight increase of values for the most part of the sample in the period 1990–2019. The northwestern Atlantic coast present values of $\alpha_0 \in [0.63, 0.66]$, while for the northwestern inland area, $\alpha_0 \in [0.67, 0.69]$; the northeastern area, now excluding station No. 11, which shows values of $\alpha_0 \in [0.60, 0.66]$ and the northern Atlantic coast, with $\alpha_0 \in [0.49, 0.53]$. In this last period, the southern part is more heterogeneous.
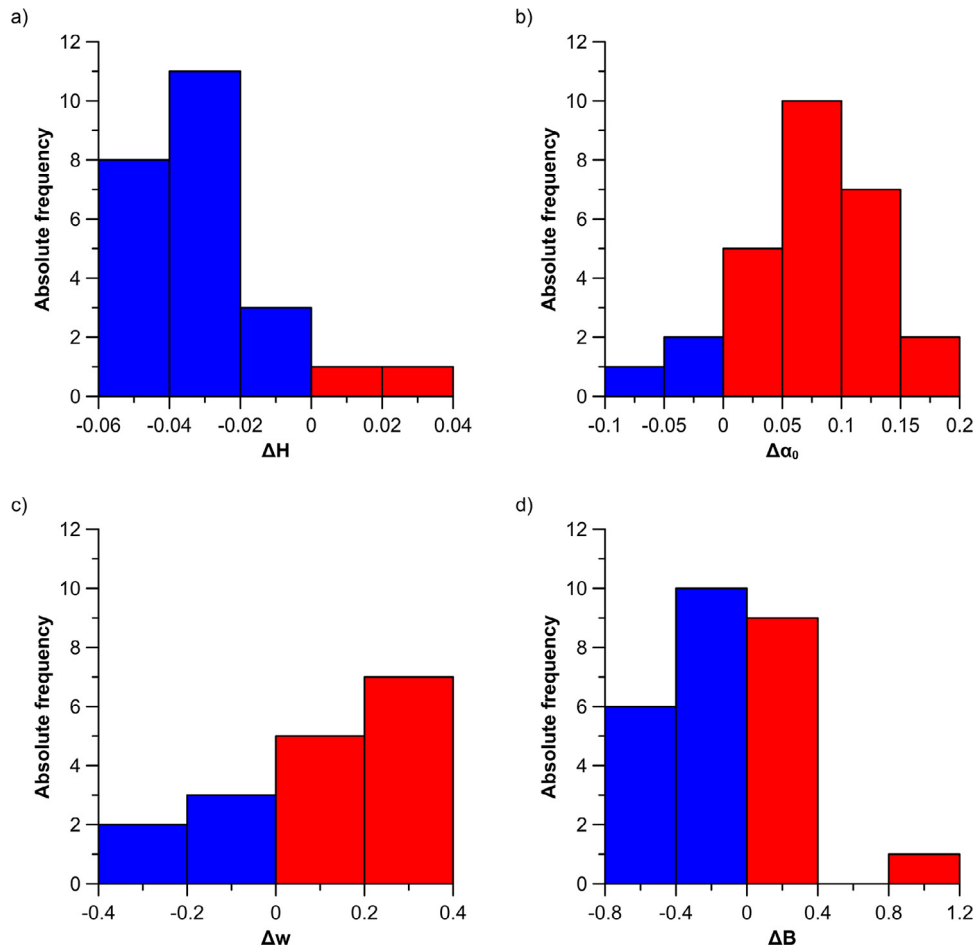
Fig. 8. Histograms of changes in parameters between periods 1960 - 1989 and 1990 - 2019. The width of the bins exceeds the largest statistical error in each parameter. Non-significant changes are omitted. (a) Hurst exponent in the scaling region (i). (b, c, d) Parameters of the multifractal spectra in the scaling region (iii).

Fig. 7(c), (d) depict the spatial distribution of the spectral width w for both subperiods. This magnitude shows a wide range of values and high spatial variability. Additionally, a little less than half of stations exhibit non-significant changes. Therefore, it cannot be identified any geographical pattern where these changes are consistent. The highest values correspond to stations No. 19 in the first period and No. 23 in the second one. This means that these time series have relatively more scaling exponents for large and low fluctuations in the respective periods and, thus, they possess a higher degree of multifractality. On the contrary, the lowest values (stations No. 24 in the period 1960–1989 and No. 10 in 1990–2019) are not significantly different from zero (see Table A.2). Hence, these signals are monofractals in the respective periods.

For the asymmetry parameter in the first period (see Fig. 7(e)), it can be observed a region with high homogeneity and positive values ($B \in [0.12, 0.39]$). This region covers the most part of the eastern area. As a result, their respective multifractal spectra are left-skewed. This means that series from the eastern part of the Peninsula in this period are characterized by being singular and having low fluctuations with "smooth-structure". Outcomes for the period 1990 - 2019 are depicted in Fig. 7(f). In this figure, the geographic pattern found in the eastern part of the Iberian Peninsula changes differently depending on the location. However, almost all the locations in this subregion show a decrease of the asymmetry coefficient, what means that they become less singular and exhibit a more complex structure of the low fluctuations.

Furthermore, some of these locations (No. 4, 25, 28 and 24) slightly vary its asymmetry from left to right-skewed, while spectra from stations No. 3 and 7 become noticeably right-skewed. Therefore, they display low fluctuations with "fine-structure" in the last period.

3.4. Global changes in H, α_0, w, and B between both periods

To clarify the general changes in H and in multifractal parameters α_0, w and B, their histograms are shown in Fig. 8. There are 22 stations that exhibit a significant decrease of the Hurst exponent between both periods (Fig. 8(a)). This denotes a global reduction of the persistence in the Iberian Peninsula at small timescales. In Fig. 8(b), an increase of α_0 is observed for large scales in 24 stations, what indicates a rise in the complexity of local fluctuations of low magnitude. The width of spectra also shows a rise between both periods, but only for 17 stations (see Fig. 8(c)). For this reason, and because no geographical patterns were found for this parameter, it cannot be discarded that these increases are due to the effect of the local conditions. Lastly, the asymmetry coefficient does not exhibit a marked tendency (see Fig. 8(d)).

4. Conclusions

48% of gauge stations present statistically significant decreasing trends in annual precipitation series between 1960 and 2019. These outcomes are also consistent with a decrease in mean and

standard deviation of annual precipitation between the subperiods 1960–1989 and 1990–2019. Most stations with decreasing annual rainfall records are distributed over the central part of Spain, which is characterized by a strong continental climate with a relatively low precipitation amount (between 400 and 600 mm/year) [10]. Thus, this region is uniformly becoming more arid in the last period (1990 - 2019).

The MF-DFA method reveals that the fluctuations of the daily precipitation series contain three distinct scaling regions. In the intermediate scales, the curves mainly differ for the fluctuations of low magnitude ($q < 0$). The analysis of the power spectrum only exhibits two different regimes, showing clear differences between the small and large timescales. This indicates that the small fluctuations at intermediate scales belong to a transition region between the mentioned regimes. Similar findings of multi-scale multifractality were also found for precipitation with hourly resolution in the United States [41]. In addition, they have also been observed in other complex systems in different fields of knowledge, such as physics [42], traffic flow [43], astronomy [44] or economics [32].

Generalized Hurst exponents depend on q moments in every case, what is a clear evidence of multifractality. The degree of multifractality is higher for small timescales. In these scales, the series exhibit a non-monotonic shape of $h(q)$ for small fluctuations ($q < 0$). This phenomenon might be a result of the influence of the time series resolution on the analysis at the smallest timescales. This led to unreliable results in the computation of the singularity spectra and the study of these ones was performed for large timescales only.

All stations present a strong long-term persistence for small timescales and weak correlations for large timescales. However, these last correlations are poorly confirmed by the power spectra for a few stations only. The standard Hurst exponent computed for small timescales shows a geographical pattern. It approximately follows the strong gradient of annual precipitation which characterizes the Iberian Peninsula. This gradient exhibits large values to the north and northwest and lower values towards the southeast [10]. The persistence is reduced in most stations between both studied periods, what might be related to the annual precipitation decrease found in the trend analysis.

The features of multifractal spectra for large timescales show more complex patterns. In fact, the spatial analysis of results is not coherent among different parameters. The main conclusions drawn are detailed next. α_0 results show that there is a global rise in complexity of low fluctuations (more presence of "fine-structure"), mainly in the Atlantic coast and the northern inland area. On the other hand, half of stations exhibit significant variations of the width, w, between both periods, although no pattern can be observed. This might denote that the degree of multifractality might be affected by the local conditions. Finally, B only shows consistent variations in the eastern part of the Iberian Peninsula, where the precipitation series become less singular and have more presence of "fine-structure" in the last period. Nevertheless, the strength of these changes varies depending on the location and is particularly notable in some stations from the central area of the Mediterranean coast and inland. This might be related to the change in the frequency and direction of the Mediterranean cyclones that affects this part of the Iberian Peninsula [45].

It has been shown that several scaling regimes with different multifractal features are present in the precipitation series of the Iberian Peninsula. The nonlinear multifractal features are proved to be more complex and irregularly distributed than those derived from the linear analysis. Furthermore, it has been observed that some of these properties change over time in different scales. This fact might reveal an important role of these parameters in the long-term change of the precipitation.

Declaration of Competing Interest

CRediT authorship contribution statement

Javier Gómez-Gómez: Conceptualization, Methodology, Software, Validation, Visualization, Formal analysis, Data curation, Investigation, Writing – original draft. **Rafael Carmona-Cabezas:** Conceptualization, Software, Investigation, Resources. **Elena Sánchez-López:** Conceptualization, Resources, Supervision. **Eduardo Gutiérrez de Ravé:** Project administration, Funding acquisition, Supervision. **Francisco José Jiménez-Hornero:** Project administration, Funding acquisition, Supervision.

Acknowledgements

Appendix A

Table A.1
Description of gauge stations of daily precipitation data series recorded at the Iberian Peninsula in the period 1960–2019.

No.	Location	Latitude (°N)	Longitude (°W)	Altitude (m a.s.l.)
1	La Coruña	43.37	8.42	58
2	Santiago de Compostela Airport	42.89	8.41	370
3	Albacete Air Base	38.95	1.86	702
4	Alicante	38.37	0.49	81
5	Badajoz Airport	38.88	6.81	185
6	Burgos Airport	42.36	3.62	891
7	Cuenca	40.07	2.13	948
8	San Sebastián, Igueldo	43.31	2.04	251
9	Hondarribia, Malkarroa	43.36	1.79	4
10	Granada Air Base	37.14	3.63	687
11	Logroño Airport	42.45	2.33	353
12	León, Virgen del Camino	42.59	5.65	912
13	Ponferrada	42.56	6.60	534
14	Getafe	40.30	3.72	620
15	Madrid Airport	40.47	3.56	609
16	Madrid, Cuatro Vientos	40.38	3.79	690
17	Madrid, Retiro	40.41	3.68	667
18	Navacerrada Pass	40.79	4.01	1894
19	Málaga Airport	36.67	4.48	5
20	Alcantarilla Air Base	37.96	1.23	75
21	Vigo Airport	42.24	8.62	261
22	Salamanca Airport	40.96	5.50	790
23	Sevilla Airport	37.42	5.88	34
24	Tortosa	40.82	−0.49	50
25	Valencia	39.48	0.37	11
26	Valladolid Airport	41.71	4.86	846
27	Zamora	41.52	5.74	656
28	Daroca	41.11	1.41	779
29	Zaragoza Airport	41.66	1.00	249

Table A.2

Multifractal spectra parameters (α_0, w and B) in the scaling region (iii) and their respective statistical errors in every location for both subperiods. Results highlighted in bold are not significantly different from zero.

No.	α_0 1960 - 1989	α_0 1990 - 2019	w 1960 - 1989	w 1990 - 2019	B 1960 - 1989	B 1990 - 2019
1	0.5940 ± 0.013	0.6356 ± 0.013	0.40 ± 0.08	0.35 ± 0.11	0.34 ± 0.04	0.20 ± 0.09
2	0.5831 ± 0.007	0.655 ± 0.03	0.17 ± 0.09	0.51 ± 0.11	**−0.05 ± 0.09**	0.14 ± 0.04
3	0.5364 ± 0.008	0.5593 ± 0.014	0.46 ± 0.14	0.51 ± 0.11	**0.17 ± 0.19**	−0.46 ± 0.08
4	0.4276 ± 0.021	0.623 ± 0.03	0.43 ± 0.11	0.37 ± 0.13	0.21 ± 0.05	−0.114 ± 0.015
5	0.5272 ± 0.019	0.661 ± 0.03	0.45 ± 0.10	0.42 ± 0.12	0.250 ± 0.023	−0.180 ± 0.021
6	0.5485 ± 0.013	0.6209 ± 0.021	0.34 ± 0.09	0.45 ± 0.08	−0.0083 ± 0.0020	−0.179 ± 0.017
7	0.6004 ± 0.010	0.5689 ± 0.011	0.26 ± 0.08	0.29 ± 0.10	0.35 ± 0.08	−0.30 ± 0.08
8	0.4501 ± 0.017	0.4939 ± 0.006	0.33 ± 0.08	0.18 ± 0.06	−0.150 ± 0.016	−0.41 ± 0.06
9	0.4853 ± 0.015	0.5218 ± 0.007	0.38 ± 0.08	0.19 ± 0.08	0.182 ± 0.017	0.083 ± 0.012
10	0.518 ± 0.03	0.5820 ± 0.005	0.53 ± 0.10	**0.14 ± 0.15**	0.122 ± 0.014	**0.00 ± 0.09**
11	0.5210 ± 0.013	0.6508 ± 0.016	0.28 ± 0.10	0.29 ± 0.10	−0.154 ± 0.014	−0.028 ± 0.013
12	0.5739 ± 0.019	0.689 ± 0.03	0.50 ± 0.09	0.68 ± 0.10	0.010 ± 0.004	0.217 ± 0.018
13	0.6145 ± 0.014	0.6723 ± 0.013	0.33 ± 0.09	0.24 ± 0.06	0.37 ± 0.05	0.038 ± 0.020
14	0.4769 ± 0.014	0.5880 ± 0.010	0.29 ± 0.08	0.30 ± 0.11	−0.049 ± 0.009	−0.17 ± 0.10
15	0.5549 ± 0.014	0.5771 ± 0.020	0.29 ± 0.08	0.37 ± 0.10	−0.33 ± 0.04	−0.128 ± 0.015
16	0.4989 ± 0.017	0.5336 ± 0.010	0.35 ± 0.07	0.22 ± 0.11	−0.26 ± 0.03	−0.082 ± 0.009
17	0.5195 ± 0.008	0.6206 ± 0.021	0.22 ± 0.09	0.44 ± 0.11	**0.04 ± 0.07**	**−0.003 ± 0.008**
18	0.5759 ± 0.021	0.630 ± 0.03	0.42 ± 0.16	0.58 ± 0.09	0.199 ± 0.020	0.25 ± 0.04
19	0.5098 ± 0.024	0.627 ± 0.05	0.57 ± 0.11	0.58 ± 0.16	0.37 ± 0.06	0.21 ± 0.03
20	0.5610 ± 0.004	0.5410 ± 0.016	0.17 ± 0.12	0.37 ± 0.10	0.29 ± 0.15	0.27 ± 0.06
21	0.5640 ± 0.006	0.6562 ± 0.018	0.18 ± 0.09	0.36 ± 0.12	0.11 ± 0.10	0.172 ± 0.019
22	0.5317 ± 0.013	0.6056 ± 0.022	0.29 ± 0.08	0.51 ± 0.09	−0.030 ± 0.007	0.187 ± 0.019
23	0.4658 ± 0.019	0.621 ± 0.04	0.46 ± 0.15	0.73 ± 0.11	−0.044 ± 0.011	0.159 ± 0.017
24	0.5573 ± 0.017	0.4808 ± 0.016	**0.14 ± 0.17**	0.36 ± 0.12	0.4 ± 0.4	−0.132 ± 0.011
25	0.5146 ± 0.022	0.5083 ± 0.012	0.52 ± 0.13	0.23 ± 0.09	0.24 ± 0.05	−0.21 ± 0.04
26	0.5504 ± 0.013	0.6720 ± 0.009	0.24 ± 0.12	0.23 ± 0.12	−0.8 ± 0.3	0.089 ± 0.017
27	0.5904 ± 0.009	0.6792 ± 0.024	0.25 ± 0.09	0.58 ± 0.11	0.19 ± 0.04	0.27 ± 0.06
28	0.5254 ± 0.015	0.6194 ± 0.016	0.41 ± 0.11	0.42 ± 0.08	0.32 ± 0.06	−0.146 ± 0.016
29	0.5488 ± 0.010	0.6071 ± 0.020	0.23 ± 0.09	0.61 ± 0.09	0.34 ± 0.06	0.037 ± 0.008

References

[1] IPCC Summary for PolicymakersClimate change 2013: the physical science basis. contribution of working group i to the fifth assessment report of the intergovernmental panel on climate change. Stocker TF, Qin D, Plattner GK, Tignor M, Allen SK, Boschung J, et al., editors. Cambridge, United KingdomNew York, NY, USA: Cambridge University Press; 2013.

[2] . Summary for policymakers. In: Field CB, Barros VR, Dokken DJ, Mach KJ, Mastrandrea MD, Bilir TE, et al., editors. Climate change 2014: impacts, adaptation, and vulnerability. part A: global and sectoral aspects. contribution of working group ii to the fifth assessment report of the intergovernmental panel on climate change. Cambridge, United KingdomNew York, NY, USA: Cambridge University Press; 2014. p. 1–32.

[3] Sankaran A, Chavan SR, Ali M, Sindhu AD, Dharan DS, Khan MI. Spatiotemporal variability of multifractal properties of fineresolution daily gridded rainfall fields over India. Nat Hazards 2021;106:1951–79. doi:10.1007/s11069-021-04523-0.

[4] Gallego MC, García JA, Vaquero JM, Mateos VL. Changes in frequency and intensity of daily precipitation over the Iberian Peninsula. J Geophys Res 2006;111:D24105. doi:10.1029/2006JD007280.

[5] de Luis M, Brunetti M, Gonzalez-Hidalgo JC, Longares LA, Martin-Vide J. Changes in seasonal precipitation in the Iberian Peninsula during 1946–2005. Glob Planet Chang 2010;74:27–33. doi:10.1016/j.gloplacha.2010.06.006.

[6] Guerreiro SB, Kilsby CG, Fowler HJ. Rainfall in Iberian transnational basins: a drier future for the Douro, Tagus and Guadiana? Clim Chang 2016;135:467–80. doi:10.1007/s10584-015-1575-z.

[7] Esteban-Parra MJ, Rodrigo FS, Castro-Diez Y. Spatial and temporal patterns of precipitation in Spain for the period 1880–1992. Int J Climatol 1998;18:1557–74 10.1002/(SICI)1097-0088(19981130)18:14<1557::AID–JOC328>3.0.CO;2-J.

[8] González-Hidalgo JC, De Luis M, Raventós J, Sánchez JR. Spatial distribution of seasonal rainfall trends in a western Mediterranean area. Int J Climatol 2001;21:843–60. doi:10.1002/joc.647.

[9] De Luis M, González-Hidalgo JC, Longares LA, Štepánek P. Seasonal precipitation trends in the Mediterranean Iberian Peninsula in second half of 20th century. Int J Climatol 2009;29:1312–23. doi:10.1002/joc.1778.

[10] Rodriguez-Puebla C, Encinas AH, Nieto S, Garmendia J. Spatial and temporal patterns of annual precipitation variability over the Iberian Peninsula. Int J Climatol 1998;18:299–316.

[11] De Lima MIP, Marques ACP, De Lima JLMP, Coelho MFES. Precipitation trends in mainland Portugal in the period 1941–2000. IAHS-AISH Publ; 2007. p. 94–102.

[12] López-Moreno JI, Vicente-Serrano SM, Angulo-Martínez M, Beguería S, Kenawy A. Trends in daily precipitation on the northeastern Iberian Peninsula, 1955–2006. Int J Climatol 2010;30:1026–41. doi:10.1002/joc.1945.

[13] de Lima MIP, Santo FE, Ramos AM, de Lima JLMP. Recent changes in daily precipitation and surface air temperature extremes in mainland Portugal, in the period 1941–2007. Atmos Res 2013;127:195–209. doi:10.1016/j.atmosres.2012.10.001.

[14] Baranowski P, Krzyszczak J, Slawinski C, Hoffmann H, Kozyra J, Nieróbca A, et al. Multifractal analysis of meteorological time series to assess climate impacts. Clim Res 2015;65:39–52. doi:10.3354/cr01321.

[15] Baranowski P, Gos M, Krzyszczak J, Siwek K, Kieliszek A, Tkaczyk P. Multifractality of meteorological time series for Poland on the base of MERRA-2 data. Chaos Solitons Fractals 2019;127:318–33. doi:10.1016/j.chaos.2019.07.008.

[16] Krzyszczak J, Baranowski P, Zubik M, Kazandjiev V, Georgieva V, Sławiński C, et al. Multifractal characterization and comparison of meteorological time series from two climatic zones. Theor Appl Climatol 2019;137:1811–24. doi:10.1007/s00704-018-2705-0.

[17] Mandelbrot BB. The fractal geometry of nature. San Francisco: WH Freeman; 1982.

[18] Feder J. Fractals. Boston, MA: Springer US; 1988. doi:101007/978-1-4899-2124-6.

[19] Telesca L, Lapenna V. Measuring multifractality in seismic sequences. Tectonophysics 2006;423:115–23. doi:10.1016/j.tecto.2006.03.023.

[20] Kalamaras N, Tzanis C, Deligiorgi D, Philippopoulos K, Koutsogiannis I. Distribution of air temperature multifractal characteristics over Greece. Atmosphere 2019;10:45. doi:10.3390/atmos10020045.

[21] Kantelhardt JW, Zschiegner SA, Koscielny-Bunde E, Havlin S, Bunde A, Stanley HE. Multifractal detrended fluctuation analysis of nonstationary time series. Phys A 2002;316:87–114.

[22] Burgueño A, Lana X, Serra C, Martínez MD. Daily extreme temperature multifractals in Catalonia. NE Spain. Phys Lett A 2014;378:874–85. doi:10.1016/j.physleta.2014.01.033.

[23] Brunet M, Jones PD, Sigró J, Saladié O, Aguilar E, Moberg A, et al. Temporal and spatial temperature variability and change over Spain during 1850–2005. J Geophys Res 2007;112:D12117. doi:10.1029/2006JD008249.

[24] State Meteorological Agency of Spain, Institute of Meteorology of Portugal. Iberian climate atlas: air temperature and precipitation (1971–2000). State Meteorological Agency of Spain, Institute of Meteorology of Portugal; 2011.

[25] da Silva HS, Silva JRS, Stosic T. Multifractal analysis of air temperature in Brazil. Phys A 2020;549:124333. doi:10.1016/j.physa.2020.124333.

[26] Kantelhardt JW, Rybski D, Zschiegner SA, Braun P, Koscielny-Bunde E, Livina V, et al. Multifractality of river runoff and precipitation: comparison of fluctuation analysis and wavelet methods. Phys A 2003;330:240–5. doi:10.1016/j.physa.2003.08.019.

[27] Koscielny-Bunde E, Kantelhardt JW, Braun P, Bunde A, Havlin S. Long-term persistence and multifractality of river runoff records: detrended fluctuation studies. J Hydrol 2006;322:120–37. doi:10.1016/j.jhydrol.2005.03.004.

[28] Livina VN, Ashkenazy Y, Bunde A, Havlin S. Seasonality effects on nonlinear properties of hydrometeorological records. In: Kropp J, Schellnhuber HJ, editors. Extremis. Berlin, Heidelberg: Springer Berlin Heidelberg; 2011. p. 266–84. doi:10.1007/978-3-642-14863-7_13.

[29] Xavier SFA, Stosic T, Stosic B, Jale JDS, Xavier ÉFM. A Brief multifractal analysis of rainfall dynamics in Piracicaba, São Paulo, Brazil. Acta Sci Technol 2018;40:35116. doi:10.4025/actascitechnol.v40i1.35116.

[30] Bunde A, Havlin S, Kantelhardt JW, Penzel T, Peter JH, Voigt K. Correlated and uncorrelated regions in heart-rate fluctuations during sleep. Phys Rev Lett 2000;85:3736–9. doi:10.1103/PhysRevLett.85.3736.

[31] Oświęcimka P, Drożdż S, Kwapień J, Górski AZ. Effect of detrending on multifractal characteristics. Acta Phys Pol A 2013;123:597–603. doi:10.12693/APhysPolA.123.597.

[32] Pavón-Domínguez P, Serrano S, Jiménez-Hornero FJ, Jiménez-Hornero JE, Gutiérrez de Ravé E, Ariza-Villaverde AB. Multifractal detrended fluctuation analysis of sheep livestock prices in origin. Phys A 2013;392:4466–76. doi:10.1016/j.physa.2013.05.042.

[33] Zhang Q, Xu CY, Chen YD, Yu Z. Multifractal detrended fluctuation analysis of streamflow series of the Yangtze River basin, China. Hydrol Process 2008;22:4997–5003. doi:10.1002/hyp.7119.

[34] Telesca L, Colangelo G, Lapenna V, Macchiato M. Fluctuation dynamics in geo-electrical data: an investigation by using multifractal detrended fluctuation analysis. Phys Lett A 2004;332:398–404. doi:10.1016/j.physleta.2004.10.011.

[35] Kavasseri R, Nagarajan R. A multifractal description of wind speed records. Chaos Solitons Fractals 2005;24:165–73. doi:10.1016/S0960-0779(04)00533-8.

[36] Gonçalvès P, Riedi R, Baraniuk R. A simple statistical analysis of wavelet-based multifractal spectrum estimation. In: Proceedings of the Conference Record of Thirty-Second Asilomar Conference on Signals, Systems and Computers (Cat. No.98CH36284), 1. Pacific Grove, CA, USA: IEEE; 1998. p. 287–91. doi:10.1109/ACSSC.1998.750873.

[37] Shimizu Y, Thurner S, Ehrenberger K. Multifractal spectra as a measure of complexity in human posture. Fractals 2002;10:103–16. doi:10.1142/S0218348X02001130.

[38] Macek WM, Wawrzaszek A. Evolution of asymmetric multifractal scaling of solar wind turbulence in the outer heliosphere. J Geophys Res 2009;114. doi:10.1029/2008JA013795.

[39] Drożdż S, Oświęcimka P. Detecting and interpreting distortions in hierarchical organization of complex time series. Phys Rev E 2015;91:030902. doi:10.1103/PhysRevE.91.030902.

[40] Gómez-Gómez J, Carmona-Cabezas R, Ariza-Villaverde AB, Gutiérrez de Ravé E, Jiménez-Hornero FJ. Multifractal detrended fluctuation analysis of temperature in Spain (1960–2019). Phys A 2021;578:126118. doi:10.1016/j.physa.2021.126118.

[41] Yang L, Fu Z. Process-dependent persistence in precipitation records. Phys A Stat Mech Appl 2019;527:121459. doi:10.1016/j.physa.2019.121459.

[42] Tadić B, Mijatović S, Janićević S, Spasojević D, Rodgers GJ. The critical Barkhausen avalanches in thin random-field ferromagnets with an open boundary. Sci Rep 2019;9:6340. doi:10.1038/s41598-019-42802-w.

[43] Shang P, Lu Y, Kamae S. Detecting long-range correlations of traffic time series with multifractal detrended fluctuation analysis. Chaos Solitons Fractals 2008;36:82–90. doi:10.1016/j.chaos.2006.06.019.

[44] Movahed MS, Jafari GR, Ghasemi F, Rahvar S, Tabar MRR. Multifractal detrended fluctuation analysis of sunspot time series. J Stat Mech Theory Exp 2006;2006:P02003 –P02003. doi:10.1088/1742-5468/2006/02/p02003.

[45] Bartholy J, Pongrácz R, Pattantyús-Ábrahám M. Analyzing the genesis, intensity, and tracks of western Mediterranean cyclones. Theor Appl Climatol 2009;96:133–44. doi:10.1007/s00704-008-0082-9.

4. CONCLUSIONES GENERALES

4. Conclusiones generales

De cada uno de los estudios llevados a cabo durante esta investigación se desprenden varias conclusiones.

Del primer estudio, en el que se aplica MF-DFA a distintas series de temperatura, se han extraído las siguientes (Gómez-Gómez et al., 2021a):

- Las variables de temperatura en superficie analizadas (máxima, mínima, media diarias y DTR) muestran distintos exponentes de escala cuando se observan las respectivas funciones de fluctuación en función de la escala, $F_q(s)$, a distintos momentos q. Esto demuestra que las series son multifractales. Además, todas las series son estacionarias y tienen correlación de largo alcance.

- Las características multifractales de las cuatro series de temperatura se modifican, en mayor o menor medida, entre los periodos 1960-1989 y 1990-2019. Esto sugiere una relación entre el cambio climático y el cambio en las propiedades fractales de estas series. No obstante, la simetría de los espectros multifractales permanece aproximadamente igual entre ambos periodos.

- Existe un mayor grado de multifractalidad en las estaciones meteorológicas costeras en ambos periodos en las variables de temperatura mínima y media que contrasta con el de las otras variables. Esto indica que el océano podría tener alguna influencia sobre la complejidad de las temperaturas mínima y media en estas áreas.

- Las temperaturas mínima y media también presentan en la mayoría de las estaciones un estrechamiento de los espectros de singularidad y, por tanto, una disminución en el grado de multifractalidad en el último periodo. Dado que este cambio no se manifiesta en la temperatura máxima, existe un comportamiento asimétrico entre las temperaturas extremas diarias. Este comportamiento puede estar relacionado con las evidencias de asimetría encontradas por otros autores en el ritmo de aumento en las temperaturas máxima y mínima en la región.

Los resultados que se han obtenido en el segundo trabajo, aplicando el marco teórico de las redes complejas a series de temperatura media, han dado lugar a las siguientes conclusiones principales (Gómez-Gómez et al., 2021b):

- Las medias anuales de las anomalías de la temperatura muestran tendencias ascendentes significativas, confirmando los resultados descritos en estudios previos en la Península Ibérica en el periodo considerado.

- Las redes HVGs de las series anuales poseen estructuras similares y propiedades que se mantienen constantes a lo largo del periodo 1960-2019, a diferencia de lo que ocurre con sus medias anuales. El calentamiento global, que influye en las medias anuales, parece no afectar a la media del grado, al exponente de la distribución del grado ni al coeficiente de agrupamiento global de las redes complejas obtenidas.

- Los resultados obtenidos en distintas localizaciones son similares, sugiriendo que las propiedades estudiadas están más relacionadas con el propio proceso natural que describen que con las variaciones en las condiciones locales.

- El algoritmo de HVG caracteriza la naturaleza de la señal estudiada. La media del grado de las series anuales indica su regularidad, típica de procesos disipativos, mientras que el exponente de la distribución en la mayoría de los casos posee un valor que revela unas correlaciones de corto alcance débiles. Además, un coeficiente de agrupamiento no muy elevado también apunta a esta presencia de correlaciones débiles, debido a que se ha hallado una correlación lineal entre este parámetro y el exponente de la distribución del grado.

Por último, el tercer estudio, que aborda los cambios en los parámetros multifractales de la precipitación en la Península Ibérica, revela las siguientes conclusiones (Gómez-Gómez et al., 2022):

- El 48% de las estaciones de medida analizadas presenta tendencias descendentes estadísticamente significativas en la precipitación anual. Estas

tendencias coinciden con un descenso en la media y la desviación estándar entre los dos periodos de 30 años, confirmando la disminución de la precipitación observada en estudios previos.

- La región central de la Península contiene la mayoría de las estaciones que registran una disminución de la precipitación anual. Por lo tanto, esta región, ya caracterizada por una precipitación escasa, se está volviendo uniformemente más árida.

- Las fluctuaciones de las anomalías de la precipitación diaria contienen tres regiones de escala distintas según el método MF-DFA. En las escalas intermedias, únicamente las pequeñas fluctuaciones difieren del resto de regiones encontradas. Contrariamente a este método, el análisis del espectro de potencia solo muestra dos regímenes distintos. Esto sugiere que las escalas intermedias pertenecen a una región de transición entre ambos para el caso de las fluctuaciones de pequeña magnitud.

- Las series de precipitación son multifractales. El grado de multifractalidad es mayor en la región de las pequeñas escalas temporales.

- Todas las estaciones presentan una gran correlación persistente para las escalas pequeñas y correlaciones débiles para las escalas grandes. Los espectros de potencia confirman el comportamiento de las primeras, mientras que para las segundas se obtienen correlaciones no significativas.

- La gran persistencia encontrada para las pequeñas escalas se distribuye sobre la Península siguiendo aproximadamente el gradiente de la precipitación anual. Además, esta persistencia disminuye en la mayoría de las estaciones analizadas en el último periodo.

- La forma no monotónica del exponente de Hurst generalizado en el régimen de las escalas pequeñas impidió la obtención de resultados fiables en esta región. En la región de las escalas temporales grandes, en cambio, se obtuvieron

espectros multifractales que indican un incremento general de la complejidad de las pequeñas fluctuaciones. Además, estos espectros manifiestan un cambio de asimetría que implica una disminución en las singularidades grandes de las series estudiadas en la región oriental de la Península, especialmente en la zona del levante. Esta mayor regularidad puede estar relacionada con el cambio observado por otros autores en la frecuencia y dirección de las borrascas Mediterráneas. Por el contrario, el grado de multifractalidad de las series no muestra ningún patrón de cambio significativo.

Las conclusiones generales, derivadas de las conclusiones individuales de cada publicación, se indican a continuación.

La dinámica de la precipitación es más compleja que la de la temperatura, distinguiéndose un mayor número de regiones de escala. Además, para ambas variables, se confirma que en general las series estudiadas son multifractales y, por tanto, muestran una jerarquía de distintos subconjuntos fractales que se entremezclan.

Las propiedades multifractales de las distintas variables de temperatura y de la precipitación se están modificando en el periodo analizado, 1960-2019. Estos cambios incluyen, fundamentalmente, reducciones en el grado de multifractalidad y complejidad de las fluctuaciones en la temperatura (especialmente, en el caso de la temperatura mínima) y un incremento de la complejidad de las fluctuaciones pequeñas de las series de precipitación a escalas grandes. En otras palabras, hay un aumento de la regularidad en la temperatura mínima y un incremento en la irregularidad de las pequeñas fluctuaciones de la precipitación. Por el contrario, la reducción de grandes singularidades en la precipitación en la zona oriental, especialmente en el levante, indica que sus grandes fluctuaciones pueden estar volviéndose más regulares en el último periodo en esta región.

En un rango amplio de escalas, las diferentes variables de temperatura presentan grandes correlaciones en ambos periodos. El grado de persistencia hallado en estas series también está variando, aunque se ha observado un patrón más claro y con mayor evidencia en el caso de la precipitación. En esta última, la alta persistencia encontrada

ocurre a escalas pequeñas y sigue la distribución espacial del fuerte gradiente de la precipitación anual característica de la Península Ibérica. Los cambios en esta variable sugieren un descenso generalizado de estas correlaciones en las series en el último periodo. Mientras tanto, a gran escala, las fluctuaciones en la precipitación manifiestan una dinámica más aleatoria, carente de correlaciones, que se mantiene en los dos periodos.

El mayor grado de multifractalidad de las temperaturas mínima y media en las zonas costeras, sugiere que la evolución de la temperatura en esas zonas tiene una jerarquía mucho más rica de exponentes. Este fenómeno puede ser debido al efecto amortiguador del océano, que parece que afecta más a las temperaturas mínimas que a las máximas en el primer periodo.

Estas conclusiones permiten confirmar la utilidad del método de MF-DFA para describir las propiedades fractales a distintas escalas y para distintos segmentos de las series. No obstante, tiene algunos inconvenientes cuando se tratan las pequeñas escalas más próximas a la resolución de las series de precipitación, impidiendo obtener resultados fiables de sus espectros multifractales.

La aplicación de HVG y el marco teórico de las redes complejas a las series de temperatura media confirman que estos grafos permiten identificar la naturaleza de las series originales y heredan sus propiedades. Las propiedades topológicas analizadas oscilan alrededor de valores medios y no muestran tendencias significativas, a pesar de la tendencia ascendente observada en el promedio anual de las anomalías de temperatura. La metodología empleada para aplicar el HVG, basada en segmentos anuales de las series desestacionalizadas, no da signos evidentes de cambio. Por lo tanto, el análisis de las series de temperatura llevado a cabo con el método HVG no detecta el cambio climático.

Finalmente, el método de análisis multifractal empleado en esta tesis permite obtener las propiedades de escala y no lineales de la temperatura y la precipitación, mejorando la descripción de estas variables. Por tanto, estas propiedades pueden ser usadas para completar la información disponible en las bases de datos que se emplean para aplicar métodos predictivos y aumentar así el conocimiento sobre la evolución del cambio climático en las próximas décadas.

5. REFERENCIAS

5. Referencias

Abaurrea, J., Asín, J., Erdozain, O., Fernández, E., 2001. Climate Variability Analysis of Temperature Series in the Medium Ebro River Basin, in: India, M.B., Bonillo, D.L. (Eds.), Detecting and Modelling Regional Climate Change. Springer Berlin Heidelberg, Berlin, Heidelberg, pp. 109–118. https://doi.org/10.1007/978-3-662-04313-4_10

Ariza-Villaverde, A.B., Pavón-Domínguez, P., Carmona-Cabezas, R., Gutiérrez de Ravé, E., Jiménez-Hornero, F.J., 2019. Joint multifractal analysis of air temperature, relative humidity and reference evapotranspiration in the middle zone of the Guadalquivir river valley. Agricultural and Forest Meteorology 278, 107657. https://doi.org/10.1016/j.agrformet.2019.107657

Baranowski, P., Krzyszczak, J., Slawinski, C., Hoffmann, H., Kozyra, J., Nieróbca, A., Siwek, K., Gluza, A., 2015. Multifractal analysis of meteorological time series to assess climate impacts. Clim. Res. 65, 39–52. https://doi.org/10.3354/cr01321

Bartholy, J., Pongrácz, R., Pattantyús-Ábrahám, M., 2009. Analyzing the genesis, intensity, and tracks of western Mediterranean cyclones. Theor Appl Climatol 96, 133–144. https://doi.org/10.1007/s00704-008-0082-9

Braga, A.C., Alves, L.G.A., Costa, L.S., Ribeiro, A.A., de Jesus, M.M.A., Tateishi, A.A., Ribeiro, H.V., 2016. Characterization of river flow fluctuations via horizontal visibility graphs. Physica A: Statistical Mechanics and its Applications 444, 1003–1011. https://doi.org/10.1016/j.physa.2015.10.102

Brunet, M., Jones, P.D., Sigró, J., Saladié, O., Aguilar, E., Moberg, A., Della-Marta, P.M., Lister, D., Walther, A., López, D., 2007. Temporal and spatial temperature variability and change over Spain during 1850–2005. J. Geophys. Res. 112, D12117. https://doi.org/10.1029/2006JD008249

Brunetti, M., Colacino, M., Maugeri, M., Nanni, T., 2001. Trends in the daily intensity of
    precipitation in Italy from 1951 to 1996. International Journal of Climatology
    21, 299–316. https://doi.org/10.1002/joc.613

Burgueño, A., Lana, X., Serra, C., Martínez, M.D., 2014. Daily extreme temperature
    multifractals in Catalonia (NE Spain). Phys. Lett. A 378, 874–885.
    https://doi.org/10.1016/j.physleta.2014.01.033

Carmona-Cabezas, R., Ariza-Villaverde, A.B., Gutiérrez de Ravé, E., Jiménez-Hornero,
    F.J., 2019. Visibility graphs of ground-level ozone time series: A multifractal
    analysis. Science of The Total Environment 661, 138–147.
    https://doi.org/10.1016/j.scitotenv.2019.01.147

Coumou, D., Rahmstorf, S., 2012. A decade of weather extremes. Nature Climate
    Change 2, 491–496. https://doi.org/10.1038/nclimate1452

da Silva, H.S., Silva, J.R.S., Stosic, T., 2020. Multifractal analysis of air temperature in
    Brazil. Physica A 549, 124333. https://doi.org/10.1016/j.physa.2020.124333

de Lima, M.I.P., Santo, F.E., Ramos, A.M., de Lima, J.L.M.P., 2013. Recent changes in
    daily precipitation and surface air temperature extremes in mainland Portugal,
    in the period 1941–2007. Atmos. Res. 127, 195–209.
    https://doi.org/10.1016/j.atmosres.2012.10.001

Drożdż, S., Kowalski, R., Oświęcimka, P., Rak, R., Gębarowski, R., 2018. Dynamical
    Variety of Shapes in Financial Multifractality. Complexity 2018, 1–13.
    https://doi.org/10.1155/2018/7015721

Durrani, S., 2022. Koch.m
    (https://www.mathworks.com/matlabcentral/fileexchange/301-koch-m),
    MATLAB Central File Exchange. Retrieved February 10, 2022.

Eensaar, A., 2021. Analysis of the Spatio-Temporal Variability of Air Temperature Near the Ground Surface in the Central Baltic Area from 2005 to 2019. Atmosphere 12. https://doi.org/10.3390/atmos12010060

El Kenawy, A., López-Moreno, J.I., Vicente-Serrano, S.M., 2012. Trend and variability of surface air temperature in northeastern Spain (1920–2006): Linkage to atmospheric circulation. Atmospheric Research 106, 159–180. https://doi.org/10.1016/j.atmosres.2011.12.006

Feder, J., 1988. Fractals. Springer US, Boston, MA. https://doi.org/10.1007/978-1-4899-2124-6

Fuwape, I.A., Ogunjo, S.T., Oluyamo, S.S., Rabiu, A.B., 2017. Spatial variation of deterministic chaos in mean daily temperature and rainfall over Nigeria. Theor Appl Climatol 130, 119–132. https://doi.org/10.1007/s00704-016-1867-x

García-Marín, A.P., Estévez, J., Sangüesa-Pool, C., Pizarro-Tapia, R., Ayuso-Muñoz, J.L., Jimenez-Hornero, F.J., 2015. The use of the exponent $K(q)$ function to delimit homogeneous regions in regional frequency analysis of extreme annual daily rainfall: MULTIFRACTAL PROPERTIES OF RAINFALL TO FORM HOMOGENEOUS REGIONS IN RFA. Hydrol. Process. 29, 139–151. https://doi.org/10.1002/hyp.10284

Gómez-Gómez, J., Carmona-Cabezas, R., Ariza-Villaverde, A.B., Gutiérrez de Ravé, E., Jiménez-Hornero, F.J., 2021a. Multifractal detrended fluctuation analysis of temperature in Spain (1960–2019). Physica A: Statistical Mechanics and its Applications 578, 126118. https://doi.org/10.1016/j.physa.2021.126118

Gómez-Gómez, J., Carmona-Cabezas, R., Sánchez-López, E., Gutiérrez de Ravé, E., Jiménez-Hornero, F.J., 2022. Multifractal fluctuations of the precipitation in Spain (1960–2019). Chaos, Solitons & Fractals 157, 111909. https://doi.org/10.1016/j.chaos.2022.111909

Gómez-Gómez, J., Carmona-Cabezas, R., Sánchez-López, E., Gutiérrez de Ravé, E., Jiménez-Hornero, F.J., 2021b. Analysis of Air Mean Temperature Anomalies by Using Horizontal Visibility Graphs. Entropy 23, 207. https://doi.org/10.3390/e23020207

Gozolchiani, A., Yamasaki, K., Havlin, S., 2011. The Emergence of El-Niño as an Autonomous Component in the Climate Network. Phys. Rev. Lett. 107, 148501. https://doi.org/10.1103/PhysRevLett.107.148501

Horton, B., 1995. Geographical distribution of changes in maximum and minimum temperatures. Atmos. Res. 37, 101–117. https://doi.org/10.1016/0169-8095(94)00083-P

Hu, K., Ivanov, P.Ch., Chen, Z., Carpena, P., Eugene Stanley, H., 2001. Effect of trends on detrended fluctuation analysis. Phys. Rev. E 64, 011114. https://doi.org/10.1103/PhysRevE.64.011114

IPCC, 2021. Summary for Policymakers, in: Masson-Delmotte, V., Zhai, P., Pirani, A., Connors, S.L., Péan, C., Berger, S., Caud, N., Chen, Y., Goldfarb, L., Gomis, M.I., Huang, M., Leitzell, K., Lonnoy, E., Matthews, J.B.R., Maycock, T.K., Waterfield, T., Yelekçi, O., Yu, R., Zhou, B. (Eds.), Climate Change 2021: The Physical Science Basis. Contribution of Working Group I to the Sixth Assessment Report of the Intergovernmental Panel on Climate Change. In press.

IPCC, 2014. Summary for policymakers, in: Field, C.B., Barros, V.R., Dokken, D.J., Mach, K.J., Mastrandrea, M.D., Bilir, T.E., Chatterjee, M., Ebi, K.L., Estrada, Y.O., Genova, R.C., Girma, B., Kissel, E.S., Levy, A.N., MacCracken, S., Mastrandea, P.R., White, L.L. (Eds.), Climate Change 2014: Impacts, Adaptation, and Vulnerability. Part A: Global and Sectoral Aspects. Contribution of Working Group II to the Fifth Assessment Report of the Intergovernmental Panel on Climate Change. Cambridge University Press, Cambridge, United Kingdom and New York, NY, USA, pp. 1–32.

IPCC, 2013. Summary for Policymakers, in: Stocker, T.F., Qin, D., Plattner, G.-K., Tignor, M., Allen, S.K., Boschung, J., Nauels, A., Xia, Y., Bex, V., Midgley, P.M. (Eds.), Climate Change 2013: The Physical Science Basis. Contribution of Working Group I to the Fifth Assessment Report of the Intergovernmental Panel on Climate Change. Cambridge University Press, Cambridge, United Kingdom and New York, NY, USA.

Javanshiri, Z., Pakdaman, M., Falamarzi, Y., 2021. Homogenization and trend detection of temperature in Iran for the period 1960–2018. Meteorology and Atmospheric Physics 133, 1233–1250. https://doi.org/10.1007/s00703-021-00805-1

Jones, P.D., Hulme, M., 1996. Calculating regional climatic time series for temperature and precipitation: Methods and illustrations. Int. J. Climatol. 16, 361–377. https://doi.org/10.1002/(SICI)1097-0088(199604)16:4<361::AID-JOC53>3.0.CO;2-F

Jones, P.D., Moberg, A., 2003. Hemispheric and Large-Scale Surface Air Temperature Variations: An Extensive Revision and an Update to 2001. J. Climate 16, 206–223.

Jones, P.D., New, M., Parker, D.E., Martin, S., Rigor, I.G., 1999. Surface air temperature and its changes over the past 150 years. Rev. Geophys. 37, 173–199. https://doi.org/10.1029/1999RG900002

Kantelhardt, J.W., Zschiegner, S.A., Koscielny-Bunde, E., Havlin, S., Bunde, A., Stanley, H.E., 2002. Multifractal detrended fluctuation analysis of nonstationary time series. Physica A 316, 87–114. https://doi.org/10.1016/S0378-4371(02)01383-3

Katsoulis, B.D., Kambetzidis, H.D., 1989. Analysis of the long-term precipitation series at Athens, Greece. Climatic Change 14, 263–290. https://doi.org/10.1007/BF00134966

Krzyszczak, J., Baranowski, P., Zubik, M., Kazandjiev, V., Georgieva, V., Sławiński, C., Siwek, K., Kozyra, J., Nieróbca, A., 2019. Multifractal characterization and comparison of meteorological time series from two climatic zones. Theor Appl Climatol 137, 1811–1824. https://doi.org/10.1007/s00704-018-2705-0

Lacasa, L., Luque, B., Ballesteros, F., Luque, J., Nuño, J.C., 2008. From time series to complex networks: The visibility graph. Proc. Natl. Acad. Sci. 105, 4972–4975. https://doi.org/10.1073/pnas.0709247105

Lacasa, L., Toral, R., 2010. Description of stochastic and chaotic series using visibility graphs. Phys. Rev. E 82, 036120. https://doi.org/10.1103/PhysRevE.82.036120

López-Moreno, J.I., Vicente-Serrano, S.M., Angulo-Martínez, M., Beguería, S., Kenawy, A., 2010. Trends in daily precipitation on the northeastern Iberian Peninsula, 1955-2006. Int. J. Climatol. 30, 1026–1041. https://doi.org/10.1002/joc.1945

Luque, B., Lacasa, L., Ballesteros, F., Luque, J., 2009. Horizontal visibility graphs: Exact results for random time series. Phys. Rev. E 80, 046103. https://doi.org/10.1103/PhysRevE.80.046103

Mali, P., 2015. Multifractal characterization of global temperature anomalies. Theor Appl Climatol 121, 641–648. https://doi.org/10.1007/s00704-014-1268-y

Mandelbrot, B., 1967. How Long Is the Coast of Britain? Statistical Self-Similarity and Fractional Dimension. Science 156, 636–638. https://doi.org/10.1126/science.156.3775.636

Mandelbrot, B.B., 1982. The fractal geometry of nature. W.H. Freeman, San Francisco.

Millán, H., Ghanbarian-Alavijeh, B., García-Fornaris, I., 2010. Nonlinear dynamics of mean daily temperature and dewpoint time series at Babolsar, Iran, 1961–2005. Atmospheric Research 98, 89–101. https://doi.org/10.1016/j.atmosres.2010.06.001

Movahed, M.S., Jafari, G.R., Ghasemi, F., Rahvar, S., Tabar, M.R.R., 2006. Multifractal detrended fluctuation analysis of sunspot time series. Journal of Statistical Mechanics: Theory and Experiment 2006, P02003–P02003. https://doi.org/10.1088/1742-5468/2006/02/p02003

Nilsson, E., 2007. Multifractal-based image analysis with applications in medical imaging. Dep. Comput. Sci. Umea Univ. Umea Sweden 33–70.

Ongoma, V., Rahman, M.A., Ayugi, B., Nisha, F., Galvin, S., Shilenje, Z.W., Ogwang, B.A., 2020. Variability of diurnal temperature range over Pacific Island countries, a case study of Fiji. Meteorol Atmos Phys. https://doi.org/10.1007/s00703-020-00743-4

Paluš, M., Hartman, D., Hlinka, J., Vejmelka, M., 2011. Discerning connectivity from dynamics in climate networks. Nonlin. Processes Geophys. 18, 751–763. https://doi.org/10.5194/npg-18-751-2011

Pavón-Domínguez, P., Serrano, S., Jiménez-Hornero, F.J., Jiménez-Hornero, J.E., Gutiérrez de Ravé, E., Ariza-Villaverde, A.B., 2013. Multifractal detrended fluctuation analysis of sheep livestock prices in origin. Physica A 392, 4466–4476. https://doi.org/10.1016/j.physa.2013.05.042

Perevedentsev, Yu.P., Vasil'ev, A.A., Shantalinskii, K.M., Gur'yanov, V.V., 2017. Long-term variations in surface air pressure and surface air temperature in the Northern Hemisphere mid-latitudes. Russian Meteorology and Hydrology 42, 461–470. https://doi.org/10.3103/S1068373917070056

Rodrigo, F.S., 2010. Changes in the probability of extreme daily precipitation observed from 1951 to 2002 in the Iberian Peninsula. Int. J. Climatol. 30, 1512–1525. https://doi.org/10.1002/joc.1987

Rodrigo, F.S., Trigo, R.M., 2007. Trends in daily rainfall in the Iberian Peninsula from 1951 to 2002. Int. J. Climatol. 27, 513–529. https://doi.org/10.1002/joc.1409

Rodríguez-Solà, R., Casas-Castillo, M.C., Navarro, X., Redaño, Á., 2017. A study of the scaling properties of rainfall in spain and its appropriateness to generate intensity-duration-frequency curves from daily records. Int. J. Climatol. 37, 770–780. https://doi.org/10.1002/joc.4738

Sarker, A., Mali, P., 2021. Detrended multifractal characterization of Indian rainfall records. Chaos, Solitons & Fractals 151, 111297. https://doi.org/10.1016/j.chaos.2021.111297

Tadić, B., Mijatović, S., Janićević, S., Spasojević, D., Rodgers, G.J., 2019. The critical Barkhausen avalanches in thin random-field ferromagnets with an open boundary. Scientific Reports 9, 6340. https://doi.org/10.1038/s41598-019-42802-w

Telesca, L., Cuomo, V., Lapenna, V., Macchiato, M., 2001. Identifying space–time clustering properties of the 1983–1997 Irpinia–Basilicata (Southern Italy) seismicity. Tectonophysics 330, 93–102. https://doi.org/10.1016/S0040-1951(00)00221-3

Telesca, L., Lapenna, V., 2006. Measuring multifractality in seismic sequences. Tectonophysics 423, 115–123. https://doi.org/10.1016/j.tecto.2006.03.023

Telesca, L., Lovallo, M., 2011a. Revealing competitive behaviours in music by means of the multifractal detrended fluctuation analysis: Application to Bach's Sinfonias. Proc. R. Soc. A Math. Phys. Eng. Sci. 467, 3022–3032. https://doi.org/10.1098/rspa.2011.0118

Telesca, L., Lovallo, M., 2011b. Analysis of the time dynamics in wind records by means of multifractal detrended fluctuation analysis and the Fisher–Shannon information plane. J. Stat. Mech. 2011, P07001. https://doi.org/10.1088/1742-5468/2011/07/P07001

Tsonis, A.A., Roebber, P.J., 2004. The architecture of the climate network. Physica A:
Statistical Mechanics and its Applications 333, 497–504.
https://doi.org/10.1016/j.physa.2003.10.045

Zhuang, Y., Zhang, J., 2020. Diurnal asymmetry in future temperature changes over the
main Belt and Road regions. Ecosystem Health and Sustainability 6, 1749530.
https://doi.org/10.1080/20964129.2020.1749530